5-2007

Effects of Quaternary Climate Change on Tributary Sedimentation and Geomorphology in Eastern Grand Canyon

Benjamin D. DeJong
Utah State University

EFFECTS OF QUATERNARY CLIMATE CHANGE ON TRIBUTARY SEDIMENTATION AND GEOMORPHOLOGY IN EASTERN GRAND CANYON

by

Benjamin D. DeJong

A thesis submitted in partial fulfillment
of the requirements for the degree

of

MASTER OF SCIENCE

in

Geology

Approved:

UTAH STATE UNIVERSITY
Logan, Utah

2007

ABSTRACT

Effects of Quaternary Climate Change on Tributary Sedimentation and Geomorphology in Eastern Grand Canyon

by

Benjamin D. DeJong, Master of Science

Utah State University, 2007

Major Professor: Dr. Joel L. Pederson
Department: Geology

Climate variability has had a dramatic impact on eastern Grand Canyon tributaries over the past ~100 ky. This is readily observed in the Lava Chuar and Comanche catchments, which host well preserved colluvial remnants and river terraces that resulted from several climate-induced cycles of aggradation and incision. This study investigates these climate responses using surveying, sedimentology, and luminescence geochronology methods to investigate the mechanisms and timing of their deposition.

The survey data demonstrate that the concavity of terrace treads is lower than modern drainages. The sedimentology suggests the prevalence of stream-flow reworking of debris flow deposits and portrays an expected down-stream fining of deposits. Results of geochronology indicate that Lava Chuar Creek aggraded from ~100-90 ka (S4), 61-55 ka (S3o), 50-35 ka (S3y), and 14-7 ka (S2). Comanche Creek similarly aggraded twice during the time period from 77-35 ka (S3) and also from 26-22 ka (S2).

The response of eastern Grand Canyon tributaries to glacial-interglacial climate cycling appears to be more complicated than formerly thought. Previous conceptual

models assumed that stream aggradation in arid settings occurred as a response to one specific set of climatic and biologic conditions, but new field data and luminescence dates on terrace materials reveal that there are at least two sets of conditions that were conducive to aggradation along local streams. First, streams aggraded during cooler, wetter climates, which is inferred to be due to increased sediment supply (e.g. S4 and S3y in Lava Chuar). With the transition to warmer interglacial climates came higher intensity storms and decreased vegetation density in catchments, based on previous paleoclimate studies. These conditions caused remobilization and redeposition of older sediment and resulted in a second set of stream aggradation phases (e.g. S3o and S2 in Lava Chuar). Meanwhile, the Colorado River aggraded only once per climate cycle during glacial advances and subsequent climate transitions. Thus, tributaries have responded more frequently and more sensitively to changing local conditions compared to the relatively insensitive Colorado River. This is supported by tighter correlation of tributary records to trends in regional paleoclimate records than to global ice records.

(122 pages)

ACKNOWLDGEMENTS

First and foremost, words cannot express my gratitude for Joel Pederson. He has a passion for geomorphology that is both contagious and inspirational, and this work would have been impossible without his keen understanding of landscape evolution and constant support. I would also like to thank my committee members, Tammy Rittenour and Jack Schmidt, for providing me with fresh ideas and helpful edits that significantly improved both the content and flow of this thesis. Thanks also to Ron Goble, Paul Hanson, and Tammy Rittenour for their guidance in collecting, processing, and running samples at the OSL Geochronology Laboratory at the University of Nebraska in Lincoln. Much thanks to all the students and research assistants associated with the Department of Geology at Utah State University for giving so freely of their time and energy to ensure a thorough collection of data by raft and by foot. Finally, I would like to thank my family for their continued encouragement and support throughout these endeavors.

Funding for this research was provided by a National Science Foundation grant awarded to Joel Pederson (EAR-0346054), a Geological Society of America student research grant, and the Utah State University Department of Geology. I am grateful to the Grand Canyon National Park for providing both backcountry and river access to eastern Grand Canyon to carry out this research.

Ben DeJong

PREFACE

The Research presented here examined hillslope and fluvial surficial deposits in the Comanche and Lava Chuar catchments in eastern Grand Canyon to gain insight into how climate variability over the past ~100 ky affected tributary sedimentation. This thesis is divided into three chapters. Chapter 1 offers a background for the study including an introduction to the study area, a review of previously developed ideas and past research concerning geomorphic response of the eastern Grand Canyon and other similar settings to past climate change, and a review of the concepts and methodology surrounding the optically stimulated luminescence dating technique used in this research. Chapter 2 sequentially takes the reader through the three primary methods used in this research and the results that came out of each method. Finally, Chapter 3 includes a discussion of the results and places them in the context of the current working conceptual model for the response of eastern Grand Canyon tributaries to climate change. The thesis ends with the main conclusions that can be taken from this research. All of the data collected during this study are included in the Appendices, including two surficial geologic maps containing the locations of survey transects and luminescence samples.

CONTENTS

LIST OF TABLES

LIST OF FIGURES

LIST OF PLATES

CHAPTER 1

BACKGROUND

INTRODUCTION

Though the Grand Canyon of northern Arizona is widely known for its classic layer-cake sequence of Precambrian and Paleozoic bedrock, an increasing body of research is focused on its more recent erosional history. Superimposed on the overall incision that carved the canyon is a well preserved Quaternary stratigraphic record of sedimentary and geomorphic responses to climate change. Dissected hillslope deposits and fluvial terraces record phases of aggradation and incision along both the mainstem Colorado River and its smaller tributaries, and these changes have been attributed to glacial-interglacial climate changes during the Pleistocene (Machette and Rosholt, 1989; Lucchitta et al., 1995, 2000; Pederson et al., 2002; Anders et al., 2005). Within the relatively narrow, steep-walled Grand Canyon, Pleistocene deposits are preserved in reaches where weaker bedrock was eroded to form wide valley floors. The Furnace Flats reach in eastern Grand Canyon provides such a setting and is host to well-exposed Colorado River and tributary deposits. Within the Furnace Flats region, the Quaternary deposits preserved in the Lava Chuar and Comanche drainages are especially well exposed, and therefore are the focus of this research.

Unglaciated drylands can be ideal settings for studying climate change because the geomorphic and biologic responses to each phase of the glacial-interglacial cycle are distinct and may be preserved in the geologic record. Erosional landscapes such as Grand Canyon are exceptionally useful, as several climate cycles may be preserved in the record and can provide insight into climatic controls

on sedimentation. Based on paleoclimate studies in the area, the Pleistocene climate changes recorded in eastern Grand Canyon deposits are similar in magnitude to those projected for upcoming centuries. Understanding landscape responses to these changes is crucial because it has been recognized that arid and semi-arid regions, and those who inhabit them, are particularly vulnerable to the effects of global warming (Dohrenwend, 1987; IPCC, 2001).

REVIEW OF DRYLAND RESPONSE TO CLIMATE CHANGE

Bull (1991) developed a conceptual model for understanding the geomorphic responses of deserts to glacial-interglacial climate cycles that is based on several lines of research (e.g. Bull and Schick, 1979; Gerson, 1982; Gerson and Grossman, 1987). In this model, cycles of aggradation and incision evident in landscape records occur in response to time-transgressive changes in hillslope processes and vegetation communities. Rates of bedrock weathering increased during the relatively colder, wetter conditions of glacial periods, which lead to enhanced rates of regolith production. Vegetation density increased during this time as well, which increased both soil cohesion and infiltration and ultimately induced sediment storage on hillslopes. The greatest geomorphic activity occured during glacial-interglacial transitions, as climate shifted to warmer and drier conditions and the southwest monsoon season developed. Increased precipitation intensity on hillslopes with diminishing vegetation prompted the mobilization of stored colluvium. Sediments were incorporated into stream systems, and drainage heads migrated up-catchment toward the toes of hillslopes. Colluvium was depleted from adjacent hillslopes by the start of the interglacial period, and streams began to incise through their own beds by the mid-Holocene. In short, Bull's model suggests sediment production and

storage during colder glacial climate, hillslope transport and stream deposition during the glacial-interglacial transition, and incision or inactivity during interglacial climates. While this model is a helpful backdrop for understanding the effects of climate change, it is primarily based on geologic records covering only the most recent glacial-interglacial cycle, it lacks robust age control, and its applicability to all drylands is unclear.

Several researchers have responded to these limitations by building upon and revising Bull's original model. Physically based numerical models (Tucker and Slingerland, 1997) and field-based research (Ritter and Gardner, 1993) provide a process-oriented perspective of changes in hillslope processes and sedimentation in non-glaciated settings during glacial-interglacial transitions. According to these studies, vegetation density increases during wetter glacial conditions and causes channel heads to retreat downslope due to an associated increase in the ratio of saturation overland flow/infiltration overland flow and/or regolith cohesion (Dietrich and Dunne, 1993). As a result, hillslopes lengthen, become mantled with colluvium, and are stabilized by vegetation. Vegetation density declines during the transition to interglacial climates and causes the ratio of saturation overland flow/infiltration overland flow and regolith cohesion to decrease. Channel heads migrate back upslope introducing a pulse of sediment to streams due to the dissection of colluvial mantles. Tucker and Slingerland (1997) demonstrated that a change in climate is not always necessary for stream incision to follow an episode of stream aggradation. As the hillslope materials are depleted, the threshold of erosion in streams can be crossed, just as Bull (1991) proposed in his original model. Second, their results predict that geomorphic responses to shifts to more arid climate conditions could be more rapid than shifts in the reverse due to the effect of high precipitation intensity from monsoons. Increased runoff intensity leads to a rapid upslope extension of the

channel network. The erosion of former side slopes leads to a large increase in sediment flux to the main channel network and results in rapid valley aggradation. Shifts to colder, glacial conditions reduce sediment transport rates, and channels undergo slow aggradation.

Pederson and others (2000, 2001) interpreted stratigraphic evidence in the Mojave Desert as indicating support for this model not only for Pleistocene records but also for those spanning back to the Miocene. In slight contrast to Bull's model, there was evidence for sediment delivery from hillslopes to piedmonts during wetter, glacial conditions, as well as major sediment pulses during glacial-interglacial transitions. They also concluded that rates of weathering, and thus sediment supply, are much greater in areas of weaker bedrock than those with more resistant bedrock.

The effects of vegetation cover on geomorphic responses to climate change in the American Southwest vary with respect to the type of vegetation and the substrate on which it is established. Harvey and Wells (1994) and Harvey and others (1999) used differing vegetation communities of California and Nevada to illustrate the role vegetation played in the geomorphic response of alluvial fans to the last glacial-interglacial transition (and the development of summer monsoons). Results of their study show that alluvial fans in the Mojave Desert of southern California experienced a pulse of sediment delivery and deposition during this period, which was attributed to the effects of a well-developed monsoon season and to relatively sparse vegetation cover on hillslopes. The vegetation in the Mojave Desert changed from temperate desert scrub during the Pleistocene to thermophilous desert scrub during the Holocene. Alluvial fans in west-central Nevada did not experience this sediment pulse during the glacial-interglacial transition, however, which was attributed primarily to its lush vegetation and relatively weak monsoon season. Vegetation in this region changed from juniper woodland with a rich grass and sagebrush

understory at lower elevations and pine forest at higher elevations during the late Pleistocene, to temperate desert scrub at low elevations and juniper and pine woodlands at higher elevations during the Holocene. By contrast, McDonald and others (2003) show that vegetation cover actually may have had limited impact on hillslope stability and sediment yield in the Providence Mountains of the eastern Mojave Desert during the Pleistocene-Holocene climatic transition. The coarse-textured colluvium on which vegetation is established has an inherently high infiltration capacity regardless of vegetation density, and modern vegetation cover (temperate desert scrub) appears to provide enough stability for the buildup of soils and colluvium. They instead attribute alluvial fan deposition primarily to an increase in extreme storm events; possibly an increase in tropical cyclones.

Nichols and others (2002) generally show that the timing of geomorphic responses may not necessarily be consistent for all settings in the American Southwest. They gained better age control for large, unconfined desert piedmonts in the Mojave Desert and found that rather than experiencing a sediment pulse during the glacial-interglacial transition as predicted, piedmonts experienced greatest sedimentation ~75 ka during wetter glacial conditions (MIS 4). There was a lag time on the order of ~30 ky before this pulse of sediment reached the distal portions of the piedmont ~3.5 km downslope. Piedmonts were therefore generally marked by the slow propagation of a sediment pulse during the glacial-interglacial transition and by erosion during the Holocene.

Recent research by Anders and others (2005) in eastern Grand Canyon tributaries targets deposits that span a larger spatial and temporal scale and offers greater opportunities for age control than most previous records. They concluded that terrace and hillslope deposits in eastern Grand Canyon reveal a more complicated relationship between tributary sedimentation and climate change. For

example, their geochronologic results reveal a temporal disconnect between the responses of tributary streams and the responses of the mainstem Colorado River to climatic forcing. Based on geochronology, tributary aggradation may have lagged behind that of the mainstem by approximately 20 ky during the late Pleistocene. Anders and others (2005) hypothesize that this lag-time may be due to prolonged sediment production and transport in tributary catchments as a function of distinct local geomorphic responses to climate cycling. This scenario could ultimately induce a style of time-transgressive sedimentation during the shift from glacial to interglacial climates where tributary aggradation progrades downstream as material is gradually made available from hillslopes. According to this model, this material is concurrently eroded upslope and redeposited downslope during warmer, drier interglacial climates.

This study aims to further explore the responses of eastern Grand Canyon tributary streams to known climate changes by focusing on the timing and patterns of sedimentation. Optically stimulated luminescence (OSL) dating is used to develop a higher-resolution chronology for tributary-stream deposition in eastern Grand Canyon, and sedimentologic descriptions and survey data provide insight into the corresponding patterns and transport mechanisms of deposits. The goal of this study is to test whether Quaternary deposits change in age and character from headwaters to the mouths of two tributary catchments in eastern Grand Canyon.

SETTING

The Comanche and Lava Chuar catchments of eastern Grand Canyon are ephemeral, mixed bedrock-alluvial drainages (Fig. 1.1). The Comanche catchment

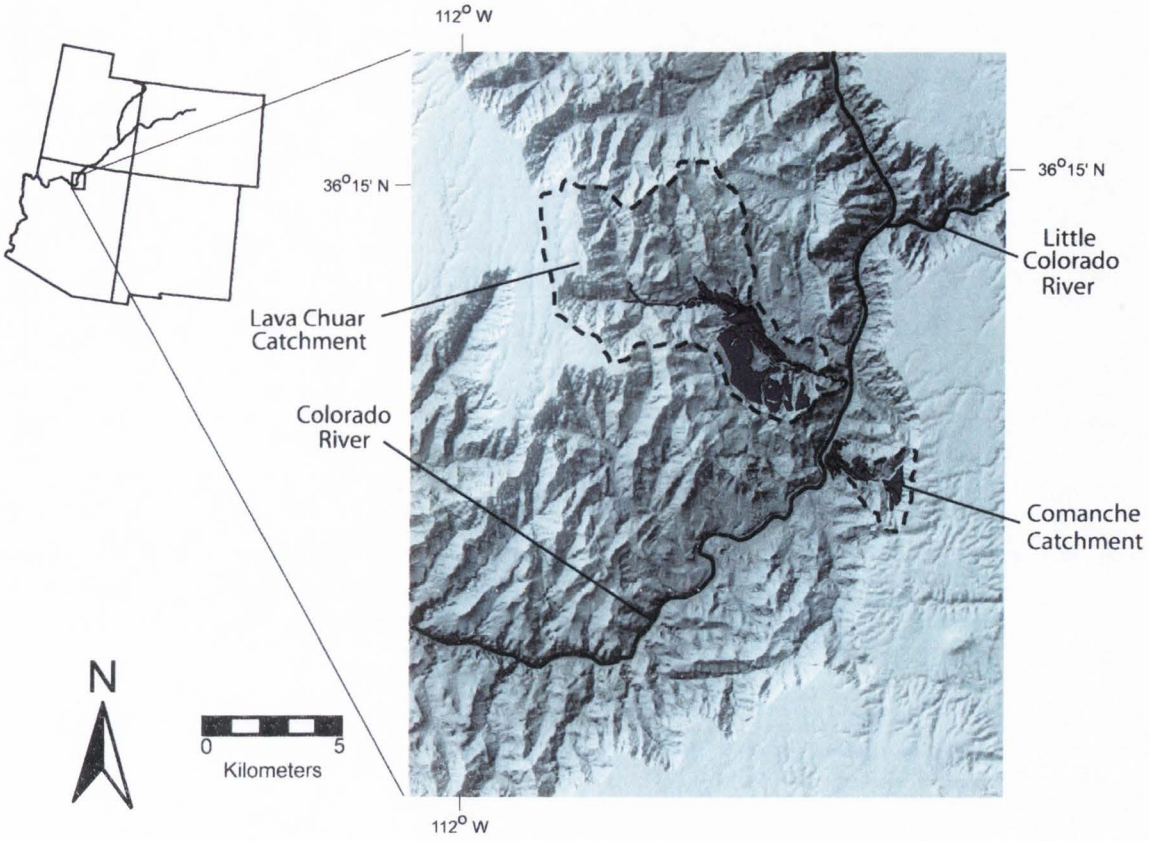

Figure 1.1 The study site in the Furnace Flats reach of eastern Grand Canyon. The two study catchments are outlined by dotted lines and tributary deposits are represented by shaded polygons.

covers a surface area of 5.4 km^2, has a very steep average gradient of 39°, and a drainage length of 4.5 km. The larger Lava Chuar catchment covers 54.7 km^2, has an average gradient of 29°, and a drainage length of 15.2 km. The contrasting geometries of these two catchments are useful for this study. The Comanche catchment was selected because its short, steep nature provides excellent exposure, and direct relationships between hillslope and tributary stream deposits can be observed. For instance, field evidence suggests that the stream deposits exposed in the Comanche catchment are stratigraphically linked to large colluvial remnants in the headwaters. By contrast, the relatively open landscape of the Lava Chuar catchment offers excellent preservation of a longer record of tributary-fill deposits.

This longer record affords a clearer understanding of their relations to each other and to changes in local climate.

Climate and vegetation vary strongly with respect to elevation within the Grand Canyon. The mean annual precipitation (MAP) is 645 mm and the mean annual temperature (MAT) is 6.0°C at the north rim, whereas the MAP is 244 mm and MAT is 20.5°C at the bottom of the canyon (http://www.wrcc.dri.edu/summary/climsmaz.html). Desert scrub communities including sagebrush (*Artemesia tridentata*), Mormon tea (*Ephedra nevadensis*), catclaw (*Acacia greggii*), and blackbrush (*Coleogyne ramosissima*) are dominant at elevations less than 1,500 m above sea level (asl) and transition to pinyon-juniper woodland (*Pinus edulis* and *Juniperus osteosperma*) at elevations between 1,500 and 2,200 m asl (Cole, 1990a, 1990b). An upland-vegetation community of Douglas-fir (*Pseudotsuga menziesii*), Ponderosa pine (*Pinus ponderosa*), Englemann spruce (*Picea engelmannii*), and quaking Aspen (*Populus tremuloides*) dominates elevations above 2,200 m asl (Cole, 1990a, 1990b; Weng and Jackson, 1999). These vegetation zones appear to have shifted vertically in response to deglaciation after the Last Glacial Maximum (LGM) due to changing MAP and MAT, as reviewed below.

Field observations indicate hillslopes are generally weathering-limited in the Lava Chuar and Comanche catchments. In eastern Grand Canyon, bedrock weathering would have been relatively rapid during wetter glacial conditions because the increased effective moisture would have accelerated rates of physical and chemical weathering. However, wetter climates also increased vegetation density, which stabilized slopes and caused regolith-mantling of hillslopes as evident by relict colluvial deposits in this landscape. Other research suggests debris flows are the dominant process responsible for transporting this stored regolith into drainages

(Melis, 1997; Griffiths et al., 2004). In eastern Grand Canyon, debris flows are usually initiated by failure and mass-movement of bedrock or colluvium due to the "firehose effect" of large volumes of water impacting slopes from pour-overs. This occurs either during intense summer monsoon storms, especially if there is antecedent soil moisture, or during low-intensity, long-duration winter-frontal storms (Webb et al., 1996; Griffiths et al., 1996). Field evidence in eastern Grand Canyon suggests that debris flows also were the primary transport mechanism and a major source of sediment for tributary-stream networks during the Pleistocene.

PREVIOUS GEOMORPHIC RESEARCH IN EASTERN GRAND CANYON

A number of researchers have studied the well preserved Quaternary deposits in eastern Grand Canyon. Most work has focused on Colorado River and tributary debris-fan deposits found along the mainstem corridor (Machette and Rosholt, 1989), but only recently have deposits upslope from the mouths of tributary drainages been studied in detail (Anders, 2003). Lucchitta and others (1995) identified seven Pleistocene Colorado River terraces as well as eight tributary-stream terraces in the Lava Chuar-Comanche reach. Machette and Rosholt (1989) also identified seven Pleistocene Colorado River terraces in the Tanner-Unkar reach just downstream (Colorado River mile 68.5L (left)-72.6R (right) where mile 0 is at Lee's Ferry, AZ). Hereford (1996) and Hereford and others (1996) identified three Holocene Colorado River deposits and interpreted them to be stratigraphically related to debris-fan surfaces in the Lava Chuar-Unkar reach. These smaller scale and finer-grained Holocene deposits, however, are distinct from older, coarser fill-terraces in the study area and are not the focus of this study.

Previous workers have largely attributed the presence of Pleistocene deposits in eastern Grand Canyon to climate-related variables. Machette and Rosholt (1989)

attribute mainstem terrace formation to changes in sediment yield in the Colorado River catchment due to glacial-interglacial climate cycles and their effects on vegetation cover. Lucchitta and others (1995) concluded that glacial advances in the Colorado River headwaters during the Pinedale (marine isotope stage (MIS) 2) and Bull Lake (MIS 6) glaciations increased sediment yield and caused two episodes of mainstem aggradation in eastern Grand Canyon. Early Holocene aggradation is conversely attributed to increased erosion of alluvial and colluvial deposits on the Colorado Plateau due to reduced vegetation cover and intense monsoonal precipitation (Lucchitta et al., 1995). By contrast, Hamblin (1994) proposed that Quaternary deposits in eastern Grand Canyon were deposited in a series of lakes that formed behind lava-dams in western Grand Canyon, in particular the prominent terraces in Lava Chuar and other tributaries.

Much of the age control associated with these earlier studies is problematic. Machette and Rosholt (1989) bracketed deposition of their seven Colorado River terraces to between 700 ka and 5 ka based on uranium-trend dating, a technique which has since been abandoned. Lucchitta and others (1995) used terrestrial cosmogenic nuclide (TCN) and radiocarbon dating to constrain terrace ages. However the TCN ages were not corrected for inheritance by the collection of shielded samples and amalgamated sampling methods were not used, as these practices were not developed by that time.

Anders (2003) studied the exposed suites of both mainstem and tributary deposits in eastern Grand Canyon. This included the detailed mapping of deposits as well as geochronologic dating of key exposures (Anders et al., 2005). Four well preserved tributary terrace deposits (S1-S4) and at least six mainstem terrace deposits (M1, M3-M7) were identified. OSL, TCN, and uranium-series (U-series) dating methods were applied to a variety of surficial deposits and landforms for age

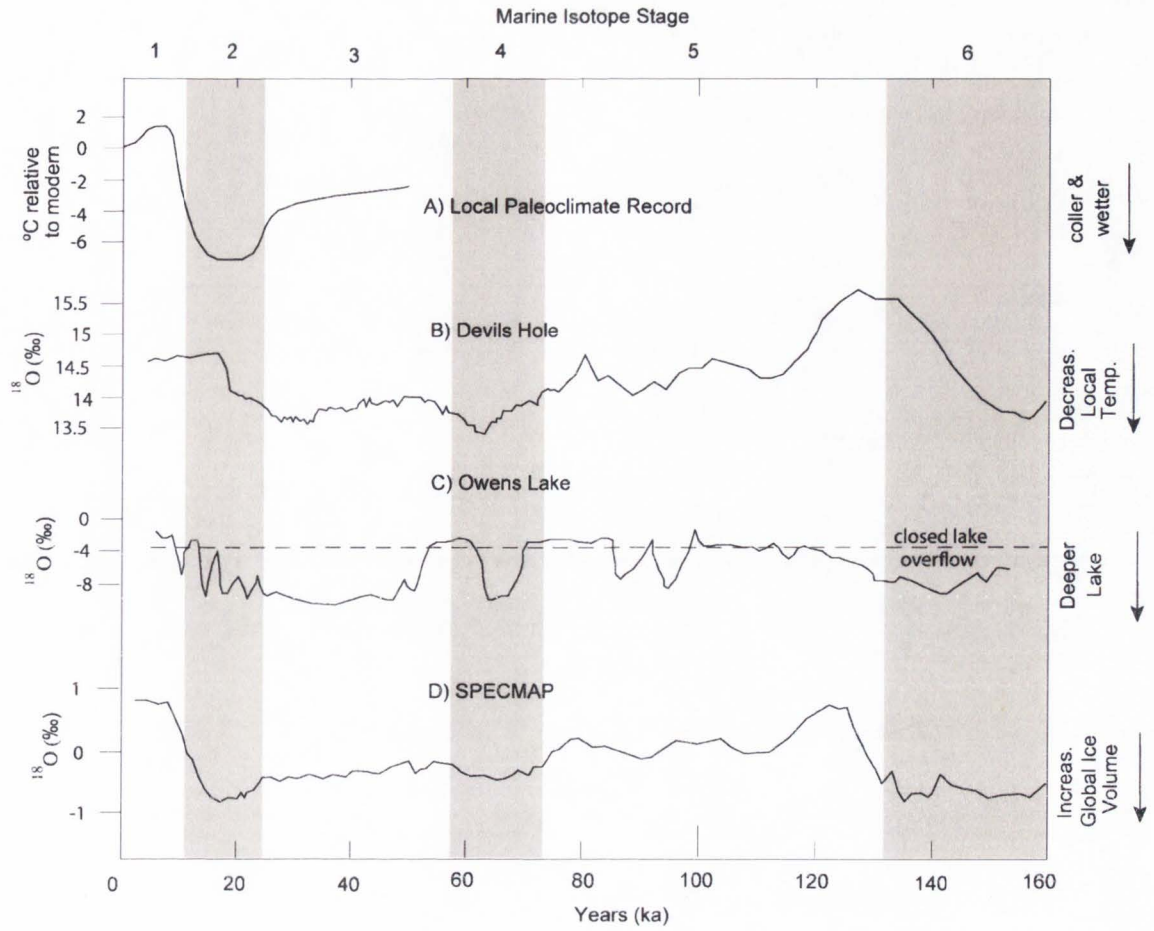

Figure 1.2 Paleoclimate records in and around eastern Grand Canyon (EGC). A) local paleoclimate record (Cole 1982, 1990a, 1990b; Coats, 1997; Weng and Jackson, 1999); B) the Devils Hole paleoclimate record (modified from Winograd et al., 1992, 2006); C) Owens Lake paleoclimate record (modified from Smith et al., 1997); D) SPECMAP paleoclimate record (modified from Winograd et al., 1992). Vertical shaded regions indicate major periods of global glaciation (MIS 2, 4, and 6).

constraints on depositional sequences and the timing of subsequent incision. By mapping the entire extent of tributary drainages and developing an initial chronology for them, Anders et al. (2005) were able to explore relations between hillslopes, tributary drainages, and the mainstem Colorado River through time. Ages obtained from the best-preserved last 80 ky of this record indicate an apparent out-of-phase relation between deposition by the Colorado River (M3) from 71 to 64 ka, and local catchments (S3), from 50 to 34 ka (Fig. 1.2). Incision of the M3 deposit had begun

Figure 1.3. Farthest upstream exposures of S2 and S3 terraces in Comanche. The S3 is stratigraphically connected to colluvium projecting to canyon walls. S2 gravels issued from eroded S3 terraces in the headwaters of Comanche Creek. See Fig. 2.6A for close-up view of S2 exposure in lower right of this photograph.

by 55 ka, which implies mainstem incision occurred at the same time as tributary aggradation. Field evidence indicates that these S3 fill-terraces are stratigraphically connected to thick colluvial mantles that blanket hillslopes and extend out into tributary drainages (Fig. 1.3). In their model, Anders et al. (2005) suggest that enhanced bedrock weathering and decreased precipitation intensity during colder, wetter conditions caused colluviation at hillslope toes and contraction of drainage networks (Fig. 1.4 A). The erosion of these colluvial mantles and then filling of S3 deposits downstream may be a hillslope-down process that occurred during this time, and ages derived for S3 deposits farther downstream were predicted to yield progressively younger ages than those upstream. With the transition to the Holocene came the development of an intense summer monsoon and the reorganization of vegetation communities, according to paleoclimate reconstructions

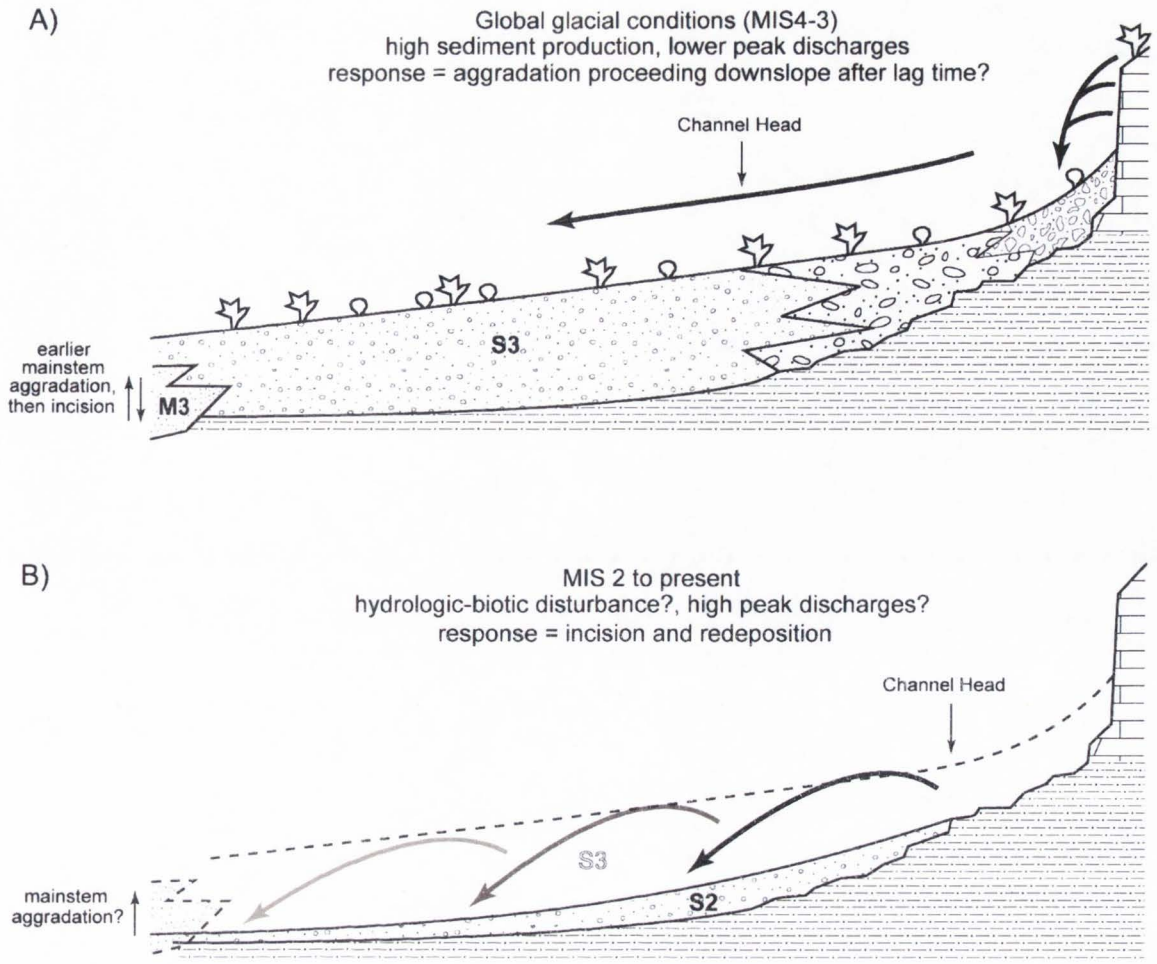

Figure 1.4. The conceptual model for landscape responses to climate change in eastern Grand Canyon tributary catchments proposed by Anders et al. (2005) based on the last ~80 kyr of record. A) Enhanced bedrock weathering and decreased precipitation causes colluviation at hillslope toes, drainage contraction, and eventually delayed tributary stream aggradation. B) Increased precipitation intensity and vegetation disturbance force drainage extention with dissection and redeposition of S3 and colluvial materials (from Anders et al., 2005).

(reviewed below). This caused an increase in stream erosivity, upslope drainage extension, and the dissection of S3 materials. S2 terraces can be traced to the toes of hillslopes and appear to originate from the eroded remnants of these dissected S3 deposits (Figs. 1.3, 1.4 B). In this way, the S2 also is a time-transgressive deposit that resulted from simultaneous upstream erosion and downstream redeposition of S3 materials. This model deviates from models for humid environments (Ritter and

Gardner, 1993; Tucker and Slingerland, 1997) and dry environments (Bull, 1991; Pederson et al., 2000). Models developed for humid regions attribute sediment yield in transport-limited landscapes almost exclusively to hydrologic processes, whereas sediment supply is largely controlled by bedrock weathering in the weathering-limited landscape of eastern Grand Canyon. The models for dryland responses to climate change cannot account for the aggradation of the dominant surficial deposit (S3) during glacial conditions (rather than during the glacial-interglacial transition) or for aggradation throughout the tributary-stream network instead of just proximal hillslope areas. These observations and a limited number of ages indicate relationships between tributary deposits that are significantly different from Bull's (1991) original model. A more robust chronology and a thorough study of the sedimentology and geometry of deposits are needed to understand relations between geomorphic response and climate change.

PALEOCLIMATE RESEARCH IN THE GREATER REGION AND AROUND EASTERN GRAND CANYON

The Owens Lake lacustrine carbonate record in California (Smith et al., 1997) and the Devils Hole terrestrial carbon isotope record in Nevada (Winograd et al., 1992, 2006) provide the highest resolution long-term paleoclimate records available for the American Southwest. The Owens Lake record traces pluvial lake level fluctuations in response to glacial-interglacial climate cycling through time. Lake levels were high (indicating a response to increased effective moisture during glacial climates) from 100-85 ka, 70-60 ka, and from 50-30 ka and fluctuated substantially from 30-13 ka, as the region responded to a gradual shift to interglacial climates (Fig. 1.2). The Devils Hole record includes a continuous time series of Pleistocene climate recorded in vein calcite cored from a cave in southern Nevada. This record

indicates full-glacial conditions at ~155 ka, 62 ka, and 30 ka. In contrast to Owens Lake, the Devils Hole record shows an overall gradual shift to colder glacial conditions during MIS 5 and the latter portion of MIS 3. So, rather than an arid interglacial climate, which is often assumed for the region during MIS 3, climate oscillated frequently to slightly colder and slightly warmer conditions during this overall cooling trend. ^{18}O excursions in the Devil's Hole record are generally in concert with the fluctuations of ice volume recorded in the global SPECMAP record, with the exception of warming episodes (Fig. 1.2). Steady warming started at ~150 ka and at ~30 ka in this part of Nevada, which is at least 10 kyr prior to the onset of the respective global deglaciations. The early warming associated with the Devils Hole record is hypothesized to have its origins in either early tropical and subtropical warming or in interhemispheric warming of sea surface temperatures. The differences between the Owens Lake and Devils Hole records reflect their contrasting settings, as the Owens Lake record indicates lake levels with a source of glacial meltwater and the Devils Hole record is a proxy for temperatures as indicated by desert rainfall.

Longer-term paleoclimate reconstructions have also been produced in the headwaters of the Colorado River drainage, and they show deviances from the patterns seen in the Devils Hole and Owens Lake records. The timing of glacial advances in the Wind River Range have been constrained using TCN dating of moraines and strath terraces (Evenson et al., 1994; Gosse et al., 1995; Chadwick et al., 1997; Phillips et al., 1997; Hancock et al., 1999) and U-series dating of pedogenic carbonate in outwash terraces (Sharp et al., 2003). There is general consensus that the Pinedale glacial peak was slightly before 22 ky and it lasted until 16 ka, which is substantially later than the glacial maximum temperature and effective precipitation recorded in the Devils Hole and Owens Lake records. The

timing of previous glacial periods in the Wind Rivers has been debated. Chadwick and others (1997) determined a peak in glaciation to have occurred between 46 and 28 ka using a linear-incision model, while Sharp and others (2003) used U-series dating of pedogenic carbonate to show a peak at 55 ka. These glacial peaks are generally in phase with the Owens Lake paleoclimate record. TCN results of three different research groups suggest another peak in glaciation between 125 and 100 ka in the Wind River Mountains (Evenson et al., 1994; Phillips et al., 1997; Hancock et al., 1999). Repka and others (1997) used TCN to date fill terraces along the Fremont River in southern Utah using depth-profile sampling to correct for inheritance and amalgamated sampling methods. Their results show fill terraces aggraded 60, 102, and 151 ka.

A shorter-term paleoclimate record has been synthesized for the headwater areas of the Colorado River in the San Juan Mountains and the Front Range of the Rocky Mountains. Alpine glaciers began to advance approximately 30 ka (Nelson et al., 1979; Madole, 1986), reached their maximum extents around 23 ka (Madole, 1986), retreated substantially in some areas by 15 ka (Maher, 1972; Madole, 1986), and had largely disappeared from cirques by 10.5 ka (Benedict, 1973; Madole, 1986; Elias et al., 1991). Floral and faunal macrofossils and pollen indicate MAT about the same as the present with MAP slightly lower than the present by approximately 9 ka. Between 9 ka and 5 ka, MAT was similar to present, but MAP was slightly higher due to persistent winter precipitation combined with the development of the summer monsoon. The most arid period of the Holocene was around 4 ka, when temperatures were ~1° warmer and MAP was less than present. Temperatures and precipitation regimes shifted to relatively cooler and wetter conditions and have been roughly similar to the present since 4 ka (Benedict, 1973; Andrews et al., 1975; Peterson and Mehringer, 1976; Nelson et al., 1979; Carrara et al., 1984; Elias et al.,

1991, Epstein et al., 1991). This Holocene record produced for the Colorado River headwaters is in general agreement with paleoclimate proxies from eolian and alluvial deposits in the Canyonlands area near the confluence of the Green and Colorado rivers (Reheis et al., 2005).

Finally, paleoclimate reconstructions based largely on pollen and macrofossil assemblages have been produced for the area in and around eastern Grand Canyon (Cole, 1990a, 1990b; Weng and Jackson, 1999). From 50 to 25 ka, a gentler winter precipitation regime dominated and the MAT was ~2.3 to 4.3°C colder than today (Fig 1.4), allowing an elevational lowering of some plant species on the order of 460-900 m (Wright et al., 1973; Anderson, 1993; Coats, 1997). The MAT was ~6.7°C lower and the MAP was 87 mm (13%) higher during full-glacial conditions 25 to 15 ka according to pollen, floral macrofossils, and isotopes in herbivore teeth (Wright et al., 1973; Mead and Phillips, 1981; Martin, 1984; Phillips, 1984; Cole, 1990a, 1990b; Anderson, 1993; Coats, 1997; Connin et al., 1998; Anderson et al, 2000). By the time glacial conditions were waning and transitioning into the Holocene around 15 ka to 9 ka, there was a major vegetation reorganization indicating a switch to warmer, dryer conditions (Cole, 1990a, 1990b; Weng and Jackson, 1999). From 9 to 7 ka, MAT was comparable to the present and MAP greater than the present due to a high flux of winter precipitation combined with the onset of a strong summer monsoon (Cole, 1982, 1990a, 1990b; Weng and Jackson, 1999). The Holocene experienced its most arid period between 7 and 4 ka, with MAT approximately 1°C warmer and MAP slightly less than the present. Since 4 ka, climate shifted to relatively cooler and wetter conditions similar to those of modern times (Cole, 1990a, 1990b; Davis and Shafer, 1992; Weng and Jackson, 1999). This climate-induced shifting of vegetation zones (and density) must have influenced rates of chemical and physical

weathering as well as infiltration, and thus sediment supply feeding the record studied here in the Lava Chuar and Comanche catchments.

OPTICALLY STIMULATED LUMINESCENCE GEOCHRONOLOGY

Optically stimulated luminescence is used to estimate the time elapsed since buried sediment grains were last exposed to sunlight. Upon burial, grains of quartz or feldspar are exposed to ionizing radiation produced by the decay of naturally occurring radionuclides (U, Th, and K) and, to a lesser extent at depth, cosmic rays (Aitken, 1998). Exposure to this radiation produces free electrons that are trapped in crystal lattice-defects in quartz and feldspar grains. The resulting charge trapped in these defects, or traps, is stable over long time periods and continues to grow until the grains are exposed to light, or "bleached". The amount of trapped charge acts as a stopwatch that starts upon burial and is stopped when the sediment is re-exposed to sunlight. The cumulative dose collected, or the equivalent dose, can be measured by exposing the unbleached sediments to light (optically stimulated luminescence) or heat (thermoluminescence). This exposure forces recombination of electrons and produces light emission (luminescence), the brightness of which reflects the amount of charge trapped in the crystal lattice, which is in turn related to the length of burial time. Dividing this amount by a dose rate calculated using the concentration of radionuclides in the surrounding material yields an age for the material:

$$\text{Age (ky)} = \text{Equivalent dose (Gy)} / \text{Dose rate (Gy/ky)}$$

Optical dating has been successfully employed to develop chronologies for both colluvial and alluvial deposits (e.g. Porat et al., 1996; Yanchou et al., 2002; Hanson et al., 2004; Anders et al., 2005; Rittenour et al., 2005), although difficulties

arise when applying OSL dating to these sedimentary environments. The preferred OSL sample is composed of well-sorted, medium-grained quartz sand that has undergone long transport distances to ensure complete bleaching of the sediment. As such, eolian deposits prove to be the best material for OSL dating. The transport mechanisms associated with hillslope-mantling colluvium and proximal alluvium in Grand Canyon tributaries, however, cannot provide such ideal conditions. Hillslope transport often occurs over short distances during pulses of mass movement, limiting the exposure of sand grains to sunlight. Similarly, alluvium is often transported under turbid water conditions or in debris flows in Grand Canyon tributaries. These conditions have the potential to either completely block light or greatly reduce light intensity and restrict the spectrum of the light reaching the sediment, which ultimately produces partial bleaching of sand grains (Aitken, 1998; Wallinga, 2002; Jain et al., 2004). Partial bleaching may cause age overestimates by the incorporation of sand grains with high residual, or inherited, luminescence signals at deposition. The heterogeneity associated with the study deposits is also problematic in determining accurate dose rates. To maximize uniformity in dose-rates through time, samples should be surrounded by at least 30 cm of homogeneous sediment and should not have undergone significant water-content variations (Aitken, 1998; Forman et al., 2000). Alluvial sands in the study catchments, in contrast, are commonly isolated as sand pockets surrounded by larger clasts that shield the sample. Furthermore, these deposits have had variable water content histories. These inconsistencies reduce the accuracy of dose-rates measured in the lab, which increases the error associated with produced ages. These complications are minimized here by the careful selection of OSL samples, and their effects are included in the errors reported with ages. The OSL dating technique is known to work in these deposits, having already produced 14 dependable ages from surrounding catchments in the Furnace Flats

region of eastern Grand Canyon (Anders et al., 2005). Single-aliquot regenerative dose OSL methods are used in this study to develop more robust chronologies for Pleistocene sedimentation in the Lava Chuar and Comanche catchments.

CHAPTER 2

THE PLEISTOCENE RECORD IN EASTERN GRAND CANYON TRIBUTARIES: METHODS AND RESULTS

INTRODUCTION

This study is organized into three complementary components that are used to quantify down-catchment chronologic and geometric patterns in sedimentation in eastern Grand Canyon tributary deposits. Surveying is used to understand the geometries of deposits; sedimentologic descriptions are used to interpret the processes involved with sediment transport; and OSL dating methods are applied along the length of the Lava Chuar and Comanche drainages to establish a robust chronology of deposition. The approach is to establish a dataset for each of these techniques at the upper, middle, and lower portions of these drainages. The naming convention used to describe terraces is the same as that used by Anders (2003) and consists of a provenance descriptor ("M" = Colorado River/mainstem terrace and "S" = tributary/side stream terrace) followed by a deposit modifier ("1" = youngest, "2" = second youngest, etc.). If an erosional tread is preserved on a terrace deposit or if two deposits are intimately associated in the landscape and difficult to distinguish, a third modifier is added to the end of the descriptor for younger and older landforms ("y" = younger, "o" = older, respectively).

A suite of four fill terraces, S1-S4, has been identified both for the Lava Chuar and Comanche drainages. All of these deposits are commonly thicker than the dimension of a single channel, have somewhat planar, but often scrolling, basal straths, and may have more than one preserved tread. Deposits have been interpreted as episodes of stream aggradation followed by subsequent incision as a direct response to glacial-interglacial climate cycling (Machette and Rosholt, 1989;

Lucchitta et al., 1995; Anders et al., 2005), but further investigation of these deposits reveals that the responses to climate are not simple.

METHODS AND RESULTS

Surveying Methods

Heights of Quaternary deposits above the modern streambed were measured using two methods that provide higher resolution than is available from large-scale topographic maps. First, five cross sections of drainages were surveyed using a geodetic total station at strategic locations where S2-S3-S4 deposit suites are well-exposed and their field relations clearly distinguishable. Second, heights of terrace treads were measured off of the present stream bottom using an Abney level and a laser range finder at locations between total station surveys. To derive heights, simple trigonometry was applied to the straight-line distance between the target and the observer (measured with a laser-rangefinder) and the angle between the observer and the target (measured using an Abney level). The survey data were used to produce both longitudinal profiles of deposit treads with respect to the modern valley long-profile and cross-sections of drainages at total station survey locations. Long profiles were produced by plotting terrace heights up from valley long profiles that were produced for both drainages using digital raster graphic (DRG) versions of USGS 1:24,000 topographic maps for reference. Cross sections from the total station surveys provide documentation of the relative position of treads and straths (where available) of deposits and allow comparison of the deposit geometries at specific points along drainages.

Terrace long-profiles help quantify the degree of concavity of terrace treads and the overall downstream divergence or convergence of deposit treads with the

modern stream channel. These characteristics can have implications to climatic and hydrologic factors such as precipitation intensity or peak stream discharge at the time of deposition (Zaprowski et al., 2005). Terrace long-profile concavity was quantified for the S2 and S3 terrace treads as well as the modern stream in both the Lava Chuar and Comanche catchments by calculating their Stream Concavity Index (SCI) on the basis of a methodology described by Demoulin (1998). A line A-B is drawn from the highest to the lowest elevation on a plot of normalized relief vs. normalized distance from the divide, forming a triangle with an area of 0.5 (Fig. 2.1). The area between the line A-B and the terrace profile is then calculated. In this study, the area was measured digitally using the freeware program "ImageJ"

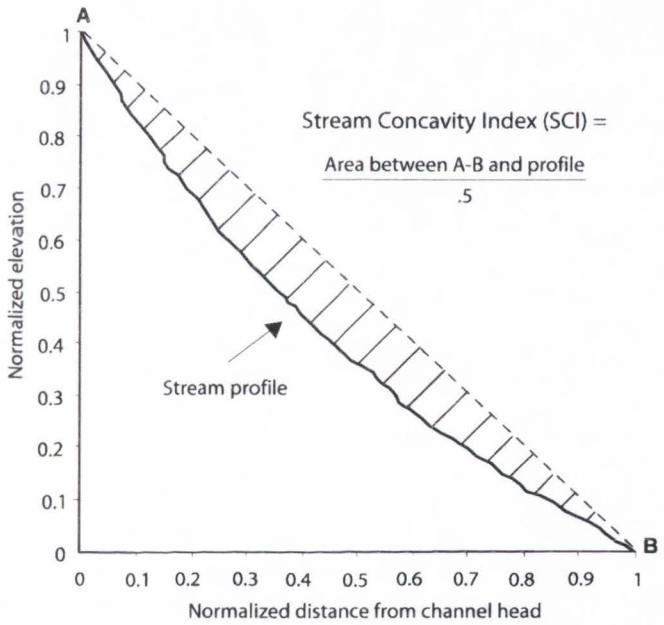

Figure 2.1. The stream concavity index (SCI) used for the terraces and modern streambeds in the Lava Chuar and Comanche catchments (modified from Zaprowski et al., 2005).

(Abramoff et al., 2004), and then divided by 0.5 to generate the SCI for that particular terrace deposit. Larger SCI values indicate greater concavity. Although it would be ideal to calculate and plot the SCI values for both treads and straths, only treads are presented here because straths are more irregular and often below grade.

For SCI values to hold importance, one must ensure that it is calculated for the entire length of streams from channel head to mouth. This is easily done for the modern streams and for the S2 in Comanche, but identifying paleo-channel heads for S2 in Lava Chuar and S3 in both catchments proves difficult. Data are lacking for the height of the S2 and the S3 along their entire length beyond the uppermost survey (LC_1U, Appendix A.1). Thus, even if a paleo-channel head were identified upstream, there is no way to trace the height of the terrace to the first data point. Because of this limitation, the heights of the S2 and S3 terraces collected at the uppermost survey is used to calculate the concavity for the rest of the stream. Because this location is below the actual paleo-channel head, the reported SCI values should be viewed as a minimum. As reviewed in Chapter 1, the S3 deposit in Comanche is thicker in the headwaters where it transitions to hillslope deposits. Because its sediment is derived chiefly from hillslope processes at the upper study locality, these outcrops are interpreted as upstream from the S3 channel head. The first well-exposed fluvial S3 deposit is almost a third of the way down-catchment, and probably substantially below the paleo-channel head. The S3 channel head is therefore projected to be just below a constriction in the channel associated with the outcropping of the underlying Cardenas Formation. Results showing geometrical characteristics of the S2 and S3 deposits therefore represent only the lower 2/3 of the Lava Chuar drainage and the entire Comanche Creek drainage.

Survey Results

Survey results were incorporated into a GIS database that previously included nine existing surveys in Lava Chuar collected by Anders (2003). Five new cross sections of the tributary terraces were produced along the Comanche drainage and two new cross sections were produced in the upper reaches of the Lava Chuar drainage (Appendix A). Heights of terrace treads above modern washes vary along the lengths of drainages, which is illustrated in the long-profile and cross-sectional diagrams of the drainages (Figs. 2.2, 2.3, 2.4).

The S3 fill terrace in the headwaters of the short, steep Comanche catchment is ~80 m above the modern streambed where it is stratigraphically linked to large colluvial remnants (Fig. 1.3). Exposure is sparse below this for the middle 1/3 of the catchment, where it converges to a height of 20 m at the next clear exposure. The S3 generally retains this height along the rest of the drainage. The S2 fill terrace in Comanche heads at the toe of the colluvial portion of the S3 deposit and locally inflates from 0 to almost 13 m above the modern streambed ~600 m downstream due to the bedrock constriction in the channel (Fig. 2.2). Below this constriction, the S2 maintains a fairly consistent height (~7m) above the modern wash down to near the mouth of the drainage, where its height increases to 10 m and then converges to the modern channel.

Survey results in Lava Chuar indicate that the S3o tread converges from a height of 53 m above the modern streambed ~50% down-catchment to 43 m above the modern streambed ~1800 m downstream and remains between 43 m and 49 m above the wash throughout the rest of the drainage (Fig. 2.2). Based on trends in other catchments and aerial photo mapping (Anders, 2003), the S2 converges upstream with the modern channel. Its tread is 23 m above the modern wash at the

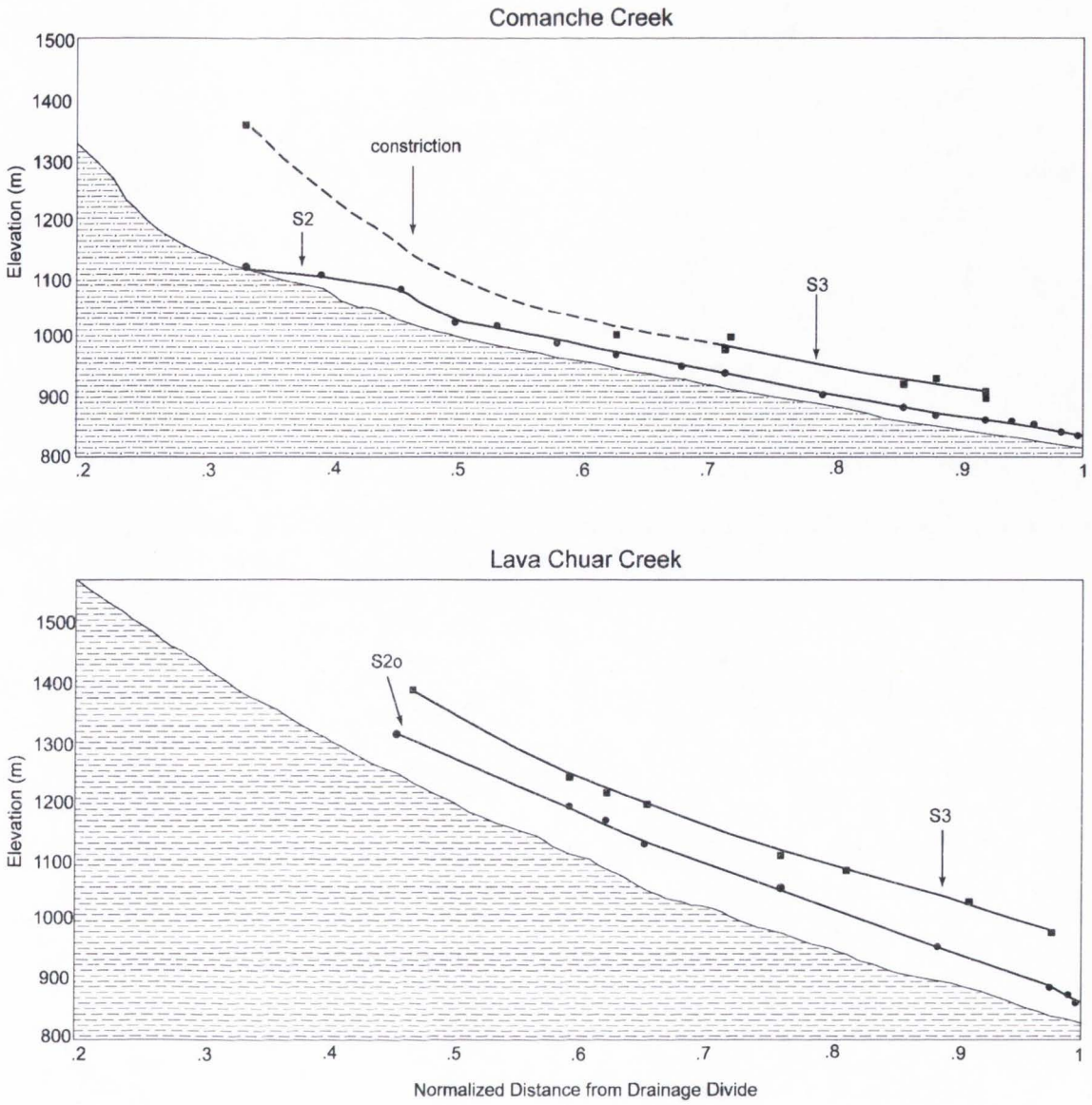

Figure 2.2. Terrace long-profiles plotted up from valley long-profiles. Squares (S3)and circles (S2) represent locations where terrace height was measured with survey equipment. Terrace heights are exaggerated 3x above valley bottoms to help distinguish them, which visually skews profile morphology. Also, normalizing distances from drainage divides makes the relatively long Lava Chuar drainage look deceptively steeper than the shorter Comanche drainage. Schematic cross-sections of catchments can be seen in Figs. 2.3 and 2.4.

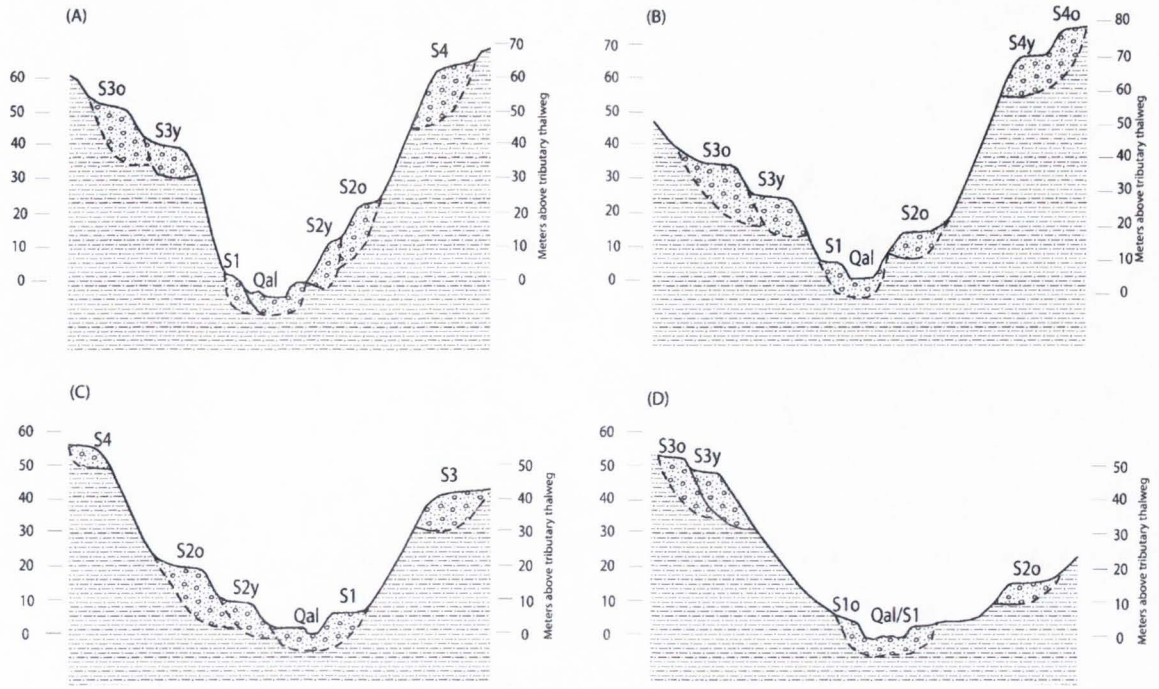

Figure 2.3. Schematic cross sections of Lava Chuar organized from upstream to downstream at its A) upper trunk, B) lower trunk, C) upper mouth and D) at mouth. Raw survey data and transects can be found in Appendix A, and locations can be found in Appendix D.

uppermost survey locality, and it gradually diverges to its greatest height of 27 m above the wash in the middle of the catchment. It finally converges back down to its lowest height of 11 m above the modern wash just upstream from the mouth of the drainage.

SCI values were calculated for the S2 and S3 deposits as well as for the modern stream in both the Lava Chuar and Comanche catchments (Table 2.1). Stream concavity appears to increase through time for the Comanche and Lava Chuar drainages, with the S3 terraces having the lowest SCI values, the S2 terraces having intermediate SCI values, and the modern streambeds having the greatest SCI values. The concavity of the modern wash measured to the uppermost survey (a false channel head) in Lava Chuar is an exception to this generalization, as it is less concave than the S2 measured over the same length of the river and approximately

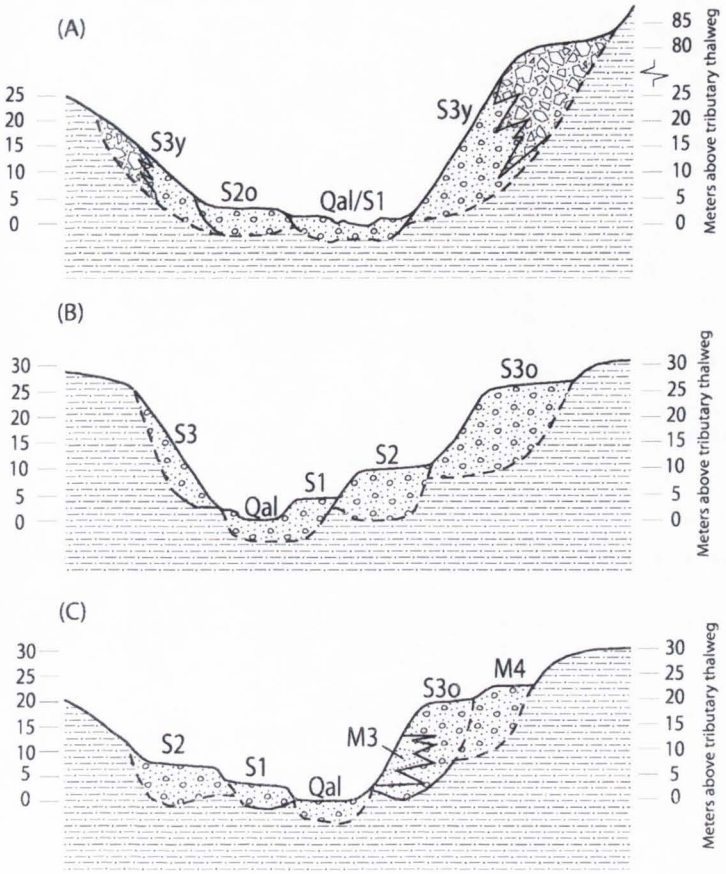

Figure 2.4. Schematic cross sections of Comanche Creek at its A) headwaters, B) trunk and C) mouth. Note the change in scale in the headwaters to accomodate the locally inflated S3. Raw survey data and transects can be found in Appendix A.

TABLE 2.1 STREAM CONCAVITY INDEX (SCI) VALUES FOR TERRACE TREADS

Surface	Lava Chuar	Comanche
S3	0.08[1]	0.07
S2	0.1[1]	0.12
Modern drainage to channel head	0.19	0.24
Modern drainage to uppermost survey	0.08	--

[1]The heights of S2 and S3 treads at the uppermost survey were used as channel heads in Lava Chuar

the same as the S3. The shorter, steeper Comanche drainage is generally more concave and records greater changes in concavity through time than Lava Chuar. All of these profiles are relatively straight (low SCI values), and the differences between them are on the order of a few percent.

Methods of Sedimentology

Key S2 and S3 exposures were photographed and described to document sedimentary facies and architecture at localities in the upstream and middle portions of drainages as well as at the mouths. The data collection began with detailed field descriptions that include information such as thicknesses of outcrops and individual beds, the topography of straths, bedding, sedimentary structures, and texture, which were used to distinguish dominant facies in deposits. Photo panels of S2 and S3 exposures at the three areas of interest in each drainage were analyzed for facies distributions and proportions by digitizing polygons over the photos and attributing them according to the representative facies (Fig. 2.5). Finally, the area of each individual polygon was calculated using ImageJ software to determine the relative proportions of facies within each photograph. The combined sedimentologic descriptions and facies proportions determined from sedimentary panels were used to interpret longitudinal trends in transport and deposition processes.

Results for Sedimentology

Tributary fill deposits are generally composed of unconsolidated, immature gravel that may be clast or matrix-supported. Nine facies were distinguished based on whether they were clast or matrix-supported and on the size of clasts (Table 2.2).

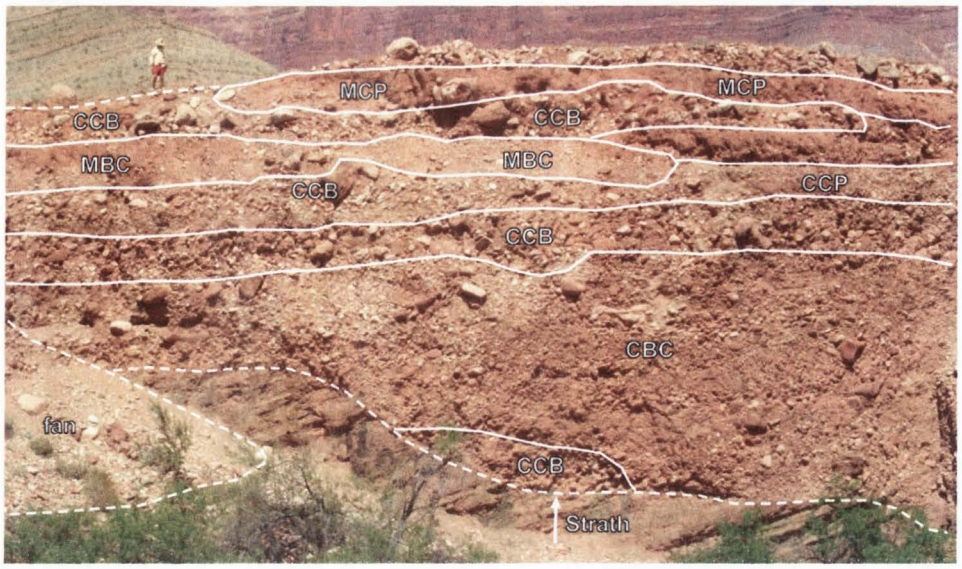

Figure 2.5. Example of the facies distribution in the S3o in the trunk of Lava Chuar with researcher for scale. Relative areas of polygons were measured using ImageJ software. Complete facies panels are found in Appendix B.

The matrix-supported material exhibits qualities similar to classic debris flow diamictons, whereas the clast-supported facies are interpreted to be alluvium deposited by tractive flow (Fig. 2.6 B) and in places represents fluvially-reworked debris flows (Fig. 2.6A). This interpretation stems from the observation that clast-supported facies in Pleistocene fills closely match modern facies found in the active wash. The modern facies are themselves commonly derived from sediment first brought to the channel in debris flows or are deposited by flood flows that may have been initiated as debris flows (Webb et al., 1996; Griffiths et al., 2004) (Fig. 2.7). The relative abundance of each facies within exposures is presented in Table 2.3.

Results indicate that terrace deposits are less mature and more closely resemble debris flow deposits in upper catchments and become finer-grained and

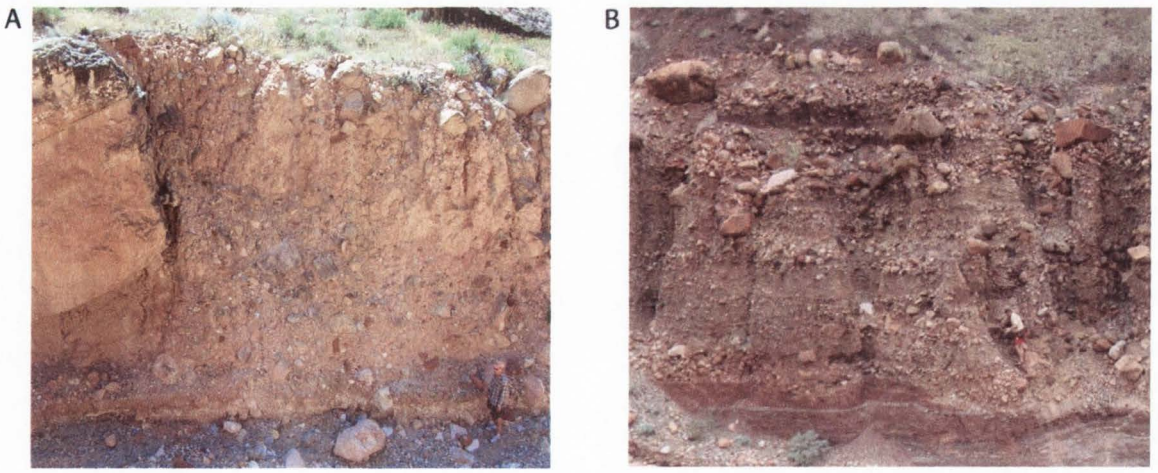

Figure 2.6. Photographs illustrating the contrast between A) a headward/upper exposure of a matrix-supported S2 diamicton, and B) a typical clast-supported S3 gravel in the lower trunk of Comanche. Researchers for scale.

TABLE 2.2. COMMON FACIES SEEN IN EASTERN GRAND CANYON PLEISTOCENE DEPOSITS

Facies	Facies name	Generalized facies descriptions
CP	Clast-supported pebble gravel	Moderately sorted, clast-supported gravel with angular-subangular granule-to-cobble sized clasts (avg. 2 cm) and a fine sand/silt matrix. Often interbedded with numerous sand lenses
CCP	Clast-supported cobble pebble gravel	Moderately sorted, clast-supported gravel with subangular-subrounded granule-to-cobble sized clasts (avg. 4 cm) and a fine sand/silt matrix. Often interbedded with numerous sand lenses
CPC	Clast-supported pebble cobble gravel	Moderately sorted, clast-supported gravel with angular-subrounded granule-to-boulder sized clasts (avg. 6 cm) and a fine sand/silt matrix. Often interbedded with numerous sand lenses
CBC	Clast-supported boulder cobble gravel	Poorly sorted, clast-supported gravel with subangular-subrounded granule-to-boulder sized clasts (avg. 15 cm) and a fine-very fine sand/silt matrix
CCB	Clast-supported cobble boulder gravel	Poorly sorted, clast-supported gravel with subangular-subrounded pebble-to-cobble sized clasts (avg. 35 cm) and a fine-very fine sand/silt matrix
MCP	Matrix-supported cobble pebble gravel	Unsorted, matrix-supported gravel with angular-subrounded granule-to-cobble sized clasts (avg. 6 cm) and a fine-very fine sand/silt matrix
MBC	Matrix-supported boulder cobble gravel	Unsorted, matrix-supported gravel with subangular-subrounded granule-to-boulder sized clasts (avg. 7 cm) and a fine-very fine sand/silt matrix
MCB	Matrix-supported cobble boulder gravel	Unsorted, matrix-supported gravel with angular-subrounded granule-to-boulder sized clasts (avg. 30 cm) and a fine-very fine sand/silt matrix

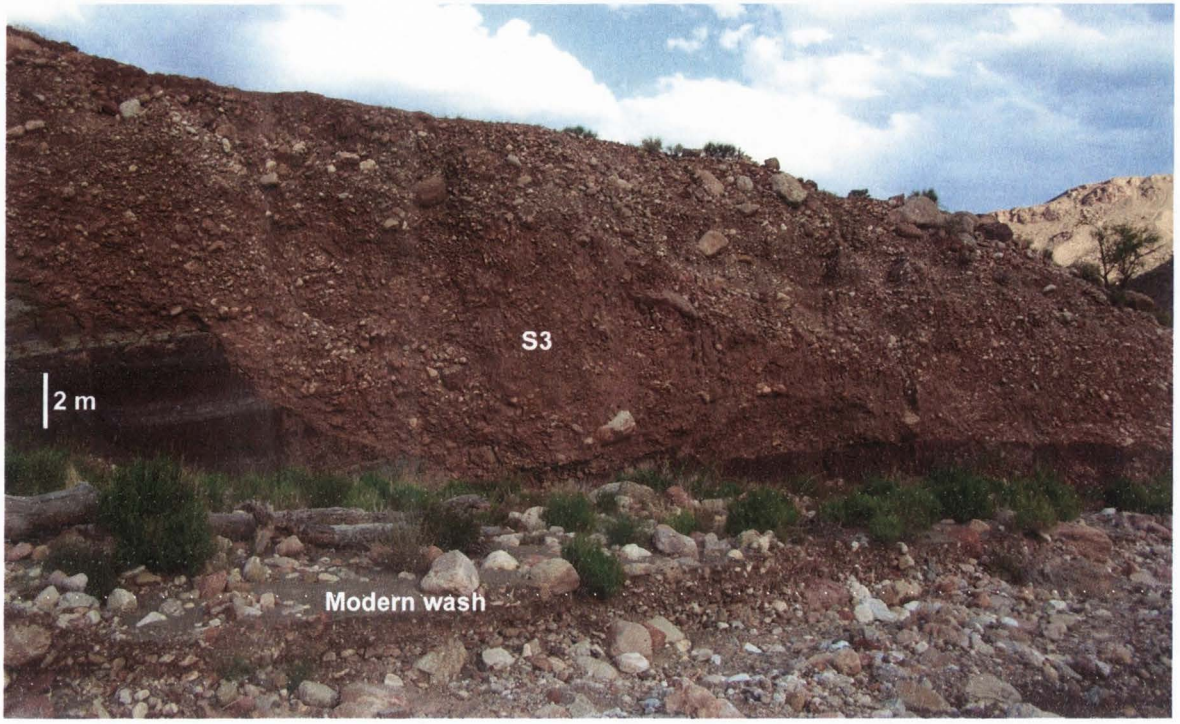

Figure 2.7. Photograph taken in the trunk of Lava Chuar showing similar facies in the modern wash and in the S3 deposit. Note small sand lenses among larger clasts in the modern, and out-sized clasts in both the modern and the S3.

more clast-supported (stream-reworked) down-catchment, as expected. For example, ~65% of the S2 and ~90% of the S3 in the headward outcrops of Comanche Creek are matrix supported (Table 2.3). Evidence for local debris flow sedimentation decreases quickly downstream, and only ~3-4% of the exposed S2 and S3 deposits near the mouth of Comanche are matrix-supported (e.g. Fig. 2.6). In general, deposits in the shorter, steeper Comanche catchment are less mature than the longer, broader Lava Chuar catchment. In Lava Chuar, the upstream exposures of S2 and S3 are almost entirely clast-supported, but they are located ~1/3 the length of the drainage downstream from the channel head. Yet, ~20% of

TABLE 2.3. FACIES PROPORTIONS IN S2 and S3 FILL DEPOSITS (BY PERCENT)[1]

Deposit	SL[2]	CP[2]	CCP[2]	CPC[2]	CBC[2]	CCB[2]	MCP[2]	MBC[2]	MCB[2]	Total Clast-Supp.	Total Matrix-Supp.
Lava Chuar											
upper S2o	--	--	16	49	--	35	--	--	--	100	--
middle S2o	--	--	30	50	--	12	8	--	--	92	8
mouth S2o	--	--	70	19	11	--	--	--	--	100	--
upper S3o	--	--	85	10	--	5	--	--	--	100	--
middle S3o	--	--	61	--	19	--	20	--	--	80	20
mouth S3o	--	3	40	31	24	--	--	--	2	98	2
Comanche											
upper S2	1	--	12	--	13	10	37	--	27	36	64
middle S2	2	--	24	--	36	38	--	--	--	100	--
mouth S2	3	--	49	32	--	12	4	--	--	96	4
upper S3	--	--	--	2	--	7	--	91	--	9	91
middle S3	--	--	51	24	--	25	--	--	--	100	--
mouth S3	--	5	60	17	2	13	--	3	--	97	3

[1]See Table 2.2 for facies definitions and descriptions, and Appendix B for facies panels of study outcrops

[2]Columns organized from fine to coarse and increasingly immature from left to right

the S3o deposit in the middle of Lava Chuar is matrix-supported, which can perhaps be attributed to local debris flow inputs.

Methods of OSL Geochronology

Identifying temporal trends in Quaternary sedimentation in the Lava Chuar and Comanche catchments hinges on the success of OSL geochronology. The sampling strategy used here focuses on the basal and upper strata of S2 and S3 deposits along the lengths of tributary drainages in an attempt to systematically constrain the timing and duration of deposition. Hypothetically, if deposits yield progressively younger ages down-catchment, sedimentation was gradually prograding from hillslope sediment sources, which is potentially consistent with increasing local sediment supply. Alternatively, if sedimentation was controlled by baselevel at drainage mouths along the Colorado River, both erosion and

sedimentation may follow a pattern of getting younger up-catchment, at least for a short distance from mouths. The first step in the OSL dating process is locating appropriate sand lenses for sampling. Lenses are not available everywhere in the basal and upper strata in the coarse-grained Pleistocene deposits. Analogous to modern stream deposits, sand lenses are rare and relatively small (Fig. 2.6). Moreover, many sand lenses were rejected because of evidence for mixing by bioturbation, which contaminates the sand and degrades its quality for OSL dating. These factors greatly limit the number of target sand lenses, and so samples were obtained wherever small, lenticular sand lenses were found in the study outcrops. Thus the oldest and youngest ages reported for deposits here do not represent the actual temporal limits of aggradation; rather they indicate the earliest and latest burial dates from those sand lenses available for OSL dating.

Dose-rate samples were collected in plastic bags and water-content samples were collected in air-tight film containers from within 30 cm of the OSL sample location. Because lenses are typically located in the lee of out-sized clasts, and only the sand fraction is analyzed for radioactive elements, dose-rates are unable to represent the radioactive contribution of larger clasts. Dose-rate samples were sent to Chemex Laboratories for elemental analysis and OSL samples were processed and run at the Luminescence Geochronology Laboratory at University of Nebraska-Lincoln. The 90-150 μm sand fraction was isolated by means of wet sieving (with the exception of 2 samples, isolated to 90-125 μm), heavy minerals were extracted via density separation using sodium polytungstate, and carbonates and feldspars were removed through a series of hydrochloric and hydrofluoric acid baths. The remaining quartz fraction was mounted on 2-mm diameter regions on disks for OSL analysis

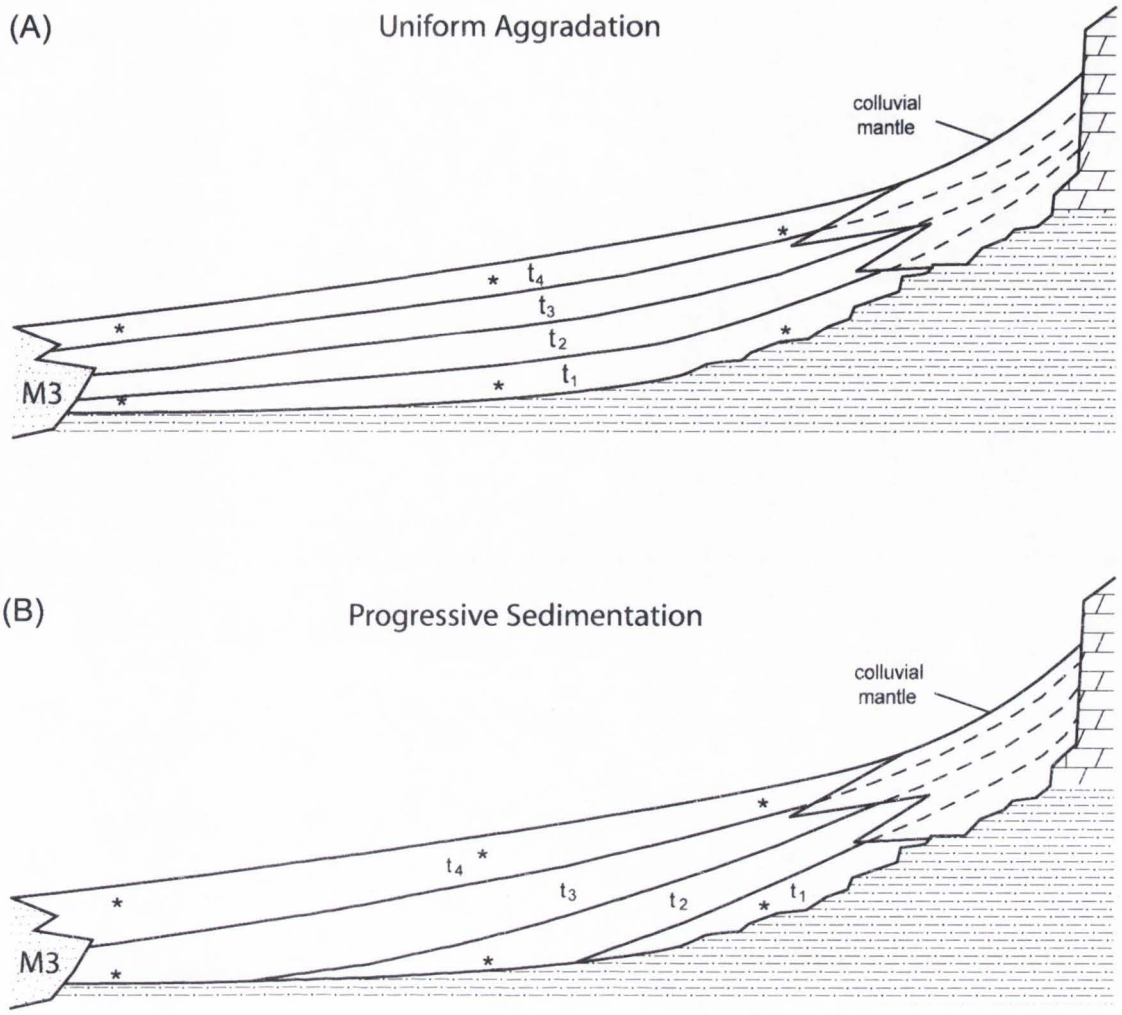

Figure 2.8. Conceptual model showing two possible styles of aggradation for the S3 deposit: (A) Uniform vertical aggradation throughout the length of the drainage; (B) Progressive sedimentation, with the time-transgressive transport of sediments down drainages from hillslopes. Episodes of time separated by solid lines; age decreasing with increasing number. Note the patterns of OSL ages that could result from the two scenarios.

performed on a RISO TL/OSL-DA-15B/C reader with blue-green light stimulation (470nm), which provided the equivalent dose used for final age calculations.

Analytical procedures used in optical dating vary extensively, and choosing the appropriate procedure depends upon the nature of the sediment. OSL dating of sand-sized quartz using the single-aliquot regenerative-dose (SAR) protocol

described by Murray and Wintle (2000) has been shown to be the best available method for luminescence dating of fluvial deposits (e.g. Wallinga, 2002). The SAR procedure used here is an 8-step measurement cycle, as shown in Table 2.4. The test dose applications aid in correcting for sensitivity changes that can result from a changing luminescence efficiency, or OSL per evicted electron (Murray and Roberts, 1998). Repeated cycling of irradiation and stimulation to single aliquots changes this efficiency, which ultimately produces scatter in the data. Applying a fixed test dose to the sample after each cycle records these changes, and dividing the regenerated curve by that of the test dose corrects the data for sensitivity change. The De is then estimated by interpolating the natural response onto a best-fit line plotted for the regenerative doses (Fig. 2.9).

TABLE 2.4. GENERALIZED SINGLE-ALIQUOT REGENERATIVE SEQUENCE

Step	Treatment	Description/reasoning
1	Give Dose (Di)	Apply the dose[1, 2]
2	Preheat to 250°C for 10 s	Heat the sample in order to empty thermal traps that could contribute to the OSL signal
3	Stimulate for 40 s at 125°C	Measure the regenerative OSL signal using blue LED's
4	Give test dose (Di)	Apply a test dose to the sample for the purpose of correcting for sensitivity change
5	Preheat to160°C for 0 sec	Heat the sample to empty thermal traps that could contribute to the OSL signal when measuring the test dose
6	Stimulate for 40 s at 125°C	Measure the test dose OSL signal
7	280°C bleach	Heat and stimulate the sample to remove any residual signals before starting the next cycle
8	Return to step 1	

[1] For the natural, i = 0 and Do = a zero dose (0 Gy)

[2] Steps 1-8 are repeated for 5 regenerative doses:

D_1 regenerative dose less than the expected equivalent dose

D_2 is regenerative dose approximately equal to the expected equivalent dose

D_3 regenerative dose greater than the expected equivalent dose

D_4 is a zero dose (similar to the natural dose) applied to check for recuperation (the residual signal observed in a SAR cycle when no regenerative dose is applied)

D_5 repeats D_1 check the recycling ratio (this shows how effectively the test doses are correcting for sensitivity change)

As previously mentioned, optical dating of deposits in hillslope and stream settings can be challenging due to their short and turbid transport histories which may lead to incomplete exposure of sand grains to sunlight, or "partial bleaching" of quartz grains. To minimize the effects of partial bleaching, small aliquots (approximately 100 grains of sand) were analyzed in this research, as it has been shown that the lowest measured dose in small (i.e. 60-100 grains) single aliquots is likely to most closely approximate the true burial dose (Olley et al., 1999). Data from aliquots with deviant behavior or that appear to be partially-bleached are discarded. The primary criteria for accepting aliquots is that they must have a recycling ratio between 0.9 and 1.1, they must produce an equivalent dose between D_1 and D_3, and the signals plots should not show large variation in OSL response.

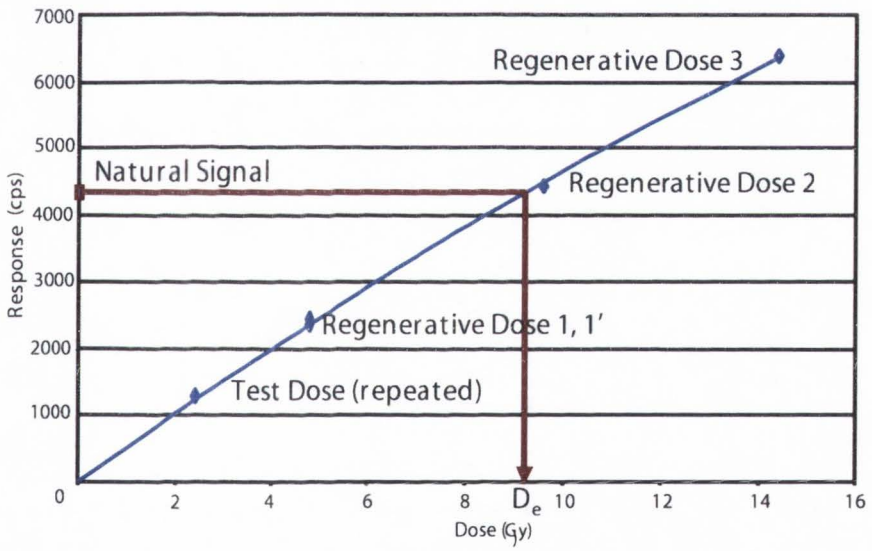

Figure 2.9 Schematic single-aliquot regenerative-dose growth curve of dose vs. OSL response in counts per second. The De is estimated by interpolating the natural signal onto the best-fit line plotted through the regenerative doses.

Results for OSL Geochronology

16 new ages are reported here for deposits in the Lava Chuar and Comanche catchments (Table 2.5). Dates are preliminary and range from having 4 to 20 acceptable disks associated with them, whereas final ages will eventually have a minimum of 20 accepted disks. Errors reported with ages are at 1-sigma and include systematic and random errors. Uncertainties will decrease with additional accepted disks, as ages are finalized. While most of the new ages build upon and agree with the previous chronology of Anders et al. (2005), several are significantly older or younger than expected based on previous mapping efforts and help to refine the stratigraphy. All pertinent OSL data can be found in Appendix C, and sample locations can be viewed in Appendix D.

Results of geochronology reveal a surprisingly complex stratigraphy. The basal portion of the S2 in Lava Chuar appears to have the same age from the upper portions of the catchment (14 ± 3 ka) to the trunk of the catchment (12 ± 3 ka; Anders et al., 2005), and finally to the upper-mouth of the catchment (11 ± 3 ka) within error (Fig. 2.10). Anders (2003) recognized both S3o and S3y terraces in Lava Chuar but could not be certain whether they were on the same fill or whether they were two distinct fills, and new OSL data reveals that they are indeed distinct in age. The S3y aggraded from 46 ± 8 – 34 ± 5 ka based on a sample collected near the mouth of the catchment in this study and a sample from the upper-middle part of a deposit in the middle of the catchment by Anders et al. (2005), respectively (Fig. 2.10). The S3o aggraded from 63 ± 11 to 55 ± 14 ka based samples collected in the mouth and middle of the catchment, which are consistent both with a cosmogenic surface age produced for the S3o (54 ka) in the middle of the catchment (Anders, 2003) as well as with S3o ages produced 1.5 km downstream in the Comanche

catchment (see below). A sample collected from the base of an S4 deposit in the upper portions of Lava Chuar yields an age of 100 ± 18 ka. Finally, a preliminary S4 age of 90 ± 16 ka is being produced for a sample collected near the base of a deposit slightly downstream from the 100 ± 18 ka sample with a tread that projects to S3 deposits downstream. Both ages are in agreement with the terrace tread TCN ages (92 ± 19 ka) produced for the S4 by Anders (2003), and the ~92 ka age suggests that the S3o in Lava Chuar may transition from an erosional landform in the upper catchment to a depositional landform downstream.

TABLE 2.5. OPTICAL AGES FROM EASTERN GRAND CANYON[a,b]

Deposit/ Location[c]	Sample number	UNL Lab Number	dose rate (Gy/ka)	De (Gy)	Disks	Optical age ± total error (ka)
Tributary terrace fills						
S2 - Lava Chuar	GC-09-11-6	UNL-171	3.64 ± 0.21	25.54 ± 5.49	NA	7 ± 2
S2 - Lava Chuar	GC-09-11-7	UNL-292	2.42 ± 0.13	28.19 ± 7.46	NA	12 ± 3
S2 - Lava Chuar	**GC-06-65.5-03**	**UNL - 1443**	**3.28 ± .14**	**37.27 ± 12.66**	**8**	**11± 3**
S2 - Lava Chuar	**GC-05-65.5-03**	**UNL-1137**	**3.26 ± .14**	**46.56 ± 11.22**	**13**	**14± 3**
S2 – Comanche	**GC-06-67-16**	**UNL-1438**	**1.31 ± .06**	**28.4 ± 8.66**	**4**	**22± 7**
S2 – Comanche	**GC-06-67-17**	**UNL-1440**	**2.34 ± .1**	**60.59 ± 12.83**	**7**	**26± 6**
S2[d] – Comanche	**GC-05-67-12**	**UNL-1136**	**1.31 ± .06**	**83.45 ± 20.45**	**7**	**64± 7**
S3 - Lava Chuar	GC-09-03-16	UNL-394	3.11 ± 0.18	105.77 ± 14.9	NA	34± 5
S3 – Lava Chuar	**GC-05-65-17**	**UNL-1171**	**2.82 ± .13**	**131.56 ± 21.03**	**15**	**46 ± 8**
S3 - Lava Chuar	**GC-05-65-18**	**UNL-1164**	**3.68 ± 0.17**	**229.81 ± 39.12**	**14**	**61 ± 11**
S3 - Lava Chuar	**GC-05-65-15**	**UNL-1178**	**3.63 ± 0.16**	**209.01 ± 57.64**	**10**	**55± 14**
S3[e] – Lava Chuar	**GC-06-65-01**	**UNL-1442**	**1.42 ± .07**	**128.37 ± 21.26**	**4**	**90 ± 16**
S3 – Comanche	**GC-05-67-14**	**UNL-1165**	**3.31 ± .15**	**206.26 ± 32.44**	**14**	**62± 10**
S3 – Comanche	**GC-04-67-01**	**UNL-1322**	**3.64 ± .16**	**209.94 ± 49.72**	**13**	**58 ± 5**
S3[f] – Comanche	**GC-05-67-09**	**UNL-1174**	**1.57 ± .07**	**60.23 ± 13.83**	**18**	**35± 9**
S3 – Comanche	**GC-04-67-03**	**UNL-1170**	**2.88 ± .13**	**222.62 ± 24.72**	**13**	**77 ± 9**
S4 - Lava Chuar	**GC-05-65.5-06**	**UNL-1130**	**2.5 ± .11**	**251.28 ± 43.03**	**13**	**100 ± 18**
Colorado River fills at the mouth of Comanche						
M3 - RM 67L	GC-09-04-19	UNL-398	2.90 ± 0.17	185.08 ± 27.24	NA	64 ± 10
M3 - RM 67L	GC-09-04-18	UNL-397	2.41 ± 0.15	164.34 ± 26.95	NA	68 ± 11
M4 – RM 67L	**GC-04-67-04**	**UNL-1167**	**2.61 ± .1**	**232.95± 46.94**	**13**	**89 ± 18**

[a] See appendix C for complete OSL geochronology data

[b] Bold samples are preliminary dates associated with this study, and others are from Anders et al. (2005).

[c] Organized by fill terrace, from upstream to downstream in catchments

[d] Interpreted as an erosional (strath) terrace on S3 materials upstream grading to a fill terrace of S2 ages downstream.

[e] Interpreted as an erosional (strath) terrace on S4 materials upstream grading to a fill terrace of S3 ages downstream.

[f] Collected from the base of reworked colluvium near the head of the Comanche catchment

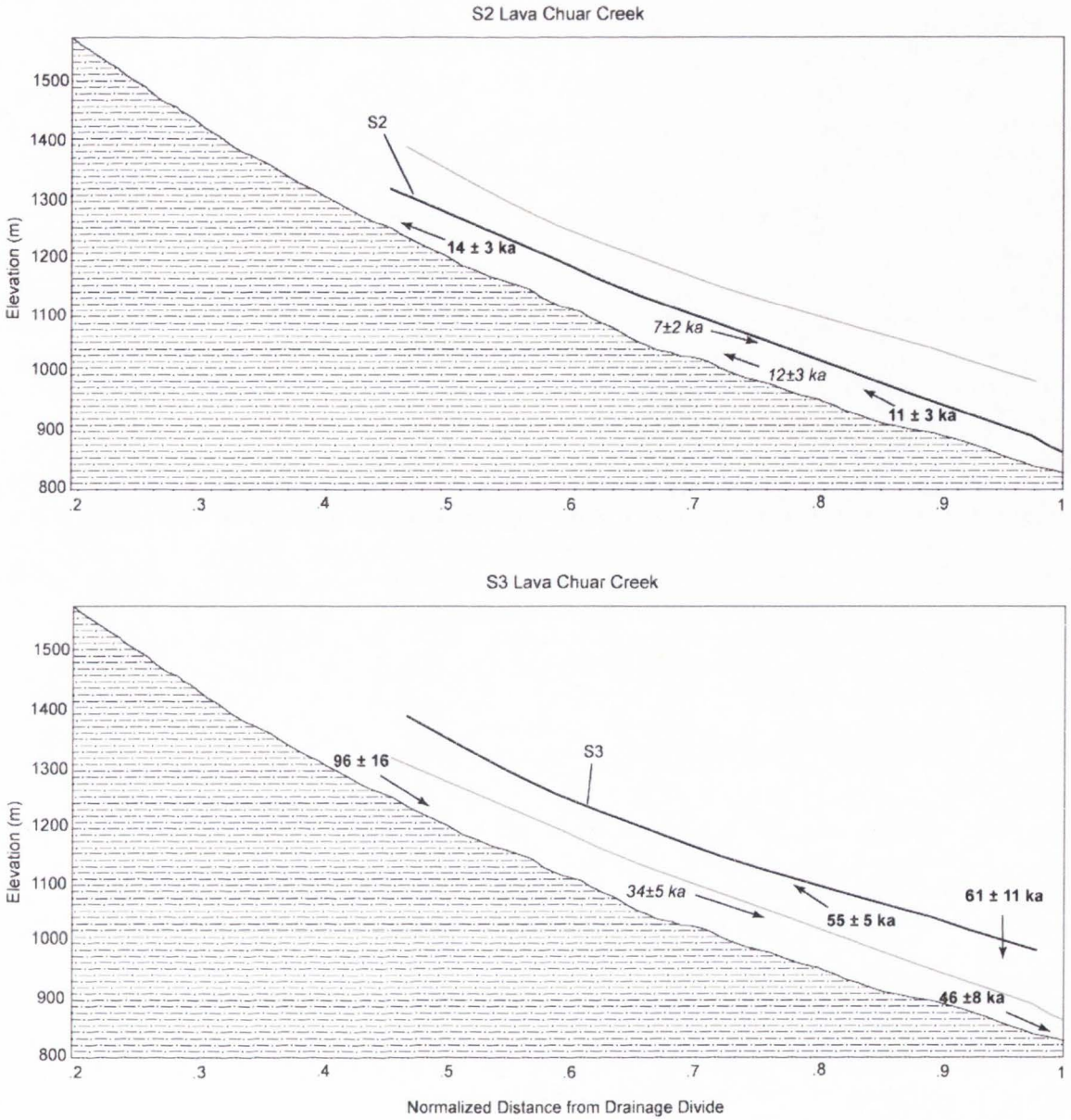

Figure 2.10 Figure illustrating the ages calculated for S2 and S3 plotted in their respective locations within terrace fills in the Lava Chuar catchment. Bold ages are preliminary ages, this study. Italicized ages are from Anders et al. (2005). The S3 ~0.5 of the distance from the divide produces S4 ages and is interpreted to be a strath terrace on an S4 fill, locally.

Preliminary ages for S2 deposits in Comanche are generally older than those in Lava Chuar. A sample taken from a 1.5 m thick deposit near what was the drainage head during S2 times yields an age of 24 ± 5 ka (Fig. 2.11). This appears to be a slackwater deposit that is positioned upstream of a debris flow "dam" issuing from a major tributary junction, and so the dated deposit is interpreted to be the result of a different process than others. But because the debris flow material is the same age as the S2 terraces that it juxtaposes, the backwater deposit should be expected to produce an S2 age as well. A preliminary age was also produced for the base of a deposit in the trunk of the Comanche catchment with a tread that clearly grades to S2 terraces both upstream and downstream. This sample has produced an unexpectedly old preliminary S3o age of 64 ± 7 ka, a relationship that is addressed in Chapter 3. A S2 sample near the mouth of Comanche has a preliminary age of 22 ± 7 ka.

Just as in Lava Chuar, S3 ages in Comanche are potentially revealing distinct older and younger deposits. The large ~80 m thick S3 headwater deposit composed of scarcely reworked colluvium is producing an age of 35 ± 9 ka approximately 20 m from the base of the deposit (Fig. 2.11). Samples from the lower portions of an S3 exposed in the trunk of Comanche produced preliminary S3 ages of 55 ± 14 and 63 ± 13 ka. Finally, two surprising preliminary ages from samples collected from the middle and top of the complicated outcrop at the mouth of Comanche (Fig. 3.1). The sample from the middle of the outcrop produced an old preliminary age of 77 ± 9 ka, apparently slightly older than mainstem M3 samples collected by Anders et al. (2005) just downstream and only slightly stratigraphically lower in the deposit. A higher sample collected 3 m below the terrace tread here appears to be a sample of mainstem sand based on petrologic evidence and has another surprisingly old

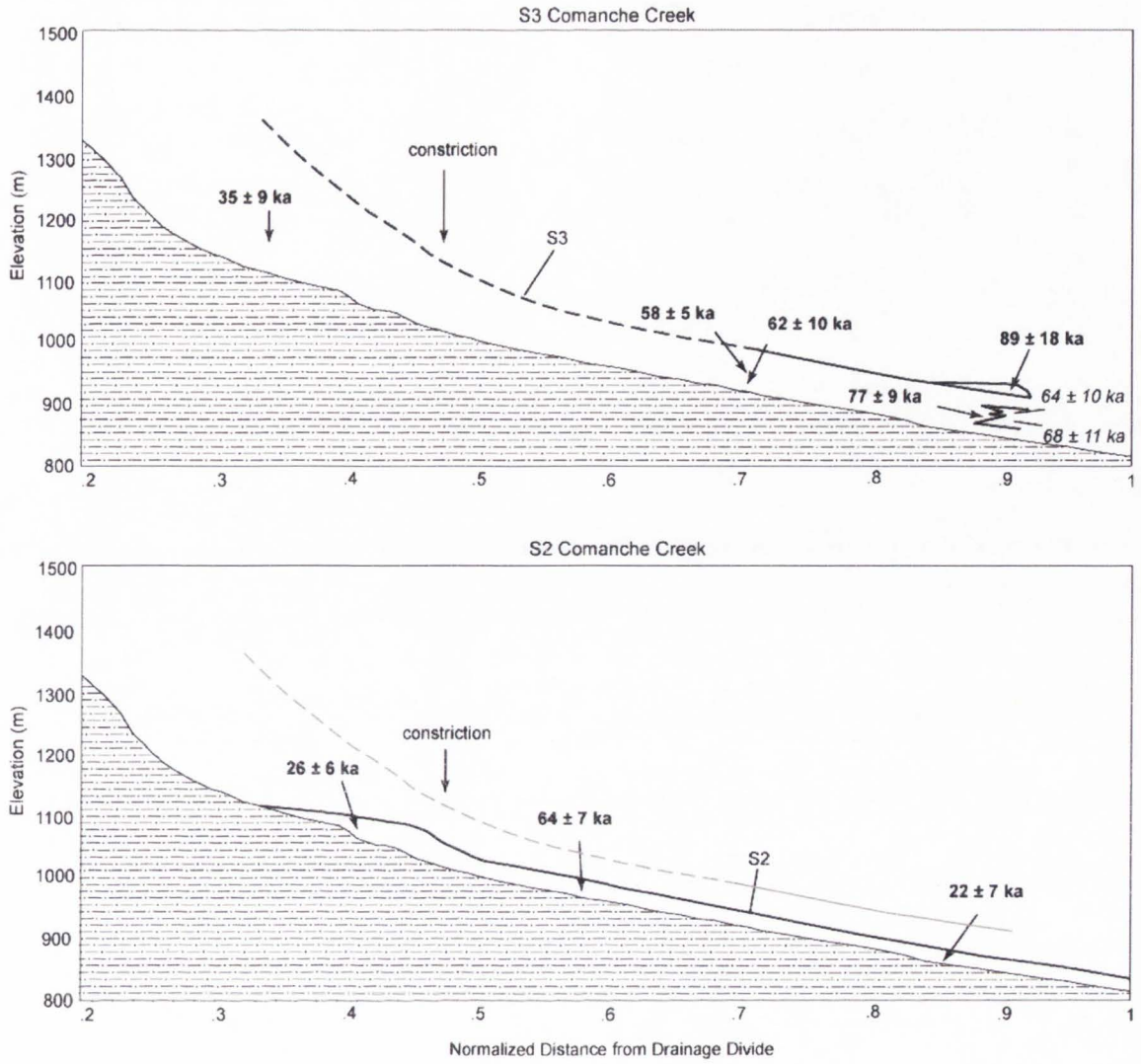

Figure 2.11 Figure illustrating the ages calculated for S2 and S3 plotted in their respective locations within terrace fills in the Comanche catchment. Bold ages are preliminary ages, this study. Italicized ages are from Anders et al. (2005). The S2 in the trunk of the catchment produces S3 ages and is interpreted to be a strath terrace on an S3o fill, locally.

preliminary age of 89±18 ka. These two samples reveal new relationships at the mouth of Comanche to be discussed in Chapter 3.

CHAPTER 3

DISCUSSION AND CONCLUSIONS

DISCUSSION

Revised stratigraphy in eastern Grand Canyon tributaries

The greatest revisions to the eastern Grand Canyon Quaternary stratigraphy are related to the unexpectedly older ages being produced for certain deposits that were previously mapped as S2 and S3. Anders (2003) correlated terraces based on stratigraphic relations observed through the process of mapping. Unconformities and inset relations between terrace deposits are extremely difficult to discern without robust chronology due to the similarity of deposits, and so deposits were conservatively lumped rather than split in this previous study. New results show this had the greatest effect on the S3 and S4 in Lava Chuar and the S2 and S3 in Comanche.

The deposit from which the sample GC-06-65-01 was collected in the upper reaches of Lava Chuar had initially been mapped as an older terrace on the S3 deposit based on the projection of its tread to those of other S3 (~70-35 ka) exposures downstream (Table 2.5). However, geochronology indicates the deposit underlying this terrace formed during S4 time (~90 ka). Similarly, GC-05-67-12 was collected from a deposit in the trunk of Comanche that was previously mapped as an S2-age fill based on the clear correlation of the terrace landform with S2 exposures downstream (Table 2.5). Likewise, the geochronology reveals that the underlying deposit formed during S3 time (~64 ka). These newly recognized erosional terraces

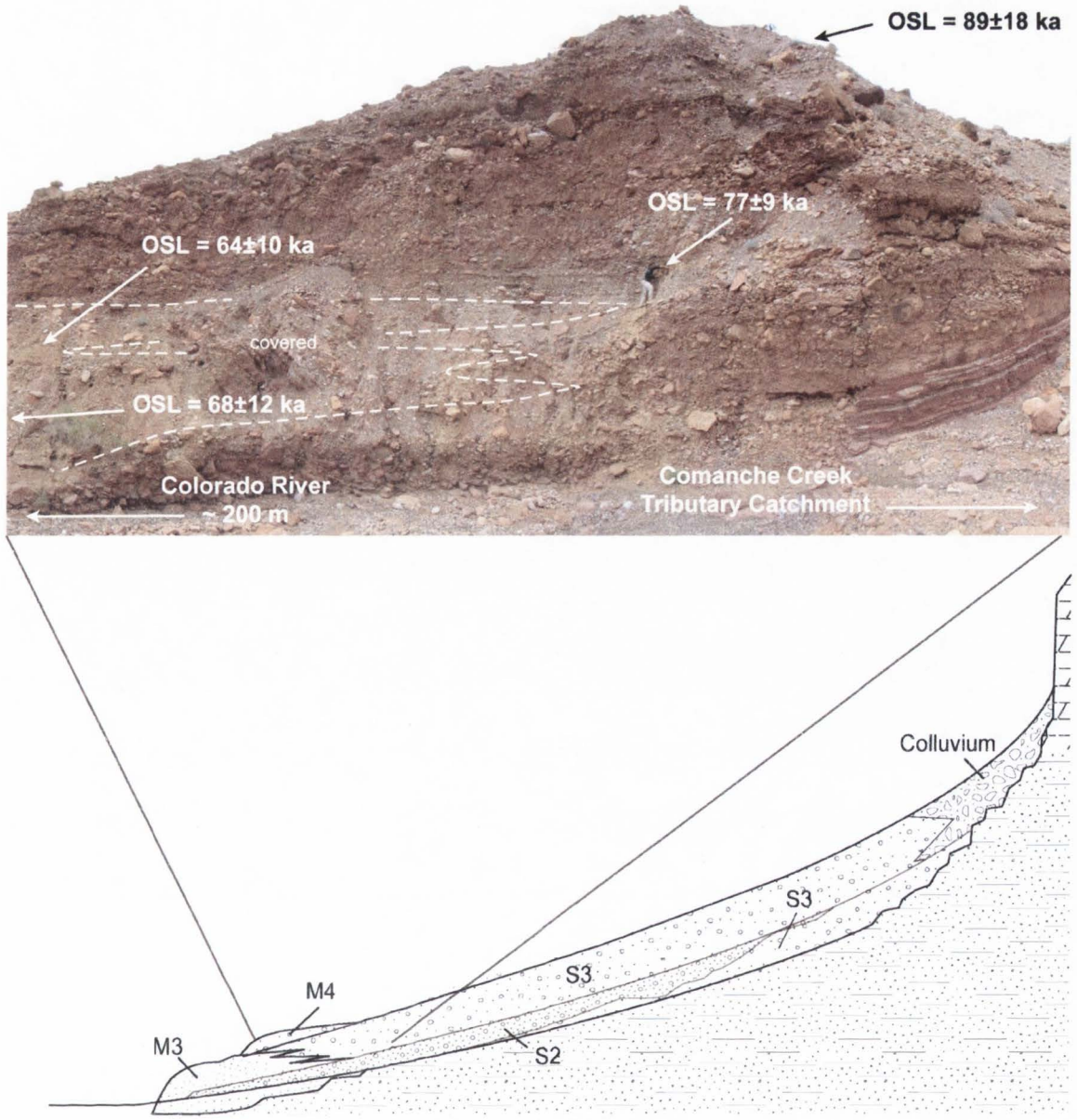

Figure 3.1. Photograph of stratigraphic relations at the mouth of Comanche and diagram of long profile stratigraphic relations, with modern wash running from right to left. Mainstem sands from the upper M3 deposit interfinger with tributary sediment in the lower 5.5 m of this outcrop as the tributary maintained grade during Colorado River aggradation. S3 materials are inset into an M4 deposit deeper into the deposit. The S2 terrace is erosional near the headwaters; a strath terrace on S3 gravels. Note researcher for scale (modified from Anders and others, 2005).

in upper reaches suggest that the S3o terrace in Lava Chuar and the S2 terrace in Comanche transition from erosional to depositional landforms down-catchment (Fig. 3.1). Streams were potentially eroding older deposits upstream (the S4 in Lava Chuar and the S3 in Comanche), while concurrently redepositing sediment farther downstream (S3 in Lava Chuar and S2 in Comanche). This is consistent with the idea that S2 aggradation represents coeval erosion and redeposition of S3y sediments suggested by Anders et al. (2005), and it is possible that the S3o-S4 couplet may be an analog to this scenario in Lava Chuar. This is also consistent with Schumm's (1973) idea of complex response wherein a single perturbation may lead to sequential incision and aggradation along a valley network through feedbacks between hillslope and channel processes (e.g. Schumm, 1973; Patton and Boison, 1986). It is also consistent with the results of related numerical models that suggest a non-linear response of drainage basins to driving forces (Tucker and Slingerland, 1997).

As previously mentioned, the deposit at the mouth of Comanche yields a confusing chrostratigraphy that must also be addressed (Fig. 3.1). Anders et al. (2005) report ages of 68 ±12 ka and 64 ± 10 ka for samples of mainstem sand that interfinger with tributary sediments from the base and middle of this outcrop, respectively. One new OSL sample was collected from tributary materials slightly upstream and stratigraphically above the contact of interfingering mainstem sands. This sample yields a preliminary age of ~77± 9 ka, which is surprisingly older than the adjacent mainstem sands. Revisiting the field site confirmed that the S3 and M3 really are interfingering here and that there is not an inset relation. This sample makes it clear that reported errors must be taken seriously, and this age is interpreted to be same as those produced by Anders et al. (2005), within error. The

interfingering of tributary and mainstem gravels at the mouth of Comanche indicates that tributaries were affected by, and responding to, high baselevel along the mainstem during this time. However, this appears to have only affected tributaries at their mouths, as S3 ages upstream in Comanche are somewhat younger. The OSL sample of mainstem sand collected from 3 m below the top of the exposure has a preliminary age of ~89 ka. In this case, field inspection indicates it is possible to interpret this as a sliver of preserved M4 with S3 gravels inset into it (Fig. 3.1).

Stream concavity

Because there are no active tectonics within the Comanche and Lava Chuar catchments, the long profiles of their terrace treads reflect stream adjustment to hydrologic and sedimentologic conditions. Long profiles are therefore logical subjects for studying the effects of climate. Channel shape has been studied in detail as far back as 1877, when Gilbert explored controls on profile gradient on drainages in the Henry Mountains. Since then, it has been established that there is a balance between erosion and deposition in graded rivers, and that terraces represent moments of equilibrium in streams (Davis, 1902; Yatsu, 1955; Leopold et al., 1964; Leopold, 1994; Pazzaglia et al., 1998). The cumulative erosion and deposition of sediment on alluvial streambeds ultimately controls long profile shape in tectonically quiescent settings. Streams that are in equilibrium, or even quasi-equilibrium, have concave profiles with gradients that are adjusted to provide sufficient transport of sediment load such that there is neither aggradation nor incision (Mackin, 1948). Leopold (1994) uses the concept of entropy (energy loss through the system) as a tool for understanding channel concavity, as entropy forces a compromise between the incompatible goals of expending minimum total work (very concave profile) and

the uniform distribution of work (straighter profile). The dissipation of this work in alluvial rivers depends primarily on the downstream increases in water discharge and channel width and the downstream decrease in bed-material size (Leopold et al., 1964; Sinha and Parker, 1996). With grain size, sediment yield, and hydrology acting as primary controls on long profile morphology, a person could potentially extract climate information from long profile changes through time as recorded in terraces.

The fact that Pleistocene deposits in the Lava Chuar and Comanche catchments show a notably lower concavity than the modern valley bottom provides insight into the climate regime at the time of deposition. Zaprowski and others (2005) explore the relationship between incision, concavity, and climate by focusing on four climatic variables: mean annual precipitation, mean precipitation intensity, mean annual discharge, and peak annual discharge. They test these variables on forty watersheds along a SE-NW trending climate gradient in the eastern High Plains using the same SCI methodology described in Chapter 2. Their results indicate all four climate variables showing a significant positive correlation to concavity, with a change to more concave profiles resulting from a shift toward stormier, more intense rainfall and greater peak discharges. Considering this, the sequential increase in profile concavity from S3 time to the modern calculated for the Lava Chuar and Comanche catchments is consistent with paleoclimate records from the region (Cole 1982, 1990a, 1990b; Weng and Jackson, 1999). During S3 deposition, a gentler winter precipitation regime dominated and was therefore conducive to a relatively straight profile. The climate transition after S3 times included the development of summer monsoons, which increased precipitation intensity and peak discharges and may have provided the hydraulic mechanism for post S3y incision prior to S2

aggradation. S2 aggradation is in accordance with sediment transport in the region during the glacial-interglacial transition (Bull, 1991; Anders et al., 2005). During the more recent past, these streams have experienced intense monsoon storms combined with a high flux of winter precipitation, resulting in the greatest relative concavity.

Timing and cause of tributary aggradation

Preliminary OSL ages produced for S4 deposits in Lava Chuar represent the first direct age control for these deposits in eastern Grand Canyon. Geochronology suggests that S4 aggradation began well before 100 ka and continued until after 90 ka (Fig. 3.2). The timing of this aggradation occurs ~25 ky after the penultimate interglacial during MIS 5e (130-120 ka). The Devils Hole and SPECMAP records indicate significant cooling from 125 to 110 ka, with the Owens Lake record indicating two significant highstands between 100 and 90 ka. Aggradation of the S4 therefore appears to have taken place under cooling conditions, with storage and transportation of sediment produced during this colder, wetter climate.

There were two identified pulses of S3 deposition in eastern Grand Canyon tributaries. The first pulse of aggradation, the S3o, began as far back as 65 ka and lasted until approximately 55 ka (Fig. 3.2). Paleoclimate records from Devils Hole and Owens Lake indicate that this coincides with the end of the glacial maximum and the transition to warmer temperatures during MIS 4. The S3o may therefore be an older analog to the S2, with deposition coinciding with and following dissection of older terrace material during a period of warming and greater precipitation intensity. The second pulse of sedimentation, the S3y, began at ~50 ka and lasted until at least 35 ka. Global ice records, the regional Devils Hole and Owens Lake records,

and local paleoclimate records all indicate an extended period of cooling during this time, but S3y deposition does not coincide with the Last Glacial Maximum (~20 ky). Likewise, these climate correlations suggest that the S3y may be an analog to the older S4 fill, with deposition correlating to greater sediment production during wetter climates.

These two distinct S3 fills are clearly recognizable in the larger, broader Lava Chuar catchment. Preliminary S3o ages have been produced for two samples: one at a depth of 3 m in the middle of the drainage (55 ka) and one from an exposure near the mouth of the drainage at a depth of 10 m (61 ka) (Fig. 2.10). One new preliminary age of 46 ka has been produced for the S3y in Lava Chuar at the base of an eroded remnant ~200 m up from the mouth of the catchment. This correlates well with an OSL age of 34 ka for a sample 7 m deep in the middle of the drainage produced by Anders et al. (2005). Importantly, the distinction of S3o and S3y fill deposits in the well-dated Lava Chuar catchment argue against the time-transgressive style of sedimentation as suggested by Anders et al. (2005) and illustrated in Figure 2.8b. Rather, S3o and S3y deposits appear to have the same age throughout catchments considering the location and depth of dated samples.

The S3o–S3y distinction in Comanche is not as clear. The OSL sample from the S3y deposit at the headwaters of Comanche that is ~20 m up from the modern streambed (60 m below the tread) produced a preliminary age of 35±9 ka (Fig. 2.11). Two samples from an S3 deposit in the trunk that are ~2 m up from the local strath (10 m below the tread) produced preliminary ages of 58±5 and 62±10 ka, which are consistent with an age of 62 ka produced for the base (10 m depth) of the S2/3 deposit ~400 m upstream. The deposit at the headwaters of the drainage is tentatively interpreted as S3y and the downstream deposits as S3o, but more OSL

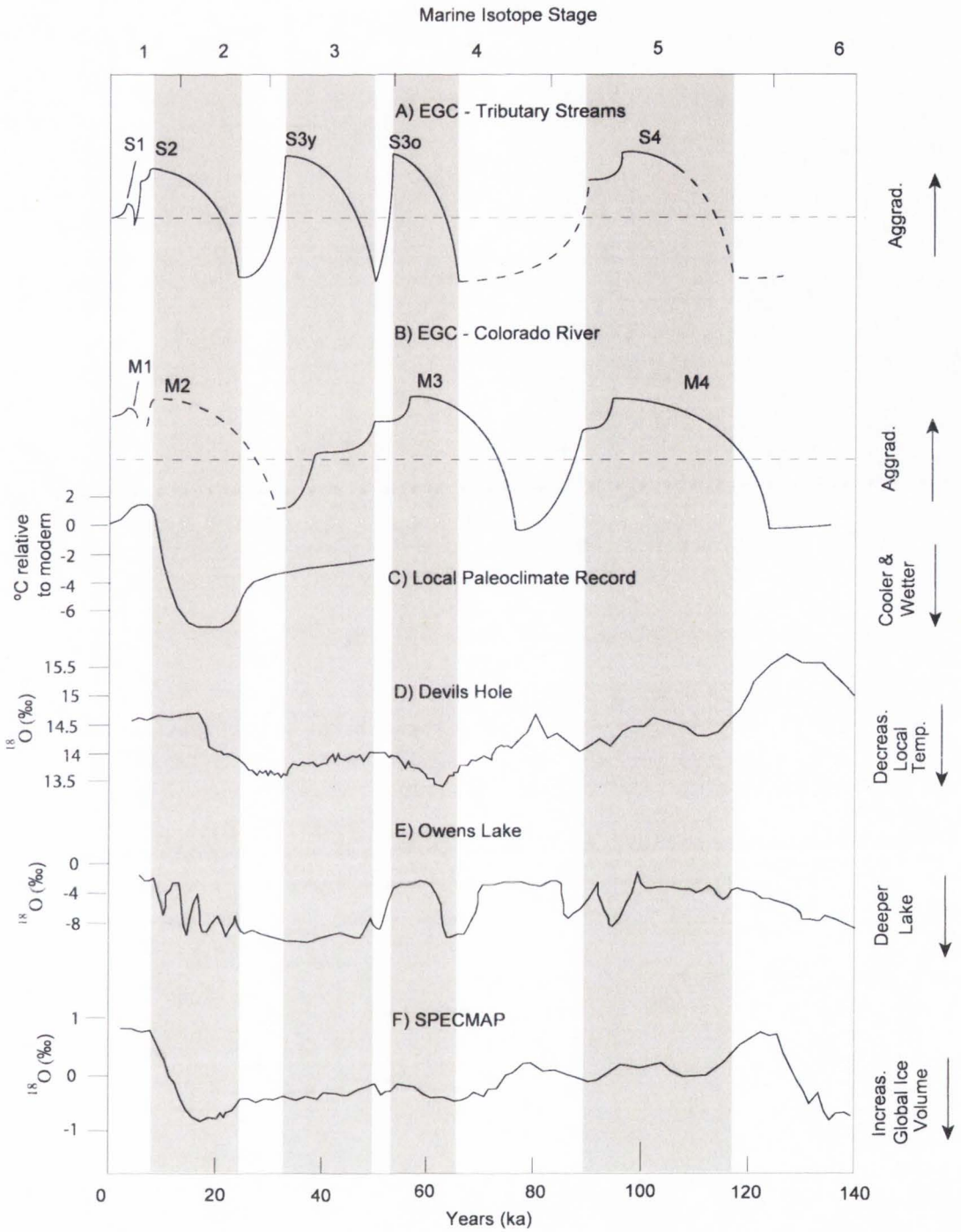

Figure 3.2. Stream activity in eastern Grand Canyon (EGC) compared to the mainstem stratigraphy and to climate records. A) tributary streams of this study; B) Colorado River based on Pederson et al (2006) and unpublished data; C) compilation of local paleoclimate records (Cole 1982, 1990a, 1990b; Coats, 1997; Weng and Jackson, 1999); D) the Devils Hole paleoclimate record (modified from Winograd et al., 1992, 2006); E) Owens Lake paleoclimate record (modified from Smith et al., 1997); F) SPECMAP paleoclimate record (modified from Winograd et al., 1992). Shaded columns represent aggradational episodes in EGC tributaries.

data are needed for Comanche to confirm that they are distinct fills. As previously mentioned, the 77±9 ka S3o deposit at the mouth of Comanche has a distinctly older age than other S3 ages, perhaps in direct response to an elevated local baselevel along the Colorado River at this time.

S2 fill terraces began aggrading ~20 ka in Comanche and continued to aggrade until at least 7 ka in Lava Chuar (Anders et al., 2005). This timing is consistent in with the transition from cold, wet conditions to drier Holocene conditions. Warming was well under way by 20 ka according to the Devils Hole record, and the Owens Lake record indicates extreme variability in climate (Fig. 3.2). Vegetation density declined locally and precipitation intensity increased with the development of intense summer monsoons during this transition (Cole, 1990a, 1990b; Weng and Jackson, 1999). These conditions drove the dissection of S3 fills and drainage extension upslope. New preliminary ages and stratigraphic evidence support Anders and others' (2005) observation that sediment for the S2 terrace was derived from older S3 deposits and colluvial mantles upstream. Despite attempts to date the basal, and thus oldest, sands from outcrops, no S2 ages in Lava Chuar are as old as those produced in Comanche. However, older S2 deposits may exist in the inaccessible portions of this catchment. The ~24 ka sample of S2 was collected from the headwater areas of Comanche, whereas the uppermost S2 OSL sample in Lava Chuar (~14 ka) was collected ~1/3 down the length of the drainage. Nevertheless, ages are largely within error of each other, and just as with the S3, there is no evidence to suggest that S2 deposits are progressively younger down-catchment.

These new data refine the working conceptual model for the landscape response to climate change in semiarid environments developed by Anders et al. (2005). In this model, the Colorado River aggraded during glacial advances and into subsequent climate reversals, whereas tributaries aggraded later in the glacial cycle and again during the glacial-interglacial transition. This apparent delay in tributary stream aggradation was hypothetically attributed to a lag time associated with generating and delivering sediment to tributary systems in this weathering-limited environment. This model is based on limited geochronologic and sedimentologic data, however, and new data indicate overlap in the timing of mainstem and tributary aggradation during both M4/S4 and M3/S3 times. So, although weathering-limited sediment supply and vegetation-assisted sediment storage likely buffered the sedimentary systems in tributaries to some degree, they did not necessarily cause a delay in sedimentation behind the mainstem. Rather, these two systems were responding to distinct sets of hydrologic and biologic conditions in their headwaters as hinted at by Anders et al. (2005). Tributaries simply responded more readily and more often to local changes in climate.

CONCLUSIONS

The hillslope and terrace deposits in the Lava Chuar and Comanche catchments indicate dramatic phases of aggradation and incision due to glacial-interglacial climate cycling. The sedimentary facies preserved in these tributaries closely match those observed in modern drainages and illustrate the prevalence of stream-flow processes that rework sediments transported to streams by debris flows. Because the facies are similar in deposits that represent responses to several climate conditions, it seems transport processes have remained consistent through

time in these tributaries. Stream concavity has not remained constant through time, however, but has increased slightly from S3 to modern time based on values calculated from terrace treads. This increase in stream concavity is consistent with the increase in precipitation intensity recorded in local paleoclimate records due to the enhancement of summer monsoons. Increasing peak discharges associated with this climate trend may provide the hydraulic mechanism for S3y incision and S2 aggradation.

Based on new geochronology and field interpretations, the stratigraphy of eastern Grand Canyon tributaries must be revised to include two distinct S3 fill deposits. Anders et al. (2005) suggested one phase of S3 aggradation from 50-34 ka, but new geochronology and field interpretations indicate another phase of deposition prior to this time. S3o (~65-55 ka) deposition began before the end of colder/wetter conditions during MIS 4 and continued as regional climate transitioned to warmer and drier conditions. The S3o appears to shift from an erosional terrace on the S4 to a fill terrace in the trunk of Lava Chuar, and so sediment for S3o aggradation is partly derived from older (S4) terrace deposits. In this way, the S3o may be an older analog to the S2, which displays the same patterns. In contrast, S3y (~50-30 ka) deposition took place during an extended period of cooling prior to the Last Glacial Maximum and was contemporaneous with colluviation in the headwaters of Comanche. The S3y may be analogous to the older S4 in this relation to climate trends. S2 aggradation appears to be the result of the erosion and redeposition of older (S3) terrace materials, as suggested by Anders et al. (2005). Importantly, this new chronology does not support the time-transgressive style of sedimentation proposed for S3 deposition by Anders et al. (2005). Rather than revealing progressively younger ages down-slope within single deposits due to long,

sustained periods of aggradation, new preliminary S3 ages reveal, if anything, multiple periods of roughly uniform vertical aggradation along the length of drainages.

Local eastern Grand Canyon tributary response to climate is more complicated than previously thought. In general, over late Quaternary time, there are more and somewhat differently timed erosion/deposition cycles preserved in tributaries compared to the mainstem Colorado River. This must reflect tributary responses to local climate conditions, which the Colorado River may be relatively insensitive to. This is supported by the tighter correlation of the tributary stratigraphy to regional paleoclimate records versus global ice records. Potentially, one type of local deposit (S4 and S3y) fills catchments as climate cools/wettens, whereas another type (S3o and S2) reworks and redeposits these stored sediments during and after transitions to warmer climate with more intense precipitation.

REFERENCES CITED

Abramoff, M.D., Magelhaes, P.J., and Ram, S.J., 2004, Image Processing with ImageJ: Biophotonics International, v. 11, no. 7, p. 36-42.

Aitken, M.J., 1998, An introduction to optical dating, The dating of Quaternary sediments by the use of photon-stimulated luminescence: Oxford, Oxford University Press, 267 p.

Anders, M.D., 2003, Quaternary geology and landscape evolution of eastern Grand Canyon, Arizona [MS thesis]: Logan, UT, Utah State University, 147 p.

Anders, M.D., Pederson, J.L., Rittenour, T.M., Sharp, W.D., Gosse, J.C., Karlstrom, K.E., Crossey, L.C., Goble, R.J., Stockli, L., and Guang, Y., 2005, Pleistocene geomorphology and geochronology of eastern Grand Canyon: linkages of landscape components duringclimate changes: Quaternary Science Reviews, v. 24, p. 2428-2448.

Anderson, R.S., 1993, A 35,000-year vegetation and climate history from Potato Lake, Mogollon Rim, Arizona: Quaternary Research, v. 40, p. 351-359.

Anderson, R. S., Betancourt, J.L., Mead, J.I., Hevly, R.H., and Adam, D.P., 2000, Middle- and late-Wisconsin paleobotanical and paleoclimatic records from the southern Colorado Plateau, USA: Palaeogeography, Palaeoclimatology, Palaeoecology, v. 155, p. 31-57.

Andrews, J.T, Carrara, P.E., King, F.B., and Stuckenrath, R., 1975, Holocene environmental changes in the alpine zone, northern San Juan Mountains, Colorado: Evidence from bog stratigraphy and palynology: Quaternary Research, v. 5, p. 173-197.

Benedict, J.B., 1973, Chronology of cirque glaciation, Colorado Front Range: Quaternary Research, v. 3, p. 584-599.

Bull, W.B., 1991, Geomorphic responses to climate change: New York, Oxford University Press, 326 p.

Bull, W.B., & Schick, A.P., 1979, Impact of climatic change on an arid watershed: Nahal Yael, Southern Israel: Quaternary Research, v. 11, p.153-171.

Carrara, P.E., Mode, W.N., Rubin, M., and Robinson, S.W., 1984, Deglaciation and postglacial timberline in the San Juan Mountains, Colorado: Quaternary Research, v. 21, p. 42-55.

Chadwick, O.A., Hall, R.D., and Phillips, F.M., 1997, Chronology of Pleistocene glacial advances in the central Rocky Mountains: Geological Society of America Bulletin, v. 109, p. 1443-1452.

Coats, L.L., 1997, Middle to late Wisconsin vegetation change at Little Nankoweap, Grand Canyon National Park, Arizona [M.S. thesis]: Flagstaff, AZ, Northern Arizona University, 139 p.

Cole, K.L., 1982, Late Quaternary zonation of vegetation in the eastern Grand Canyon: Science, v. 217, p.1142-1145.

Cole, K.L., 1990a, Reconstruction of past desert vegetation along the Colorado River using packrat middens: Palaeogeography, Palaeoclimatology, Palaeoecology, v. 76, p. 349-366.

Cole, K.L., 1990b, Late Quaternary vegetation gradients through the Grand Canyon, *in* Betancourt, J.L., Van Devender, T.R., and Martin, P.S., eds., Packrat middens: The last 40,000 years of biotic change: Tucson, University of Arizona Press, p. 240-258.

Connin, S.L., Betancourt, J., and Quade, J., 1998, Late Pleistocene C_4 plant dominance and summer rainfall in the southwestern United States from isotopic study of herbivore teeth: Quaternary Research, v. 50, p. 179-193.

Davis, W.M., 1902, Base-level, grade, and peneplain: Journal of Geology, p. 77-111.

Davis, O.K., and Shafer, D.S., 1992, A Holocene climatic record for the Sonoran desert from pollen analysis of Montezuma Well, Arizona, USA: Palaeogeography, Palaeoclimatology, Palaeoecology, v. 92, p. 107-119.

Demoulin, A., 1998, Testing the tectonic significance of some parameters of longitudinal river profiles; the case of the Ardenne (Belgium, NW Europe): Geomorphology, v. 24, no. 2-3, p.189-208.

Dietrich, W.E., and Dunne, T., 1993, The channel head, *in* Beven, K., and Kirkby, M.J., eds., Channel network hydrology: New York, John Wiley and Sons, Ltd., p. 175-219.

Dohrenwend J.C., 1987, Basin and Range, *in* Geomorphic Systems of North America, Graf WL, ed., Centennial Special Volume 2. Geological Society of America: Boulder, Colorado, p. 303–342.

Elias, S.A., Carrara, P.E., Toolin, L.J., and Jull, A.J.T., 1991, Revised age of deglaciation of Lake Emma based on new radiocarbon and macrofossil analyses: Quaternary Research, v. 36, p. 307-321.

Epstein, S., Xu, X., and Carrara, P., 1991, A climatic record from ^{14}C-dated wood fragments from southwestern Colorado: Global Biogeochemical Cycles, v. 13, no. 3, p. 781-784.

Evenson, E.B., Klein, J., Lawn, B., and Middleton, R., 1994, Glacial chronology of the Wind River Mountains from measurements of cosmogenic radionuclides in boulders: Geological Society of America Abstract with Programs, v. 26, p. A-511.

Forman S.L., Pierson, J. and Lepper, K., 2000, Luminescence geochronology, *in* Quaternary geochronology: Methods and Applications, American Geophysical Union Reference Shelf v. 4, p. 157-176.

Gerson, R., 1982, Talus relicts in deserts: A key to major climate fluctuations: Israel: Journal of Earth-Sciences, v. 31, p. 123-132.

Gerson, R., and Grossman, S., 1987, Geomorphic activity on escarpments and associated fluvial systems in hot deserts, *in* Rampino, M.R., Sanders J.E., Newman W.S., and Konigsson L.K., eds., Climate: History, periodicity, and predictability: New York, Van Nostrand Reinhold Co., p. 300-322.

Gosse, J.C., Klein, J., Evenson, E.B., Lawn, B., and Middleton, R., 1995, Beryllium-10 dating of the duration and retreat of the last Pinedale glacial sequence: Science, v. 268, p. 1329-1333.

Griffiths, P.G., Webb, R.H., and Melis, T.S., 1996, Initiation and frequency of debris flows in Grand Canyon, Arizona: U.S. Geological Survey Open-File Report 96-491, 35 p.

Griffiths, P.G., Webb, R.H., and Melis, T.S., 2004, Frequency and initiation of debris flows in Grand Canyon, Arizona. Journal of Geophysical Research, v. 109, F04002, doi: 10.1029/2003JF000077.

Hamblin, W.K., 1994, Late Cenozoic lava dams in the western Grand Canyon: Geological Society of America Memoir 183, p. 139.

Hancock, G.S., Anderson, R.S., Chadwick, O.A., and Finkel, R.C., 1999, Dating fluvial terraces with ^{10}Be and ^{26}Al profiles: Application to the Wind River, Wyoming: Geomorphology, v. 27, p. 41-60.

Hanson, P.R., Mason, J.A., and Goble, R.J., 2004, Episodic Late Quaternary slopewash deposition as recorded in colluvial aprons, Southeastern Wyoming: Quaternary Science Reviews, v. 23, p. 1835-1846.

Harvey, A.M. and Wells, S.G., 1994, Late Pleistocene and Holocene changes in hillslope sediment supply to alluvial fan systems: Zzyzx, California, *in* Millington, A.C., and Pye, K., eds., Environmental change in drylands: Biogeographical and geomorphological perspectives: New York, John Wiley and Sons, p. 67-84.

Harvey, A.M., Wigand, P.E., and Wells, S.G., 1999, Response of alluvial fan systems to the late Pleistocene to Holocene climatic transition: Contrasts between the margins of pluvial Lakes Lahontan and Mojave, Nevada and California, USA: Catena, v. 36, p. 255-281.

Hereford, R., 1996, Map showing surficial geology and geomorphology of the Palisades Creek area, Grand Canyon National Park, Arizona: U.S. Geological Survey Miscellaneous Investigations Series, Map I-2449, Scale 1:2,000.

Hereford, R., Thompson, K.S., Burke, K.J., and Fairley, H.C., 1996, Tributary debris fans and the late Holocene alluvial chronology of the Colorado River, eastern Grand Canyon, Arizona. GSA Bulletin, v. 108, no. 1, p. 3-19.

Intergovernmental Panel on Climate Change (IPCC), 2001, Contribution of working group 1 to the third assessment report of the IPCC. *in* Houghton, J.T., et al., eds., Climate Change 2001: The Scientific Bias: Cambridge, Cambridge University Press, 892 p.

Jain, M., Murray, A.S., and Botter-Jensen, L., 2004, Optically stimulated luminescence dating: How significant is incomplete light exposure in fluvial environments?: Quaternaire, v. 15, no. 1-2, p. 143-157.

Leopold, L.B., 1994, A view of the river: Cambridge, Mass., Harvard Univ. Press, 298 pp.

Leopold, L.B., Wolman, G., and Miller, J.B., 1964, Fluvial processes in geomorphology: New York, W.H. Freeman, 522 pp.

Lucchitta, I., Dehler, C.M., Davis, M.E., Basdekas, P.G., and Burke, K.J., 1995, Quaternary geologic map of the Palisades Creek-Comanche Creek area, eastern Grand Canyon, Arizona, *Open-File Report 95-832*, U.S. Geological Survey,Denver, 39 p.

Lucchitta, I., Curtis, G.H., Davis, M.E., Davis, S.W., and Turrin, B., 2000, Cyclic aggradation and downcutting, fluvial response to volcanic activity, and calibration of soil carbonate stages in western Grand Canyon, Arizona: Quaternary Research, v. 53, p. 23-33.

Machette, M.N., and J.N. Rosholt, 1989, Quaternary terraces in Marble Canyon and eastern Grand Canyon, Arizona, *in* Elston, D.P., Billingsley, G.H., and Young, R.A., eds., Geology of Grand Canyon, Northern Arizona (with Colorado River Guides), Lees Ferry to Pierce Ferry Arizona: Washington, D.C. American Geophysical Union, p. 205-211.

Mackin, J.H., 1948, Concept of athe graded river: GSA Bulletin, v. 59, p. 463-512.

Madole, R.F., 1986, Lake Devlin and Pinedale glacial history, Front Range, Colorado: Quaternary Research, v. 25, p. 43-54.

Maher, L.J., Jr., 1972, Nomograms for computing 0.95 confidence limits of pollen data: Reviews in Palaeobotany and Palynology, v. 13, p. 85-93.

Martin, P.S., 1984, Stanton's Cave during and after the last ice age, *in* Euler, R.C., ed., The archaeology, geology, and paleobiology of Stanton's Cave, Grand Canyon National Park, Arizona: Grand Canyon Natural History Association Monograph 6, p. 131-137.

McDonald, E.V., McFadden, L.D., and Wells, S.G., 2003. Regional response of alluvial fans to the Pleistocene-Holocene climate transition, Mojave Desert, California. *in* Enzel, YI, Wells, S.G., Lancaster, N., eds., Paleoenvironments and paleohydrology of the Mojave and southern Great Basin Deserts: Boulder, Colorado, Geological Society of America Special Paper 368, p. 189-205.

Mead, J.I., and Phillips, A.M. III, 1981, The late Pleistocene and Holocene fauna and flora of Vulture Cave, Grand Canyon, Arizona: The Southwestern Naturalist, v. 26, no. 3, p. 257-288.

Melis, T.S., 1997, Geomorphology of debris flows and alluvial fans in Grand Canyon National Park and their influence on the Colorado River below Glen Canyon Dam, Arizona, [Ph.D. thesis]: Tucson, University of Arizona, 490 p.

Murray, A. S., and Roberts, R. G.,1998, Measurement of the equivalent dose in quartz using a regenerative-dose single-aliquot protocol: Radiation Measurements v. 29, p. 503-515.

Murray, A. S., and Wintle, A. G., 2000, Luminescence dating of quartz using an improved single-aliquot regenerative-dose protocol: Radiation Measurements v. 32, p. 57-73.

Nelson, A.R., Millington, A.C., Andrews, J.T., and Nichols, H., 1979, Radiocarbon-dated upper Pleistocene glacial sequence, Fraser Valley, Colorado Front Range: Geology, v. 7, p. 410-414.

Nichols, K.K., Bierman, P.R., Hooke, R.L., Clapp, E.M., and Caffee, M., 2002, Quantifying sediment transport on desert piedmonts using ^{10}Be and ^{26}Al: Geomorphology, v. 45, p. 105-125.

Olley, J. M., Caitcheon G. G., and Roberts R. G., 1999, The origin of dose distributions in fluvial sediments, and the prospect of dating single grains from fluvial deposits using optically stimulated luminescence: Radiation Measurements v. 30, p. 201-217.

Patton, P.C. and Boison, P.J., 1986, Processes and rates of formation of Holocene terraces in Harris Wash, Escalante River basin, south-central Utah: Geological Society of America Bulletin, v. 97, p. 369-378.

Pazzaglia, F.J., Gardner, T.W., and Merritts, D.J., 1998, Bedrock fluvial incision and longitudinal profile development over geologic time scales determined by fluvial terraces, *in* eds. Tinkler, K.J., and Wohl, E.E. Rivers Over Rock: Fluvial Processes in Bedrock Channels: Washington D.C, Geophysical Monograph 107, AGU, p. 207-236.

Pederson, J.L., Pazzaglia, F., and Smith, G., 2000, Ancient hillslope deposits: Missing links in the study of climate controls on sedimentation: Geology, v. 28, no. 1, p. 27-30.

Pederson, J.L., Smith, G., and Pazzaglia, F., 2001, Comparing the Modern, Quaternary, and Neogene records of climate-controlled hillslope sedimentation in southwest Nevada: Geological Society of America Bulletin, v. 113, p. 305-319.

Pederson, J.L., Karlstrom, K., Sharp, W., and McIntosh, W., 2002, Differential incision of the Grand Canyon related to Quaternary faulting – Constraints from U-series and Ar/Ar dating: Geology, v. 30, no. 8, p. 739-742.

Peterson, K.L., and Mehringer, P.J., 1976, Postglacial timberline fluctuations, La Plata Mountains, southwestern Colorado: Artic and Alpine Research, v. 8, no. 3, p. 275-288.

Phillips, A.M., 1977, Packrats, plants, and the Pleistocene in the lower Grand Canyon [Ph.D. thesis]: Tucson, University of Arizona, 123 p.

Phillips, A.M., 1984, Shasta ground sloth extinction: Fossil packrat midden evidence from the western Grand Canyon, *in* Martin, P.S., and Klein, R.G., eds., Quaternary Extinctions: Tucson, University of Arizona Press, p. 148-158.

Phillips, F.M., Zreda, M.G., Gosse, J.C., Klein, J, Evenson, E.B., Hall, R.D., Chadwick, O.A., and Sharma, P., 1997, Cosmogenic ^{36}Cl and ^{10}Be ages of Quaternary glacial and fluvial deposits of the Wind River Range, Wyoming: Geological Society of America Bulletin, v. 128, p. 1453-1463.

Porat, N., Wintle, A.G., Amit, R., Enzel, Y., 1996, Late Quaternary earthquake chronology from luminescence dating of colluvial and alluvial deposits of the Arava Valley, Israel: Quaternary Research v. 46, p. 107-117.

Repka, J.L., Anderson, R.S., Dick, G.S., and Finkel, R.C., 1997, Quaternary geology and geomorphology, northern Henry Mountains region: dating the Fremont River terraces: Part 7, *in* Link, P.K., and Kowallis, B.J., eds., Mesozoic to Recent geology of Utah: Geology Studies, v. 42, p. 398-404.

Reheis, R. C., Reynolds, R.L., Goldstein, H., Roberts, H.M., Yount, J.C., Axford, Y., Cummings, L.S., and Shearin, N., 2005, Late Quaternary eolian and alluvial response to paleoclimate, Canyonlands, southeastern Utah: GSA Bulletin, v. 117, no. 7/8, p. 1051-1069.

Rittenour, T.M., Goble, R.J., and Blum, M.D., 2005, Development of an OSL chronology for late Pleistocene channel belts in the lower Mississippi valley: Quaternary Science Reviews, v. 24, p. 2539-2554.

Ritter, J.B., and Gardner, T.W., 1993, Hydrologic evolution of drainage basins Disturbed by surface mining, central Pennsylvania: Geological Society of America Bulletin, v. 105, p. 101-115.

Schumm, S. A., 1973: Geomorphic thresholds and complex response of drainage Systems, *in* Morisawa, M., Ed., Fluvial Geomorphology, p. 299-310.

Sharp, W.D., Ludwig, K.R., Chadwick, O.A., Amundson R., and Glaser, L.L., 2003, Dating fluvial terraces by ^{230}Th/U on pedogenic carbonate, Wind River Basin, Wyoming: Quaternary Research, v. 59, p. 139-150.

Sinha, S.K., and Parker, G., 1996, Causes of concavity in longitudinal profiles of rivers: Water Resources Research, v. 32, no. 5, p. 1417-1428.

Smith, G.I., Bischoff, J.L., and Bradbury, J.P., 1997, Synthesis of the paleoclimate record from Owens Lake core OL-92, *in* Smith, G.I., and Bischoff, J.L., eds., An 800,000-year paleoclimatic record from core OL-92, Owens Lake, southeast California: Geological Society of America Special Paper 317, p. 143-160.

Tucker, G.E., and Slingerland, R., 1997, Drainage basin responses to climate change: Water Resources Research, v. 33, no. 8, p. 2031-2047.

Wallinga, J., 2002, Optically stimulated luminescence dating of fluvial deposits: a review: Boreas v. 31, p. 303-322.

Webb, R.H., Melis, T.S., Wise, T.W., and Elliott, J.G., 1996, "The great cataract," effects of late Holocene debris flows on Lava Falls rapid, Grand Canyon National Park and Hualapai Indian Reservation, Arizona: U.S. Geological Survey Open-File Report 96-460, 96 p.

Weng, C., and Jackson, S.T., 1999, Late glacial and Holocene vegetation history and paleoclimate of the Kaibab Plateau, Arizona: Paleogeography, Paleoclimatology, Paleoecology, v. 153, p. 179-201.

Western Regional Climate Center, 2005. Arizona Climate Summaries http://www.wrcc.dri.edu/summary/climsmut.html.

Winograd, I.J., Coplen, T.B., Landwehr, J.M., Riggs, A.C., Ludwig, K.R., Szabo, B.J., Kolesar, P.T., and Revesz, K.M., 1992, Continuous 500,000-year climate records from vein calcite in Devils Hole, Nevada: Science, v. 258, p. 255-260.

Winograd, I.J., Landwehr, J.M., Coplen, T.B., Sharp, W.D., Riggs, A.C., Ludwig, K.R., and Kolesar, P.T., 2006, Devils Hole, Nevada, δ^{18}O record extended to the mid-Holocene: Quaternary Research v. 66, p. 202-212.

Wright, H.E., Bent, A.M., Hansen, B.S., and Maher, L.J., 1973, Present and past vegetation of the Chuska Mountains, northwestern New Mexico: Geological Society of America Bulletin, v. 84, p. 1155-1180.

Yatsu, E., 1955, On the longitudinal profile of graded river. Eos Trans. AGU, v. 36, p. 655-663.

Yanchou, L., Prescott, J.R., Hua, Z., Jie, C., and Lanying, W., 2002, Optical dating of colluvial deposits from Xiyangfang, China, and the relation to palaeo-earthquake events: Quaternary Science Reviews. v. 21, p. 1087-1097.

Zaprowski, B.J., Pazzaglia, F.J., and Evenson, E.B., 2005, Climatic influences on profile concavity and river incision: Journal of Geophysical Research, v. 110, F03004, doi: 10.1029/2004JF000138.

APPENDICES

APPENDIX A. TERRACE CROSS SECTIONS AND RAW SURVEY DATA

Figures A.1 through A.6 are graphics of total-station transects always viewed from upstream looking downstream. The locations of transects can be seen in the plates of Appendix D, and the following table presents all data associated with them.

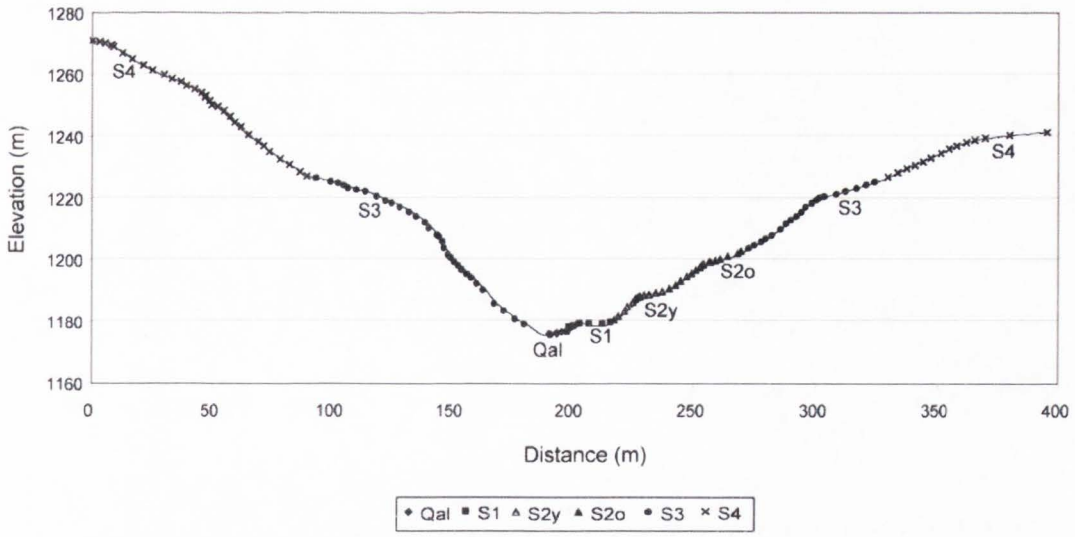

Figure A.1. Lava Chuar transect LC_1U

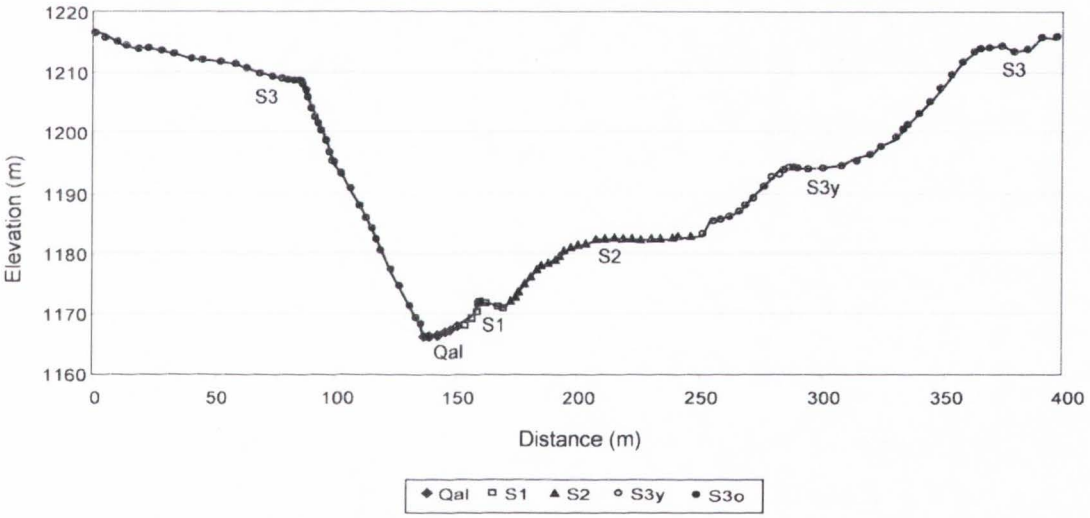

Figure A.2. Lava Chuar transect LC_2U

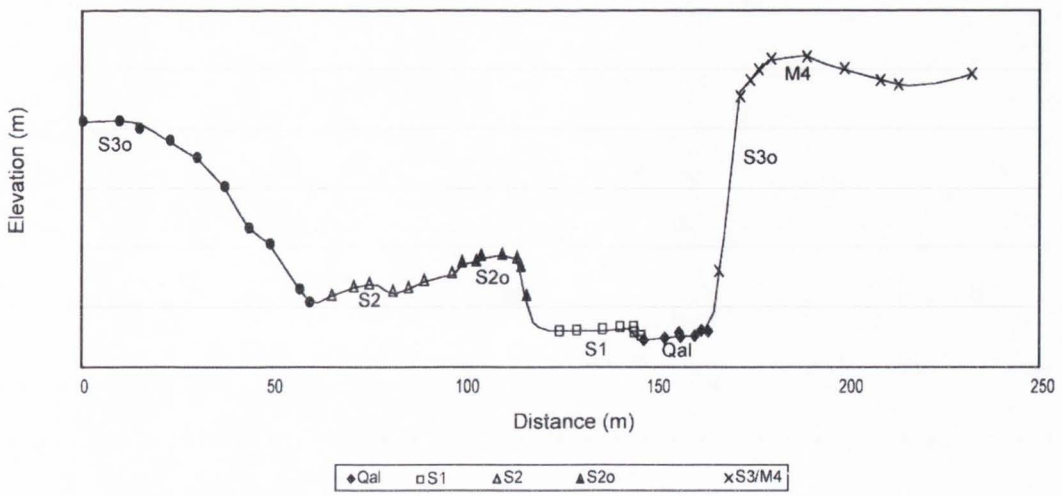

Figure A.3. Comanche transect com_mouth

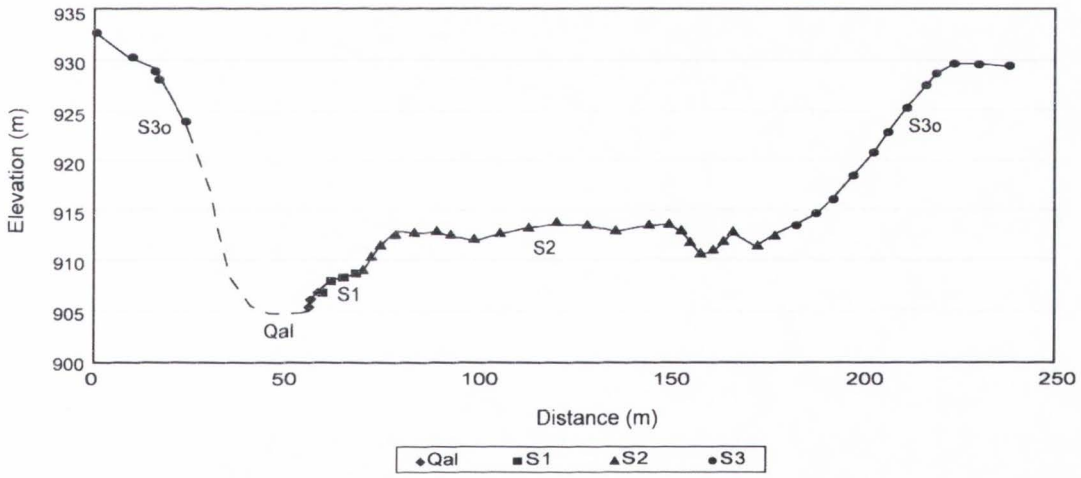

Figure A.4. Comanche transect com_trunk

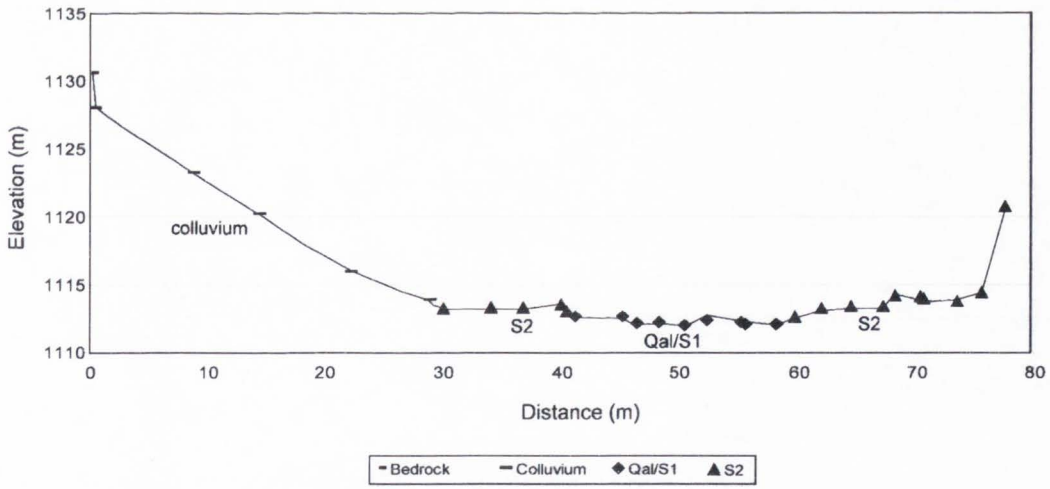

Figure A.5. Comanche transect CH1

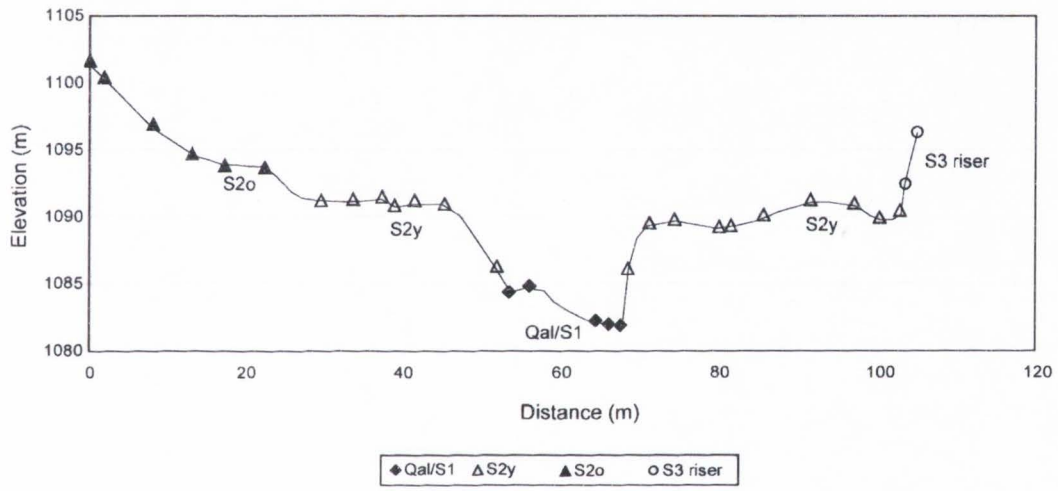

Figure A.6. Comanche transect CH2

TABLE A.1. RAW SURVEY DATA

Cross sections were created from easting, northing, and elevation survey data in NAD 1983 projection. In order to capture terrace relations, transects sometimes had turns or were briefly perpendicular with the drainage axis. To correct for this, all data points were projected at right angles onto a line perpendicular to the drainage axis. The "distance along transect" column represents where the data points fell along the projection line. The "adjusted elevation" column presents the elevation of each point at the projection line and was calculated using the average gradient of the valley bottom in the vicinity of the transect. Therefore, data points down-valley of the projection line increased in elevation and the points upstream decreased in elevation.

Transect	Pt-ID	UTM - Easting	UTM - Northing	Elevation	Dist. Along Transect	Adjusted Elev.
LC-1U	2	420898.80	4003017.58	1245.20	395.39	1241.34
LC-1U	3	420913.36	4002999.21	1243.17	380.04	1240.34
LC-1U	4	420915.12	4002988.77	1241.96	370.11	1239.34
LC-1U	5	420916.54	4002984.00	1241.32	365.69	1238.83
LC-1U	6	420918.65	4002980.22	1240.28	362.36	1237.96
LC-1U	7	420920.65	4002975.83	1239.10	358.42	1236.94
LC-1U	8	420921.66	4002972.36	1238.05	355.20	1235.98
LC-1U	9	420922.31	4002968.68	1236.50	351.71	1234.51
LC-1U	10	420923.69	4002963.95	1234.84	347.31	1232.97
LC-1U	11	420925.50	4002960.39	1233.60	344.15	1231.88
LC-1U	12	420926.59	4002956.72	1232.33	340.75	1230.71
LC-1U	13	420926.41	4002953.38	1231.27	337.43	1229.68
LC-1U	14	420927.48	4002949.36	1229.82	333.68	1228.34
LC-1U	15	420928.42	4002945.28	1228.35	329.85	1226.96
LC-1U	16	420929.82	4002939.45	1226.56	324.38	1225.31
LC-1U	17	420932.56	4002935.44	1225.31	320.94	1224.26
LC-1U	18	420932.33	4002931.21	1224.27	316.74	1223.25
LC-1U	19	420933.53	4002926.54	1223.05	312.38	1222.16
LC-1U	20	420935.07	4002922.27	1221.96	308.47	1221.20
LC-1U	21	420937.19	4002916.93	1221.06	303.62	1220.48
LC-1U	22	420938.05	4002914.98	1220.53	301.86	1220.01
LC-1U	23	420938.54	4002913.65	1219.95	300.65	1219.47
LC-1U	24	420939.25	4002911.53	1218.77	298.69	1218.36
LC-1U	25	420939.28	4002911.52	1218.79	298.69	1218.38
LC-1U	26	420939.38	4002908.79	1217.45	296.03	1217.08
LC-1U	27	420940.14	4002906.76	1215.81	294.17	1215.50
LC-1U	28	420941.35	4002904.53	1214.23	292.20	1214.02
LC-1U	29	420942.43	4002902.19	1212.94	290.11	1212.82
LC-1U	30	420943.43	4002900.00	1211.77	288.14	1211.73
LC-1U	31	420945.03	4002897.24	1209.81	285.73	1209.88
LC-1U	32	420945.78	4002893.58	1207.91	282.27	1208.06
LC-1U	33	420946.61	4002890.92	1206.57	279.81	1206.80
LC-1U	34	420947.67	4002888.89	1205.56	278.01	1205.87
LC-1U	35	420947.49	4002886.00	1204.48	275.13	1204.82
LC-1U	36	420948.10	4002883.45	1203.52	272.75	1203.92

LC-1U	37	420949.43	4002880.08	1202.25	269.68	1202.76
LC-1U	38	420950.44	4002878.35	1201.67	268.17	1202.25
LC-1U	39	420951.18	4002874.17	1200.49	264.20	1201.17
LC-1U	40	420952.66	4002870.91	1199.62	261.27	1200.42
LC-1U	41	420954.45	4002868.39	1199.03	259.13	1199.95
LC-1U	42	420954.50	4002868.41	1199.03	259.15	1199.96
LC-1U	43	420955.26	4002866.12	1198.48	257.05	1199.47
LC-1U	44	420955.57	4002865.57	1198.32	256.56	1199.34
LC-1U	45	420957.00	4002863.02	1197.59	254.33	1198.71
LC-1U	46	420957.39	4002862.39	1197.21	253.78	1198.36
LC-1U	47	420957.65	4002861.31	1196.48	252.76	1197.66
LC-1U	48	420958.92	4002859.36	1195.44	251.09	1196.72
LC-1U	49	420959.66	4002857.46	1194.41	249.35	1195.75
LC-1U	50	420960.68	4002855.44	1193.19	247.56	1194.61
LC-1U	51	420961.77	4002852.60	1191.71	244.97	1193.22
LC-1U	52	420962.71	4002850.19	1190.36	242.78	1191.95
LC-1U	53	420964.14	4002847.27	1189.10	240.17	1190.80
LC-1U	54	420965.67	4002844.26	1188.05	237.49	1189.88
LC-1U	55	420966.03	4002841.52	1187.47	234.88	1189.34
LC-1U	56	420966.68	4002838.36	1186.96	231.89	1188.90
LC-1U	57	420967.22	4002836.40	1186.60	230.07	1188.60
LC-1U	58	420968.61	4002834.33	1186.10	228.29	1188.20
LC-1U	59	420968.88	4002833.37	1185.91	227.39	1188.03
LC-1U	60	420969.37	4002832.43	1185.33	226.56	1187.48
LC-1U	61	420971.20	4002831.05	1184.05	225.55	1186.33
LC-1U	62	420972.40	4002828.50	1182.46	223.26	1184.83
LC-1U	63	420974.14	4002826.80	1180.70	221.91	1183.20
LC-1U	64	420975.31	4002824.19	1179.17	219.57	1181.75
LC-1U	65	420977.08	4002821.84	1177.71	217.58	1180.43
LC-1U	66	420977.85	4002820.23	1176.94	216.14	1179.72
LC-1U	67	420979.51	4002816.58	1176.42	212.86	1179.33
LC-1U	68	420978.98	4002811.24	1176.32	207.52	1179.26
LC-1U	69	420976.32	4002807.61	1176.50	203.47	1179.32
LC-1U	70	420973.87	4002805.70	1176.04	201.13	1178.75
LC-1U	71	420972.57	4002804.05	1175.75	199.27	1178.39
LC-1U	72	420970.66	4002803.83	1174.32	198.70	1176.86
LC-1U	73	420968.73	4002801.87	1174.31	196.42	1176.76
LC-1U	74	420967.65	4002799.96	1174.09	194.34	1176.50
LC-1U	75	420967.05	4002800.00	1173.60	194.26	1175.98
LC-1U	76	420964.16	4002797.97	1173.57	191.74	1175.80
LC-1U	77	420963.22	4002797.14	1174.00	190.74	1176.19
LC-1U	78	420962.44	4002796.22	1174.16	189.70	1176.32
LC-1U	79	420962.32	4002795.86	1175.20	189.32	1177.35
LC-1U	80	420960.38	4002792.09	1175.99	185.25	1178.07
LC-1U	81	420957.44	4002792.25	1175.07	184.87	1176.98
LC-1U	82	420954.22	4002788.56	1177.28	180.64	1179.05
LC-1U	83	420951.18	4002784.99	1179.08	176.57	1180.71
LC-1U	84	420952.74	4002780.18	1181.69	172.13	1183.46
LC-1U	85	420951.20	4002776.35	1184.16	168.09	1185.88
LC-1U	86	420951.45	4002771.30	1188.57	163.17	1190.37

LC-1U	87	420951.49	4002768.75	1190.65	160.67	1192.47
LC-1U	88	420950.57	4002766.50	1192.36	158.29	1194.16
LC-1U	89	420949.88	4002764.82	1193.68	156.51	1195.46
LC-1U	90	420949.77	4002764.75	1193.69	156.41	1195.46
LC-1U	91	420949.12	4002762.69	1194.95	154.27	1196.70
LC-1U	92	420949.30	4002761.26	1196.32	152.91	1198.10
LC-1U	93	420949.17	4002759.42	1197.67	151.07	1199.46
LC-1U	94	420949.39	4002757.86	1199.00	149.57	1200.83
LC-1U	95	420949.02	4002756.82	1200.00	148.48	1201.81
LC-1U	96	420950.61	4002754.88	1201.85	146.88	1203.77
LC-1U	97	420952.48	4002753.78	1203.81	146.15	1205.86
LC-1U	98	420953.52	4002752.33	1205.36	144.91	1207.48
LC-1U	99	420953.69	4002751.32	1205.91	143.95	1208.05
LC-1U	100	420955.75	4002747.57	1207.94	140.65	1210.24
LC-1U	101	420956.71	4002745.56	1209.75	138.85	1212.12
LC-1U	102	420955.78	4002742.07	1211.67	135.25	1214.03
LC-1U	103	420955.23	4002739.14	1213.08	132.27	1215.44
LC-1U	104	420954.69	4002735.26	1214.63	128.36	1217.00
LC-1U	105	420953.50	4002731.82	1216.16	124.76	1218.49
LC-1U	106	420953.63	4002729.34	1216.78	122.34	1219.15
LC-1U	107	420953.38	4002725.55	1218.15	118.57	1220.55
LC-1U	108	420953.33	4002725.52	1218.16	118.53	1220.56
LC-1U	109	420950.37	4002721.19	1219.92	113.73	1222.19
LC-1U	110	420948.03	4002717.88	1220.60	110.04	1222.78
LC-1U	111	420946.23	4002714.80	1221.07	106.68	1223.18
LC-1U	112	420943.89	4002713.38	1222.10	104.85	1224.09
LC-1U	113	420939.15	4002711.88	1223.03	102.50	1224.76
LC-1U	114	420935.47	4002709.40	1223.78	99.37	1225.33
LC-1U	115	420930.52	4002704.38	1225.04	93.52	1226.36
LC-1U	116	420927.96	4002700.98	1225.97	89.71	1227.19
LC-1U	117	420924.87	4002698.58	1227.44	86.78	1228.50
LC-1U	118	420921.68	4002694.91	1229.86	82.58	1230.78
LC-1U	119	420919.15	4002691.18	1231.91	78.44	1232.73
LC-1U	120	420916.80	4002687.24	1234.33	74.13	1235.06
LC-1U	121	420914.61	4002685.20	1236.33	71.73	1236.95
LC-1U	122	420911.67	4002683.28	1237.75	69.30	1238.23
LC-1U	123	420907.29	4002679.86	1240.47	65.11	1240.73
LC-1U	124	420904.03	4002677.27	1243.02	61.96	1243.12
LC-1U	125	420900.40	4002675.47	1244.61	59.52	1244.53
LC-1U	126	420894.18	4002674.63	1246.85	57.55	1246.43
LC-1U	127	420888.65	4002673.05	1248.98	54.97	1248.25
LC-1U	128	420883.14	4002671.26	1250.72	52.19	1249.70
LC-1U	129	420880.18	4002669.27	1251.38	49.68	1250.21
LC-1U	130	420876.70	4002667.70	1252.48	48.72	1251.51
LC-1U	131	420871.76	4002664.92	1253.06	46.90	1252.40
LC-1U	132	420867.96	4002664.46	1253.65	47.15	1253.21
LC-1U	133	420863.55	4002661.88	1254.34	45.44	1254.18
LC-1U	134	420858.86	4002658.18	1255.23	42.68	1255.38
LC-1U	135	420853.63	4002653.63	1255.95	39.17	1256.44
LC-1U	136	420847.01	4002650.05	1256.72	36.88	1257.63

LC-1U	137	420842.68	4002645.20	1257.38	32.92	1258.59
LC-1U	138	420842.73	4002645.27	1257.39	32.98	1258.60
LC-1U	140	420838.85	4002641.29	1258.47	29.79	1259.94
LC-1U	141	420831.74	4002634.89	1259.50	24.82	1261.44
LC-1U	142	420826.75	4002630.23	1260.73	21.17	1263.01
LC-1U	143	420821.91	4002624.74	1262.56	16.68	1265.17
LC-1U	144	420816.31	4002619.63	1263.89	12.69	1266.87
LC-1U	145	420811.18	4002614.76	1265.66	8.86	1268.99
LC-1U	146	420808.61	4002613.36	1266.09	7.96	1269.58
LC-1U	147	420806.06	4002610.39	1266.45	5.51	1270.12
LC-1U	148	420803.06	4002607.41	1266.77	3.14	1270.65
LC-1U	149	420801.25	4002603.87	1266.97	0.00	1270.98
LC-2U	151	421011.14	4002658.33	1217.40	0.00	1216.78
LC-2U	152	421014.01	4002663.16	1216.83	3.90	1215.97
LC-2U	153	421015.27	4002668.68	1216.27	8.90	1215.25
LC-2U	154	421015.80	4002672.57	1215.73	12.52	1214.62
LC-2U	155	421018.95	4002678.44	1215.34	17.85	1214.07
LC-2U	156	421024.59	4002680.91	1215.27	21.72	1214.28
LC-2U	157	421028.36	4002685.65	1214.71	27.28	1213.86
LC-2U	158	421031.87	4002689.90	1213.98	32.30	1213.27
LC-2U	159	421037.39	4002695.90	1213.04	39.54	1212.54
LC-2U	160	421042.31	4002699.22	1212.55	44.03	1212.28
LC-2U	161	421047.59	4002705.92	1212.01	51.88	1211.93
LC-2U	162	421051.83	4002711.16	1211.46	58.05	1211.54
LC-2U	163	421055.87	4002714.90	1210.73	62.72	1210.98
LC-2U	164	421059.71	4002719.36	1209.69	68.02	1210.08
LC-2U	165	421063.35	4002724.02	1208.97	73.48	1209.50
LC-2U	166	421068.97	4002726.56	1208.49	77.40	1209.29
LC-2U	167	421072.46	4002728.39	1208.02	80.08	1208.99
LC-2U	168	421074.93	4002730.43	1207.76	82.70	1208.85
LC-2U	169	421076.32	4002732.30	1207.71	84.87	1208.84
LC-2U	170	421077.01	4002732.89	1207.49	85.62	1208.65
LC-2U	171	421077.53	4002733.43	1207.01	86.28	1208.20
LC-2U	172	421078.26	4002734.74	1206.10	87.73	1207.30
LC-2U	173	421080.00	4002734.82	1204.85	88.27	1206.15
LC-2U	174	421081.13	4002735.89	1202.91	89.60	1204.25
LC-2U	175	421081.88	4002737.53	1201.38	91.38	1202.74
LC-2U	176	421082.18	4002738.73	1200.34	92.61	1201.70
LC-2U	177	421081.80	4002740.07	1199.24	93.80	1200.56
LC-2U	178	421082.33	4002742.13	1197.50	95.93	1198.81
LC-2U	179	421082.27	4002742.08	1197.50	95.86	1198.82
LC-2U	180	421080.86	4002744.14	1195.71	97.48	1196.92
LC-2U	181	421080.11	4002745.50	1194.36	98.61	1195.51
LC-2U	182	421081.10	4002746.02	1194.18	99.36	1195.37
LC-2U	183	421081.76	4002748.61	1192.27	102.04	1193.46
LC-2U	184	421083.05	4002752.43	1189.85	106.06	1191.05
LC-2U	185	421083.50	4002756.01	1187.06	109.64	1188.23
LC-2U	186	421083.67	4002758.73	1184.93	112.31	1186.07
LC-2U	187	421084.37	4002760.93	1183.24	114.61	1184.39
LC-2U	188	421084.96	4002762.72	1181.47	116.49	1182.62

LC-2U	189	421085.93	4002764.54	1179.58	118.50	1180.76
LC-2U	190	421087.88	4002768.52	1176.39	122.85	1177.61
LC-2U	191	421090.13	4002771.63	1173.57	126.45	1174.88
LC-2U	192	421094.36	4002775.03	1170.08	130.83	1171.57
LC-2U	193	421096.32	4002777.05	1168.03	133.30	1169.60
LC-2U	194	421097.03	4002778.98	1167.00	135.35	1168.58
LC-2U	195	421097.53	4002779.83	1164.78	136.30	1166.38
LC-2U	196	421099.58	4002781.86	1164.73	138.79	1166.41
LC-2U	197	421101.75	4002784.74	1164.86	142.14	1166.61
LC-2U	198	421099.43	4002782.04	1164.76	138.93	1166.42
LC-2U	199	421101.71	4002784.82	1164.88	142.21	1166.63
LC-2U	200	421104.12	4002787.75	1165.38	145.68	1167.23
LC-2U	201	421104.98	4002789.65	1165.57	147.73	1167.43
LC-2U	202	421106.30	4002792.34	1166.19	150.67	1168.08
LC-2U	203	421107.43	4002795.14	1166.30	153.67	1168.22
LC-2U	204	421108.97	4002798.00	1167.52	156.83	1169.48
LC-2U	205	421110.58	4002799.55	1168.51	158.75	1170.54
LC-2U	206	421110.17	4002800.36	1169.94	159.43	1171.93
LC-2U	207	421110.34	4002800.98	1170.23	160.07	1172.22
LC-2U	208	421108.68	4002803.84	1170.15	162.39	1172.01
LC-2U	209	421102.07	4002810.89	1170.01	167.47	1171.39
LC-2U	210	421101.12	4002813.47	1169.88	169.71	1171.16
LC-2U	211	421100.98	4002816.66	1171.08	172.75	1172.31
LC-2U	212	421100.18	4002818.99	1171.90	174.78	1173.05
LC-2U	213	421100.20	4002820.26	1172.75	176.02	1173.88
LC-2U	214	421100.85	4002822.76	1174.07	178.60	1175.20
LC-2U	215	421100.96	4002825.13	1175.36	180.92	1176.46
LC-2U	216	421100.51	4002828.02	1176.56	183.58	1177.59
LC-2U	217	421101.31	4002829.60	1177.15	185.32	1178.20
LC-2U	218	421102.41	4002832.45	1177.55	188.36	1178.62
LC-2U	219	421103.73	4002834.94	1178.04	191.10	1179.14
LC-2U	220	421104.52	4002836.51	1178.72	192.83	1179.84
LC-2U	221	421105.56	4002838.26	1179.59	194.79	1180.75
LC-2U	222	421106.69	4002840.74	1180.04	197.48	1181.22
LC-2U	223	421108.16	4002843.36	1180.44	200.39	1181.67
LC-2U	224	421109.28	4002846.71	1180.75	203.92	1181.99
LC-2U	225	421110.24	4002850.32	1181.37	207.65	1182.60
LC-2U	226	421109.26	4002854.45	1181.59	211.39	1182.71
LC-2U	227	421108.40	4002858.89	1181.88	215.44	1182.88
LC-2U	228	421106.65	4002862.94	1181.81	218.90	1182.65
LC-2U	229	421104.95	4002867.37	1181.98	222.72	1182.66
LC-2U	230	421102.93	4002871.64	1182.08	226.31	1182.58
LC-2U	231	421103.29	4002876.09	1182.28	230.70	1182.73
LC-2U	232	421102.43	4002879.90	1182.40	234.15	1182.75
LC-2U	233	421101.96	4002885.25	1182.56	239.19	1182.79
LC-2U	234	421093.23	4002889.83	1183.47	241.32	1183.15
LC-2U	235	421090.07	4002896.14	1183.75	246.59	1183.16
LC-2U	236	421087.85	4002902.07	1184.34	251.73	1183.53
LC-2U	237	421084.85	4002907.27	1186.71	255.96	1185.65
LC-2U	238	421084.82	4002910.17	1187.02	258.74	1185.92

LC-2U	239	421083.93	4002914.18	1187.62	262.39	1186.41
LC-2U	240	421084.02	4002918.35	1188.43	266.43	1187.16
LC-2U	241	421084.41	4002921.04	1189.55	269.13	1188.27
LC-2U	242	421085.38	4002924.12	1190.65	272.35	1189.37
LC-2U	243	421086.34	4002928.10	1192.68	276.45	1191.39
LC-2U	245	421088.36	4002930.58	1194.22	279.37	1193.01
LC-2U	246	421075.01	4002943.71	1196.73	288.54	1194.57
LC-2U	247	421092.67	4002932.87	1194.34	282.71	1193.34
LC-2U	248	421094.63	4002934.27	1195.09	284.58	1194.18
LC-2U	249	421096.10	4002935.92	1195.39	286.55	1194.53
LC-2U	250	421097.72	4002939.12	1195.24	290.06	1194.43
LC-2U	251	421099.39	4002943.03	1195.08	294.27	1194.29
LC-2U	252	421102.18	4002948.84	1195.06	300.61	1194.34
LC-2U	253	421105.20	4002955.80	1195.40	308.13	1194.75
LC-2U	254	421107.33	4002961.67	1196.15	314.35	1195.53
LC-2U	255	421108.52	4002966.87	1197.30	319.68	1196.66
LC-2U	256	421109.13	4002971.35	1198.62	324.16	1197.95
LC-2U	257	421110.79	4002976.92	1200.15	329.97	1199.49
LC-2U	258	421110.75	4002980.22	1201.59	333.14	1200.88
LC-2U	259	421111.01	4002982.01	1202.34	334.94	1201.62
LC-2U	260	421112.52	4002986.47	1204.22	339.64	1203.51
LC-2U	261	421113.00	4002990.74	1206.23	343.89	1205.49
LC-2U	262	421113.54	4002995.28	1208.39	348.41	1207.61
LC-2U	263	421114.08	4002999.79	1210.70	352.91	1209.88
LC-2U	264	421115.14	4003004.44	1212.88	357.67	1212.04
LC-2U	265	421116.73	4003008.97	1214.48	362.46	1213.67
LC-2U	266	421116.80	4003011.65	1215.02	365.06	1214.16
LC-2U	267	421116.80	4003015.36	1215.30	368.64	1214.39
LC-2U	268	421116.05	4003020.81	1215.62	373.71	1214.59
LC-2U	269	421115.32	4003025.99	1214.91	378.51	1213.76
LC-2U	270	421115.07	4003031.79	1215.31	384.04	1214.05
LC-2U	271	421113.15	4003038.38	1217.58	389.90	1216.11
LC-2U	272	421111.78	4003045.16	1217.84	396.08	1216.20
LC-2U	273	421108.99	4003051.87	1218.01	401.83	1216.11
CM	276	425822.24	3996837.59	862.17	0.00	860.69
CM	277	425821.80	3996847.21	862.06	9.54	860.66
CM	278	425822.00	3996852.61	861.42	14.81	860.08
CM	279	425822.04	3996860.95	860.28	23.01	859.03
CM	280	425822.38	3996868.28	858.74	30.16	857.59
CM	281	425821.98	3996875.62	856.24	37.45	855.15
CM	282	425823.74	3996882.64	852.57	44.04	851.65
CM	283	425824.18	3996888.11	851.10	49.34	850.26
CM	284	425825.44	3996896.33	847.18	57.19	846.50
CM	285	425825.69	3996899.09	846.04	59.86	845.41
CM	286	425826.02	3996904.75	846.58	65.37	846.03
CM	287	425827.04	3996910.93	847.25	71.27	846.81
CM	288	425827.43	3996915.27	847.42	75.47	847.05
CM	289	425829.16	3996922.01	846.57	81.78	846.37
CM	290	425830.22	3996926.20	846.76	85.71	846.66
CM	291	425830.71	3996930.51	847.37	89.86	847.35

CM	292	425833.08	3996938.35	847.77	97.14	847.96
CM	293	425833.83	3996940.97	848.56	99.59	848.82
CM	294	425834.13	3996944.75	848.62	103.25	848.94
CM	295	425834.46	3996946.21	849.07	104.63	849.43
CM	296	425834.33	3996951.67	849.05	110.03	849.45
CM	297	425834.62	3996955.73	848.73	113.97	849.20
CM	298	425834.99	3996956.82	848.03	114.97	848.53
CM	299	425834.96	3996958.52	845.55	116.65	846.07
CM	300	425833.80	3996966.97	842.44	125.17	842.98
CM	301	425833.29	3996971.66	842.52	129.87	843.08
CM	302	425831.52	3996978.09	842.66	136.52	843.19
CM	303	425831.40	3996982.61	842.75	140.98	843.32
CM	304	425830.45	3996985.94	842.78	144.43	843.32
CM	305	425830.42	3996986.20	842.34	144.69	842.88
CM	306	425830.67	3996987.92	842.01	146.34	842.59
CM	307	425830.71	3996988.71	841.66	147.10	842.25
CM	308	425831.59	3996994.38	841.71	152.52	842.41
CM	309	425833.27	3996998.33	842.02	156.11	842.85
CM	310	425833.45	3996998.97	841.66	156.71	842.51
CM	311	425834.73	3997002.84	841.61	160.28	842.58
CM	312	425835.70	3997004.86	842.01	162.09	843.05
CM	313	425836.61	3997006.72	841.86	163.76	842.97
CM	314	425837.90	3997009.83	846.78	166.58	848.00
CM	315	425837.61	3997015.25	861.49	171.97	862.75
CM	316	425839.51	3997018.32	862.76	174.64	864.16
CM	317	425841.18	3997020.82	863.52	176.80	865.04
CM	318	425844.43	3997024.69	864.21	180.02	865.96
CM	319	425848.08	3997034.93	864.09	189.43	866.16
CM	320	425849.01	3997044.91	862.91	199.08	865.13
CM	321	425853.71	3997055.35	861.56	208.50	864.16
CM	322	425857.54	3997060.87	860.86	213.24	863.73
CM	323	425867.19	3997082.11	861.02	232.39	864.67
CH1	325	427868.25	3995768.02	1130.52	0.22	1130.58
CH1	326	427868.64	3995767.65	1127.97	0.45	1128.01
CH1	327	427877.14	3995768.13	1123.25	8.90	1123.23
CH1	328	427882.75	3995768.62	1120.25	14.52	1120.20
CH1	329	427890.34	3995770.48	1115.97	22.31	1115.95
CH1	330	427896.92	3995771.63	1113.91	28.99	1113.90
CH1	331	427898.07	3995771.49	1113.31	30.10	1113.27
CH1	332	427902.06	3995772.19	1113.35	34.15	1113.32
CH1	333	427904.82	3995772.27	1113.40	36.88	1113.34
CH1	334	427907.86	3995773.25	1113.59	40.04	1113.56
CH1	335	427908.37	3995773.25	1113.04	40.55	1113.00
CH1	336	427909.08	3995773.35	1112.66	41.26	1112.62
CH1	337	427913.02	3995774.13	1112.66	45.28	1112.63
CH1	338	427914.25	3995774.17	1112.20	46.50	1112.15
CH1	339	427916.08	3995774.82	1112.22	48.41	1112.19
CH1	340	427918.12	3995775.45	1111.96	50.53	1111.95
CH1	341	427920.00	3995775.74	1112.37	52.43	1112.36
CH1	342	427922.73	3995776.94	1112.20	55.33	1112.23

CH1	343	427923.07	3995777.00	1112.01	55.67	1112.04
CH1	344	427925.56	3995777.74	1111.98	58.25	1112.02
CH1	345	427927.03	3995777.77	1112.52	59.70	1112.55
CH1	346	427929.18	3995778.67	1113.14	61.98	1113.20
CH1	347	427931.46	3995779.73	1113.26	64.40	1113.36
CH1	348	427934.29	3995779.71	1113.33	67.19	1113.40
CH1	349	427935.27	3995779.70	1114.10	68.15	1114.16
CH1	350	427937.41	3995780.18	1114.08	70.35	1114.15
CH1	351	427937.73	3995780.19	1113.87	70.66	1113.93
CH1	352	427940.60	3995780.62	1113.72	73.56	1113.78
CH1	353	427942.57	3995780.98	1114.38	75.57	1114.45
CH1	354	427944.61	3995781.14	1120.70	77.60	1120.75
CH2	362	427829.21	3995982.22	1101.69	0.02	1101.69
CH2	363	427830.70	3995983.26	1100.47	1.82	1100.46
CH2	364	427836.16	3995986.54	1097.02	8.08	1096.93
CH2	365	427840.62	3995989.15	1094.86	13.13	1094.72
CH2	366	427844.67	3995990.80	1094.06	17.25	1093.83
CH2	367	427848.77	3995994.04	1093.94	22.47	1093.69
CH2	368	427852.64	3995996.26	1093.58	26.83	1093.27
CH2	369	427854.72	3995998.01	1091.52	29.55	1091.22
CH2	370	427858.69	3995999.87	1091.71	33.73	1091.32
CH2	371	427862.05	3996001.48	1091.90	37.31	1091.46
CH2	372	427863.47	3996002.20	1091.37	38.86	1090.90
CH2	373	427865.13	3996004.36	1091.66	41.53	1091.23
CH2	374	427866.88	3996008.09	1091.29	45.32	1090.94
CH2	375	427868.27	3996016.44	1086.38	51.94	1086.34
CH2	376	427869.60	3996017.23	1084.41	53.46	1084.35
CH2	377	427871.22	3996019.19	1084.85	55.98	1084.81
CH2	379	427877.09	3996025.24	1082.24	64.39	1082.24
CH2	380	427878.34	3996026.26	1082.01	66.00	1082.00
CH2	381	427879.66	3996027.07	1081.99	67.53	1081.97
CH2	382	427881.89	3996025.99	1086.31	68.46	1086.15
CH2	384	427882.39	3996029.65	1089.56	71.28	1089.54
CH2	385	427884.91	3996031.47	1089.82	74.37	1089.78
CH2	386	427888.35	3996036.16	1089.31	80.06	1089.34
CH2	387	427889.62	3996037.04	1089.41	81.59	1089.43
CH2	388	427892.66	3996039.66	1090.18	85.61	1090.19
CH2	389	427897.15	3996043.31	1091.35	91.38	1091.35
CH2	390	427900.72	3996047.55	1090.99	96.88	1091.04
CH2	391	427903.01	3996049.79	1089.96	100.08	1090.00
CH2	392	427904.55	3996052.04	1090.41	102.73	1090.49
CH2	393	427910.01	3996054.76	1090.21	108.61	1090.20
CH2	394	427912.48	3996044.27	1092.97	103.42	1092.42
CH2	395	427914.06	3996044.91	1096.89	105.03	1096.30

APPENDIX B. FACIES PANELS

Figure B.1. is a map with the locations of facies panels shown in Figs. B.2. through B.7. in Lava Chuar catchment. Figure B. 8. similarly shows the locations of facies panels B.9. through B.14. in Comanche catchment.

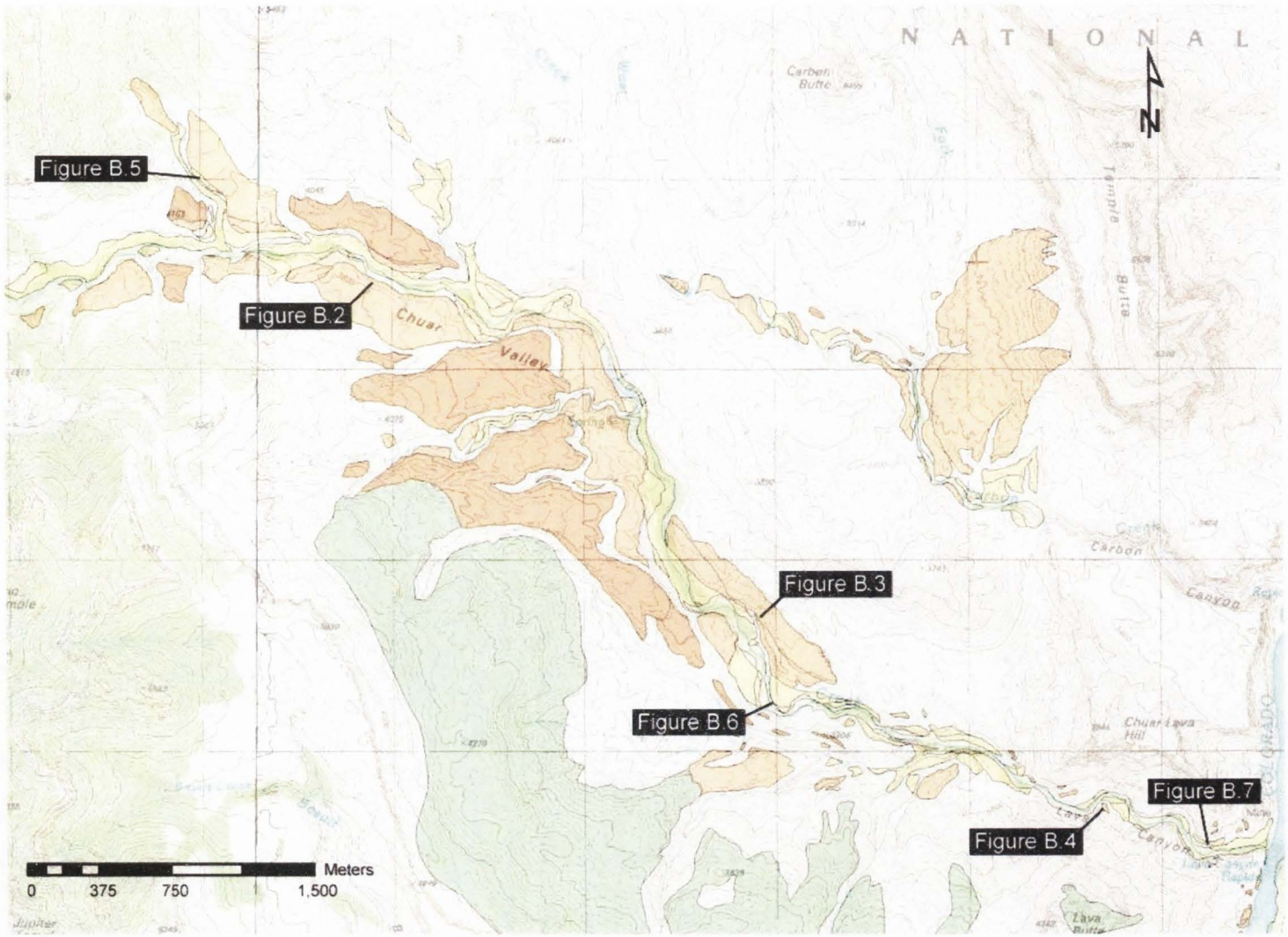

Figure B.1. Surficial geologic map of Lava Chuar showing locations of photos in Figs. B.2 through B.7.

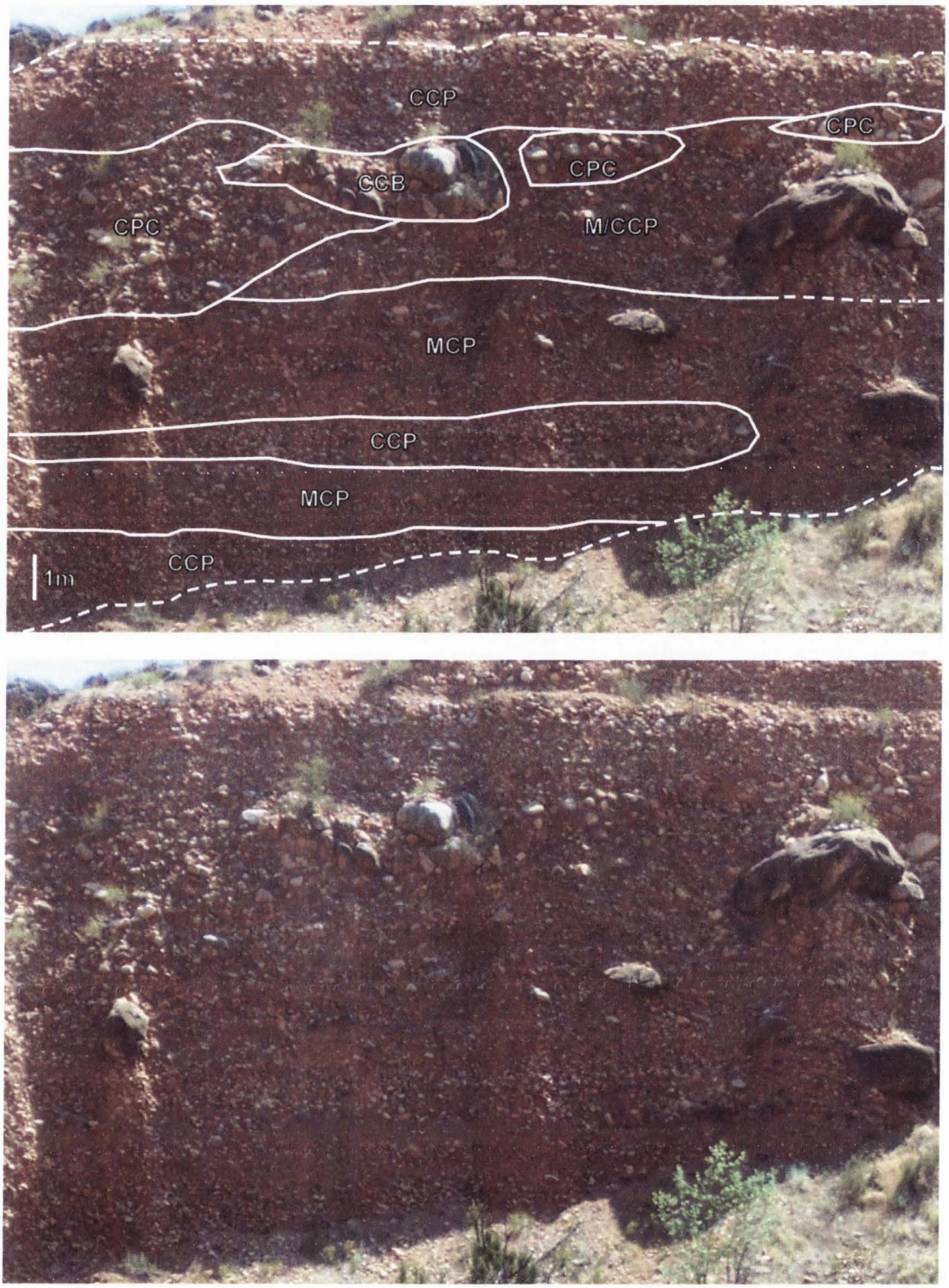

Figure B.2. Sedimentary facies in an S3 exposure in the upper trunk of Lava Chuar

Figure B.3. Sedimentary facies in an S3 exposure in the lower trunk of Lava Chuar

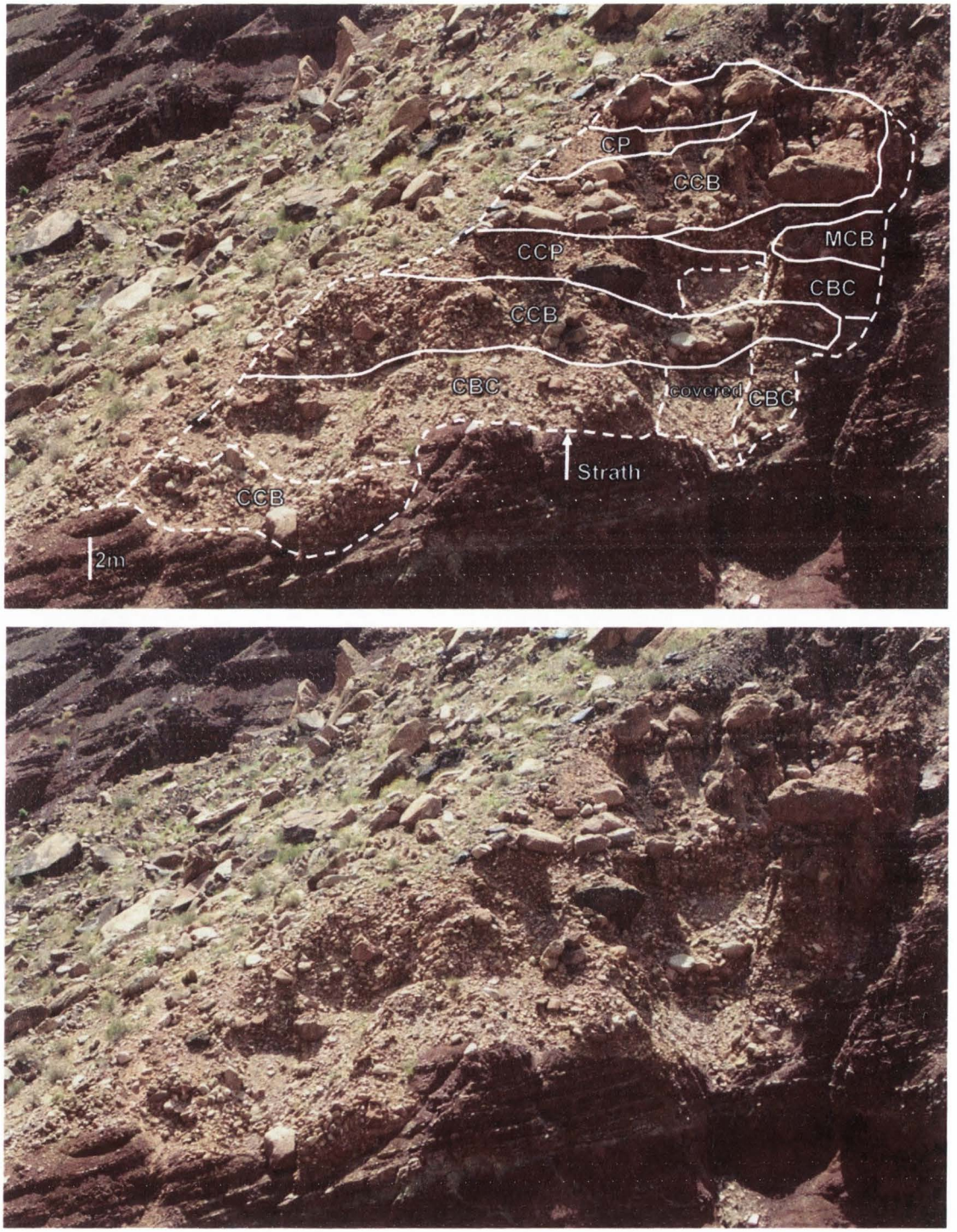

Figure B.4. Sedimentary facies in an S3 exposure near the mouth of Lava Chuar

Figure B.5. Sedimentary facies in an S2 exposure in the upper trunk of Lava Chuar

Figure B.6. Sedimentary facies in an S2 exposure in the lower trunk of Lava Chuar

Figure B.7. Sedimentary facies in an S2 exposure near the mouth of Lava Chuar

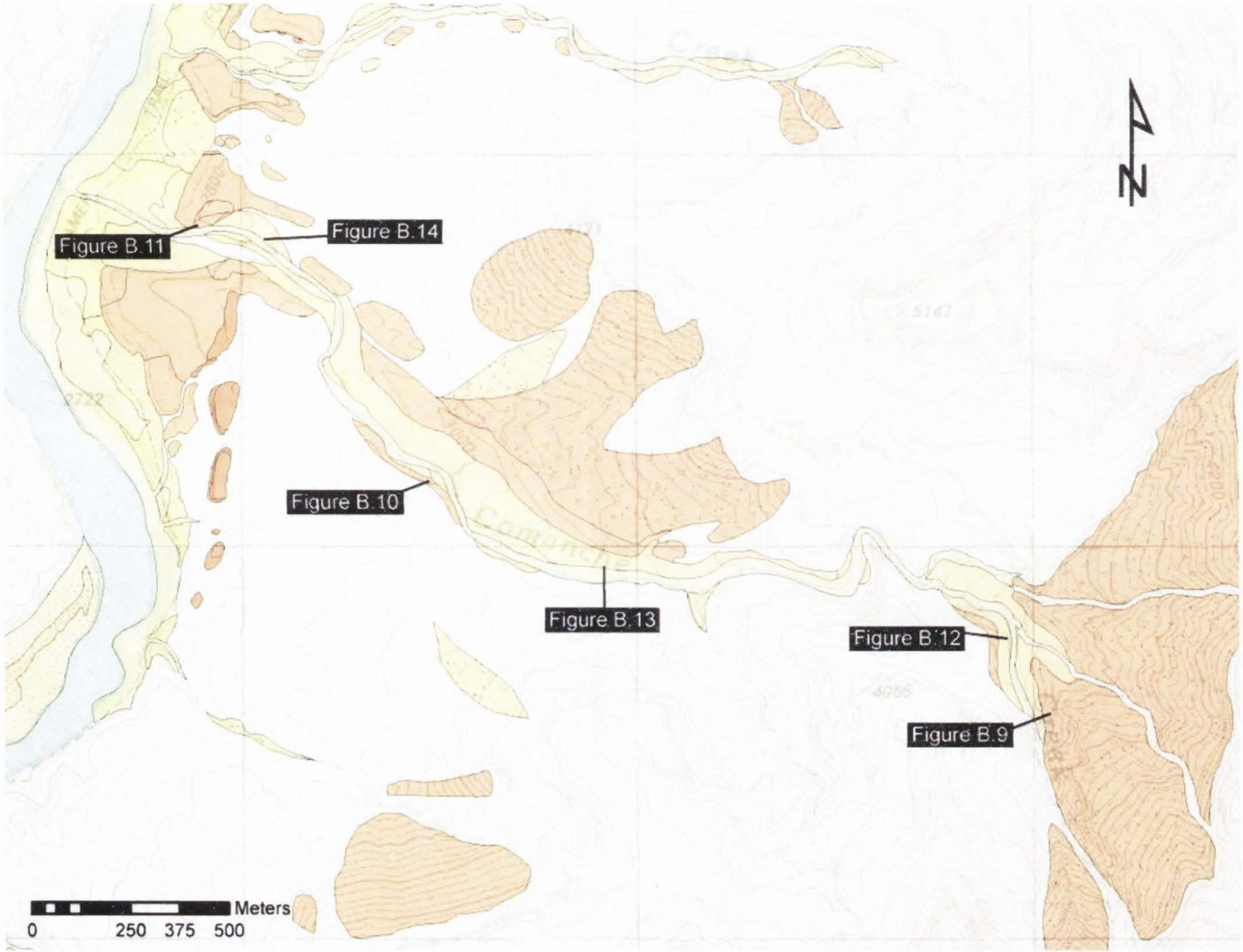

Figure B.8. Surficial geologic map of Comanche showing locations of photos in Figs. B.9. through B.14.

Figure B.9 Sedimentary facies in an S3 exposure in the headwaters of Comanche

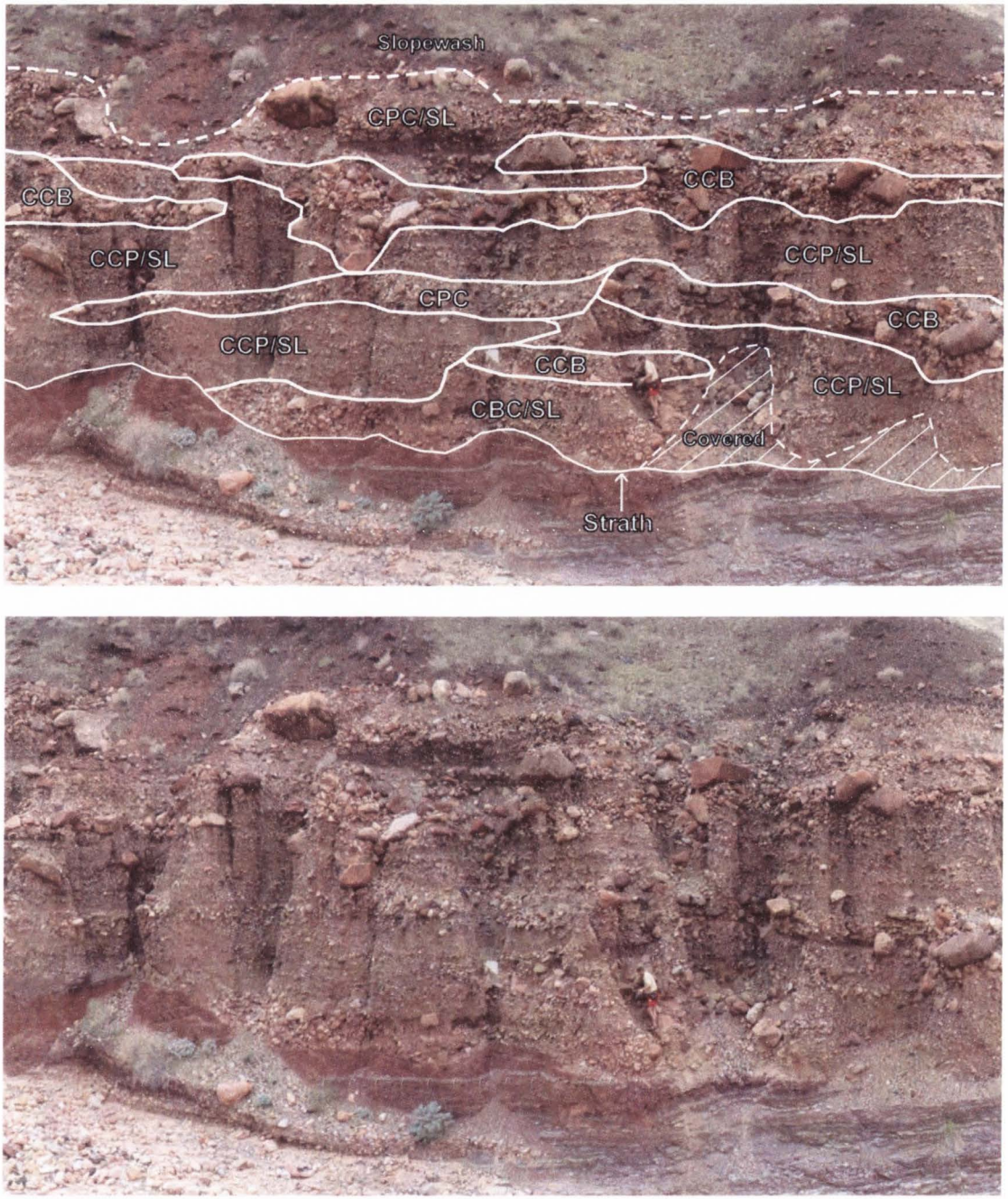

Figure B.10 Sedimentary facies in an S3 exposure in the trunk of Comanche

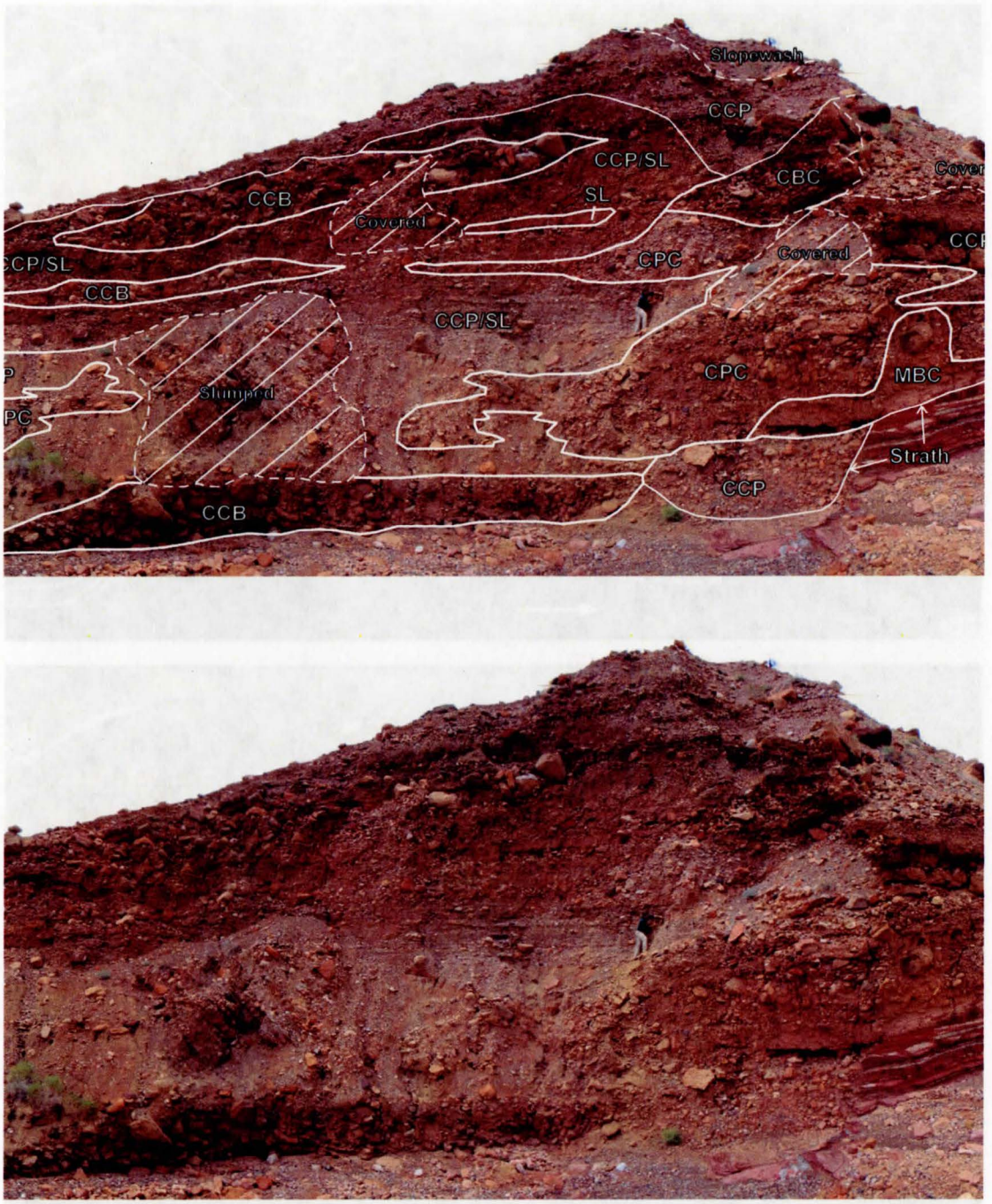

Figure B.11 Sedimentary facies in an S3 exposure near the mouth of Comanche

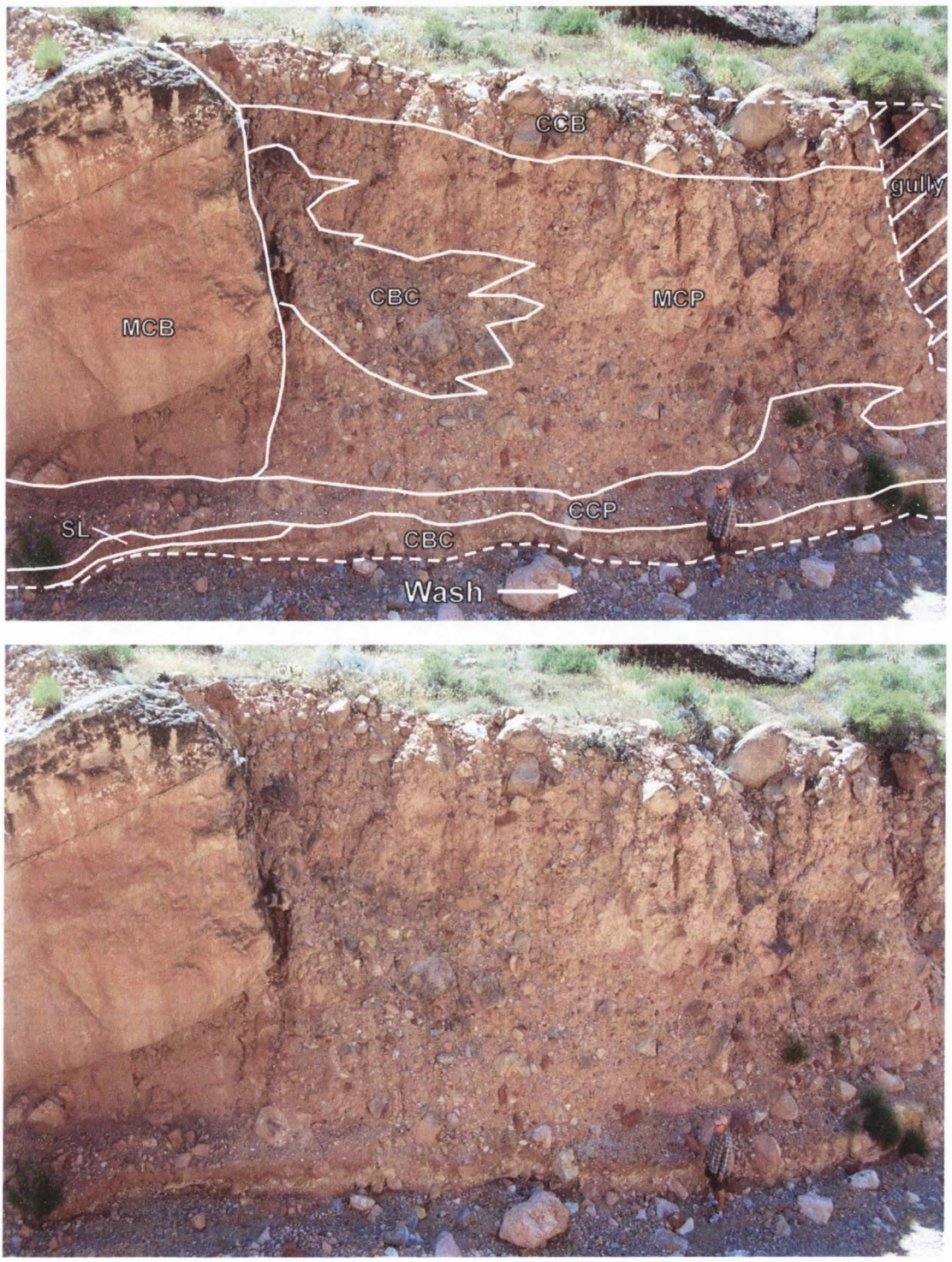

Figure B.12 Sedimentary facies in an S2 exposure in the headwaters of Comanche

Figure B.13 Sedimentary facies in an S2 exposure in the trunk of Comanche

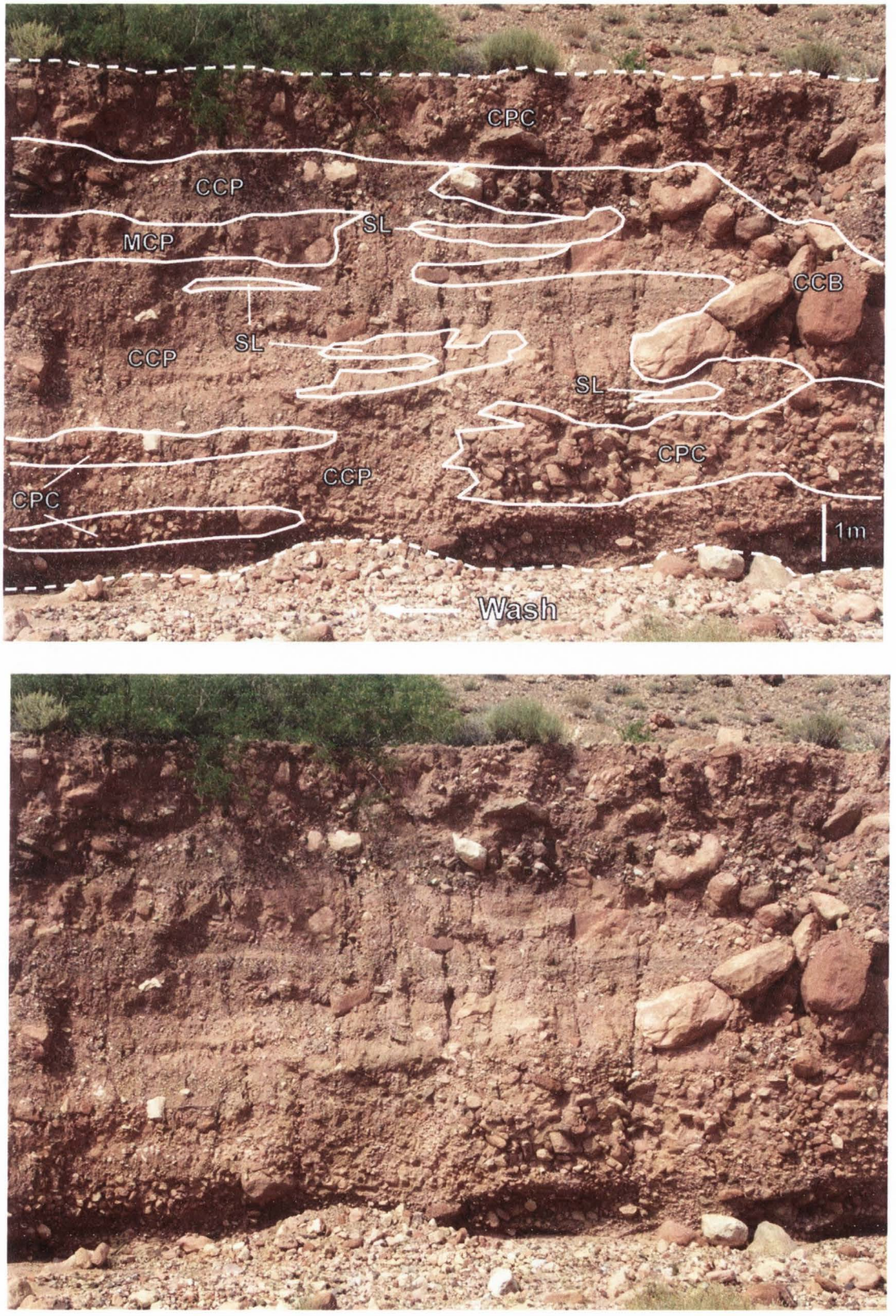

Figure B.14 Sedimentary facies in an S2 exposure near the mouth of Comanche

APPENDIX C. OPTICALLY STIMULATED LUMINESCENCE DATA

Table C.1. lists all OSL samples analyzed in this study. The following tables include all applicable data associated with each sample and are ordered in the same fashion as Table C.1.

TABLE C.1. OVERVIEW OF OPTICAL AGES FROM EASTERN GRAND CANYON

Deposit/ Location[a]	Sample number	UNL Lab Number	Depth (m)	dose rate (Gy/ka)	De (Gy)	Optical age ± total error (ka)
Tributary terrace fills						
S2 - Lava Chuar	GC-06-65.5-03	UNL - 1443	3.0	3.28 ± .14	37.3 ± 12.7	11± 3
S2 - Lava Chuar	GC-05-65.5-03	UNL-1137	7.0	3.26 ± .14	46.6 ± 11.2	14± 3
S2 – Comanche	GC-06-67-16	UNL-1438	7.0	1.31 ± .06	28.4 ± 8.7	22± 7
S2 – Comanche	GC-06-67-17	UNL-1440	1.0	2.34 ± .1	60.6 ± 12.8	26± 6
S2[b] – Comanche	GC-05-67-12	UNL-1136	7.0	1.31 ± .06	83.5 ± 20.5	64± 7
S3 – Lava Chuar	GC-05-65-17	UNL-1171	0.3	2.82 ± .13	131.6 ± 21.0	46 ± 8
S3 - Lava Chuar	GC-05-65-18	UNL-1164	3.8	3.68 ± 0.17	229.8 ± 39.1	61 ± 11
S3 - Lava Chuar	GC-05-65-15	UNL-1178	3.0	3.63 ± 0.16	209.0 ± 57.6	55± 14
S3[c] – Lava Chuar	GC-06-65-01	UNL-1442	10.0	1.42 ± .07	128.4 ± 21.3	90 ± 16
S3 – Comanche	GC-05-67-14	UNL-1165	11.5	3.31 ± .15	206.3 ± 32.4	62± 10
S3 – Comanche	GC-04-67-01	UNL-1322	10.7	3.64 ± .16	209.9 ± 49.7	58 ± 5
S3[d] – Comanche	GC-05-67-09	UNL-1174	65.5	1.57 ± .07	60.2 ± 13.8	35± 9
S3 – Comanche	GC-04-67-03	UNL-1170	8.0	2.88 ± .13	222.6 ± 24.7	77 ± 9
S4 - Lava Chuar	GC-05-65.5-06	UNL-1130	30.0	2.5 ± .11	251.3 ± 43.0	100 ± 18
Colorado River fill at the mouth of Comanche						
M4 – RM 67L	GC-04-67-04	UNL-1167	4.0	2.61 ± .1	232.9± 46.9	89 ± 18

[a]Organized by fill terrace, from upstream to downstream in catchments

[b] Interpreted as an erosional (strath) terrace on S3 materials upstream grading to a fill terrace of S2 ages downstream.

[c] Interpreted as an erosional (strath) terrace on S4 materials upstream grading to a fill terrace of S3 ages downstream.
[d] Collected from the base of reworked colluvium near the head of the Comanche catchment

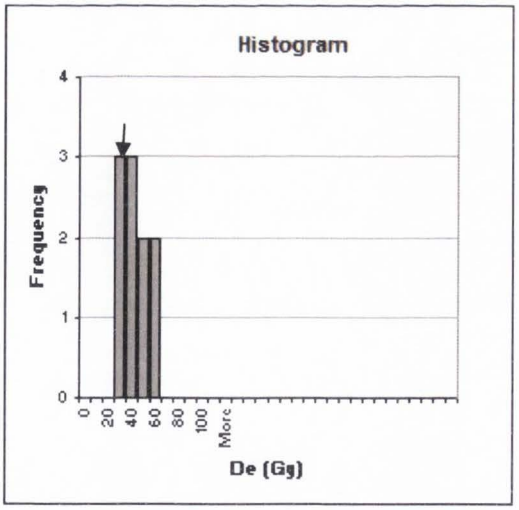

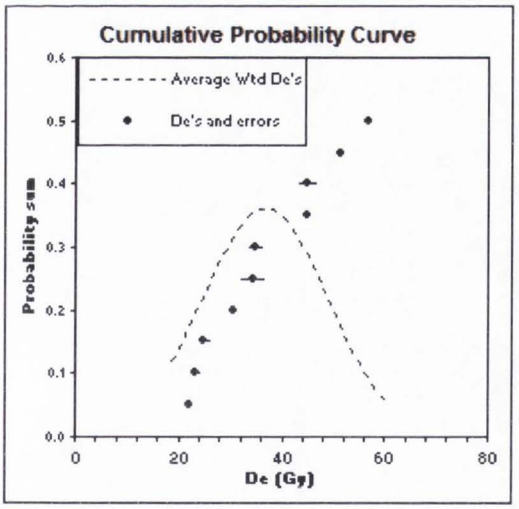

GC-06-65.5-03	S2, Lava Chuar			
UNL-1443				
	De (Gy)	±	Age (ka)	±
wt Mean =	36.79	12.16	11.2	3.8
Min =	22.01		6.7	2.2
Max =	56.88		17.4	5.8
S.D. =	12.16	used here		
Standard error =	3.85			
Random Errors=	33.14	%		
Systematic Error=	4.73	%		
Total Error=	33.48	%		
Bin Width =	10	Gy		
n =	10	Disks		
		+/-		
dose rate=	3.28	0.15	Gy/ka	
U =	2.30	0.2	ppm	
Th =	8.20	0.7	ppm	
K2O =	2.41	0.06	wt. %	
Rb2O=	92.2	3.7	ppm	
H2O=	0.5	3.0	wt. %	
Cosmic=	0.16	Gy/ka		
depth =	3.0	m		
latitude=	36	degrees (north positive)		
longitude=	-112	degrees (east positive)		
elevation=	0.90	km asl		

De (Gy)	Error	Age (ka)	±
22.01	0.21	6.71	2.25
23.38	1.02	7.13	2.39
24.85	1.33	7.58	2.54
30.67	0.78	9.36	3.13
34.35	2.56	10.48	3.51
34.86	1.46	10.64	3.56
44.65	0.53	13.62	4.56
44.92	1.97	13.71	4.59
51.35	0.68	15.67	5.25
56.88	0.34	17.35	5.81

Sample descript: Collected from the middle of an exposure of S2 near the mouth of Lava Chuar

UTM : Z 12, 426034E, 3999748N

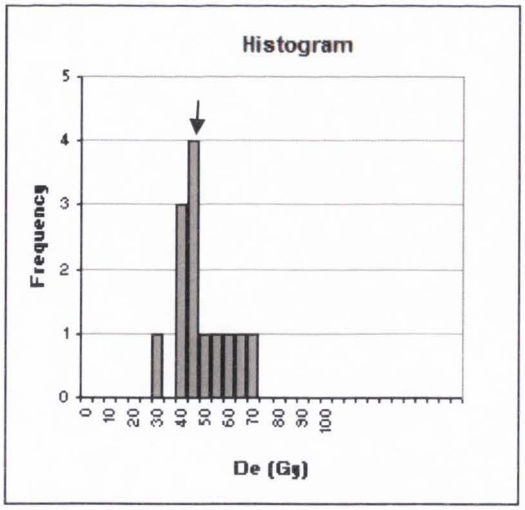

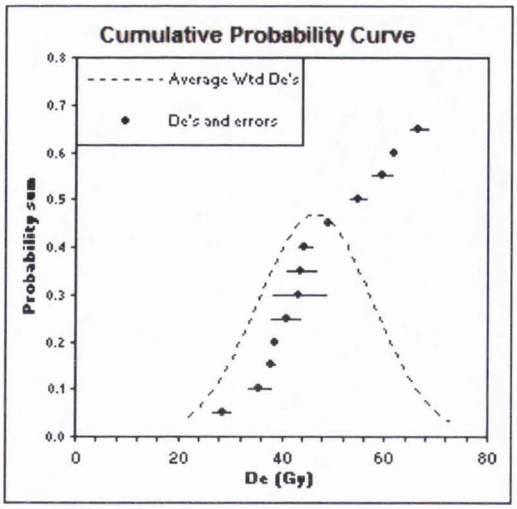

GC-05-65.5-03	S2, Lava Chuar				De (Gy)	Error	Age (ka)	±
UNL-1137					28.46	2.00	8.73	2.15
	De (Gy)	±	Age (ka)	±	35.67	2.42	10.94	2.70
wt Mean =	46.56	11.22	14.3	3.5	37.98	1.06	11.65	2.87
					38.66	0.72	11.85	2.92
					40.91	3.26	12.54	3.09
Min =	28.46		8.7	2.2	43.34	5.58	13.29	3.28
Max =	66.55		20.4	5.0	43.84	3.31	13.44	3.32
					44.57	1.74	13.67	3.37
S.D. =	11.22	used here			49.18	0.90	15.08	3.72
Standard error =	3.11				54.87	1.91	16.82	4.15
					59.53	2.20	18.25	4.50
Random Errors=	24.19	%			61.73	0.14	18.93	4.67
Systematic Error=	4.81	%			66.55	2.10	20.41	5.03
Total Error=	24.67	%		

Bin Width =	5	Gy	
n =	13	Disks	
		+/-	
dose rate=	3.26	0.14	Gy/ka
U =	2.10	0.1	ppm
Th =	7.20	0.6	ppm
K2O =	2.64	0.07	wt. %
Rb2O=	72.7	2.9	ppm
H2O=	1.0	3.0	wt. %

Cosmic=	0.10	Gy/ka
depth =	7.0	m
latitude=	36	degrees (north positive)
longitude=	-112	degrees (east positive)
elevation=	0.90	km asl

Sample descript: Collected from near the base of an S2 exposure up side channel in upper trunk of Lava Chuar

UTM: Z 12 420934E, 4003206N

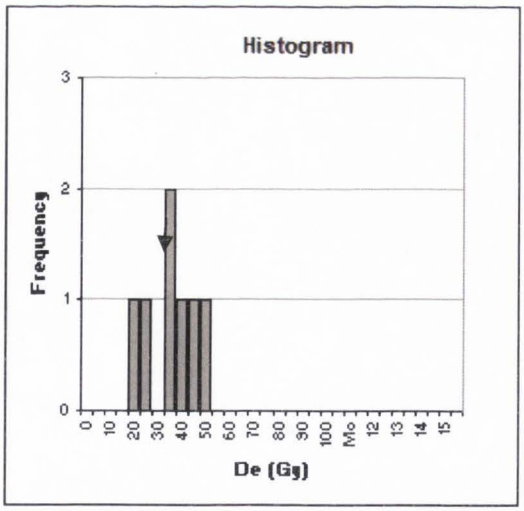

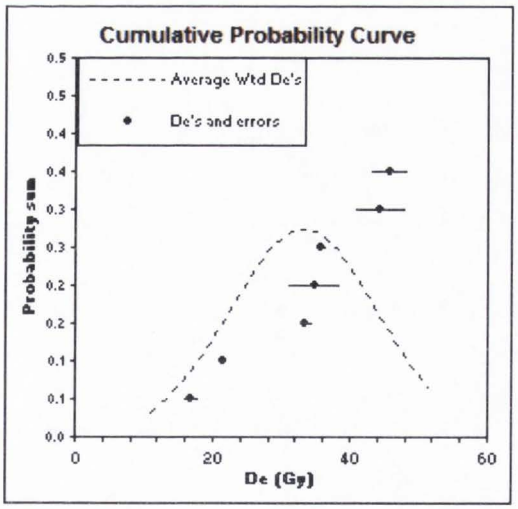

GC-06-67-16	S2 Comanche				De (Gy)	Error	Age (ka)	±
UNL-1438					16.89	1.21	12.86	4.24
	De (Gy)	±	Age (ka)	±	21.33	0.29	16.24	5.36
wt Mean =	33.17	10.79	25.3	8.3	33.44	1.11	25.46	8.40
					34.65	4.03	26.38	8.70
Min =	16.89		12.9	4.2	35.69	0.73	27.18	8.96
Max =	45.76		34.8	11.5	44.42	3.78	33.82	11.15
					45.76	2.76	34.84	11.49
S.D. =	10.79	used here						
Standard error =	4.08							
Random Errors=	32.64	%						
Systematic Error=	4.68	%						
Total Error=	32.98	%						
Bin Width =	5	Gy						
n =	7	Disks						
		+/-						
dose rate=	1.31	0.06	Gy/ka					
U =	1.10	0.1	ppm					
Th =	2.90	0.3	ppm					
K2O =	0.90	0.02	wt. %					
Rb2O=	30.5	1.2	ppm					
H2O=	0.5	3.0	wt. %					
Cosmic=	0.10	Gy/ka						
depth =	7.0	m						
latitude=	36	degrees (north positive)						
longitude=	-112	degrees (east positive)						
elevation=	0.90	km asl						

Sample descript: Collected from a small sand lense behind a slumped boulder in an S2 near the mouth of Comanche

UTM: Z 12 426131E, 3996857N

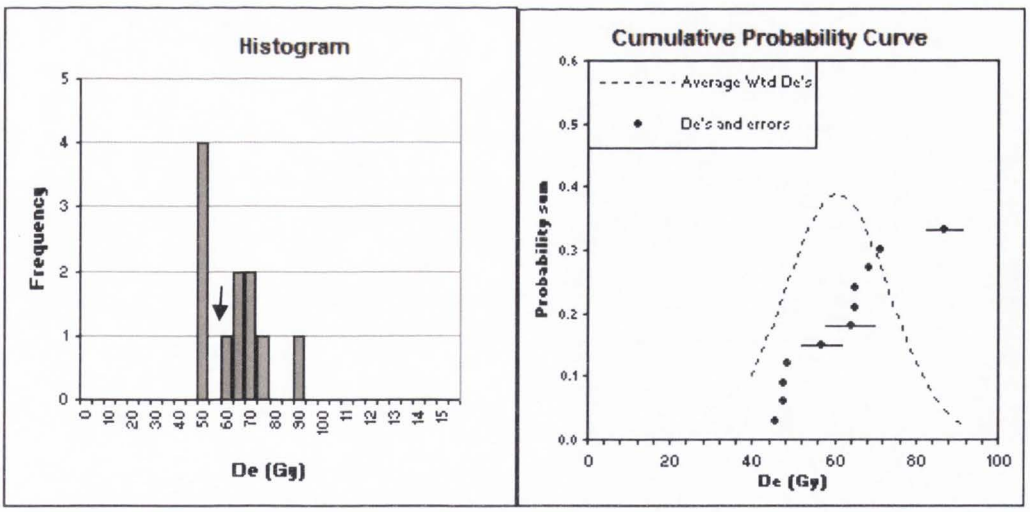

GC-06-67-17	S2 Comanche				De (Gy)	Error	Age (ka)	±
UNL-1440					45.41	0.65	19.43	4.24
	De (Gy)	±	Age (ka)	±	47.62	0.77	20.38	4.45
wt Mean =	60.59	12.83	25.9	5.7	47.80	0.45	20.46	4.46
					48.31	0.43	20.67	4.51
Min =	45.41		19.4	4.2	56.80	5.26	24.31	5.30
Max =	86.89		37.2	8.1	63.88	6.38	27.34	5.96
					64.87	0.09	27.76	6.06
S.D. =	12.83	used here			65.15	0.36	27.88	6.08
Standard error =	3.87				68.51	0.94	29.32	6.40
					71.24	1.17	30.49	6.65
Random Errors=	21.32	%			86.89	4.81	37.19	8.11
Systematic Error=	4.64	%						
Total Error=	21.82	%						

Bin Width =	5	Gy	
n =	11	Disks	
		+/-	
dose rate=	2.34	0.10	Gy/ka
U =	2.00	0.1	ppm
Th =	5.30	0.5	ppm
K2O =	1.54	0.04	wt. %
Rb2O=	54.1	2.2	ppm
H2O=	0.5	3.0	wt. %

Cosmic=	0.21	Gy/ka
depth =	1.0	m
latitude=	36	degrees (north positive)
longitude=	-112	degrees (east positive)
elevation=	0.90	km asl

Sample descript: Taken from the top of an S2 exposed near the head of Comanche

UTM: Z 12, 427895E, 3995901N

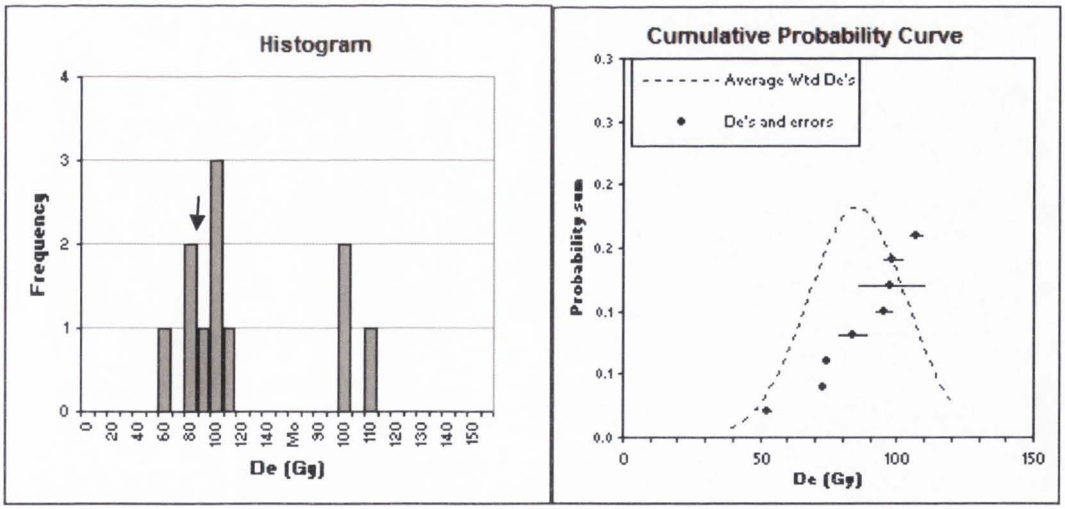

GC-05-67-12	S3, Comanche				De (Gy)	Error	Age (ka)	±
UNL-1136					52.38	2.31	39.86	3.67
	De (Gy)	±	Age (ka)	±	73.12	0.96	55.64	5.13
wt Mean =	85.29	6.36	64.9	6.0	74.14	1.86	56.41	5.20
					83.89	5.80	63.83	5.88
Median =	89.62		68.2	6.3	95.36	3.73	72.56	6.69
Min =	52.38		39.9	3.7	97.71	12.68	74.35	6.85
Max =	107.19		81.6	7.5	98.53	4.23	74.97	6.91
					107.19	2.73	81.56	7.51
S.D. =	18.00	used here						
Standard error =	6.36							
Random Errors=	7.94	%						
Systematic Error=	4.67	%						
Total Error=	9.21	%						
Bin Width =	10	Gy						
n =	8	Disks						
		+/-						
dose rate=	1.31	0.06	Gy/ka					
U =	1.10	0.1	ppm					
Th =	3.10	0.3	ppm					
K2O =	0.88	0.02	wt. %					
Rb2O=	31.1	1.2	ppm					
H2O=	0.1	3.0	wt. %					
Cosmic=	0.10	Gy/ka						
depth =	7.0	m						
latitude=	36	degrees (north positive)						
longitude=	-112	degrees (east positive)						
elevation=	0.90	km asl						

Sample descript: Collected from an S2 landorm on S3o sediments

UTM: Z12, 426473E, 3996301N

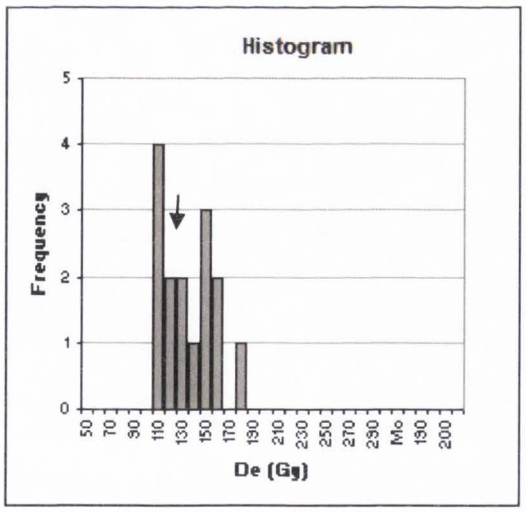

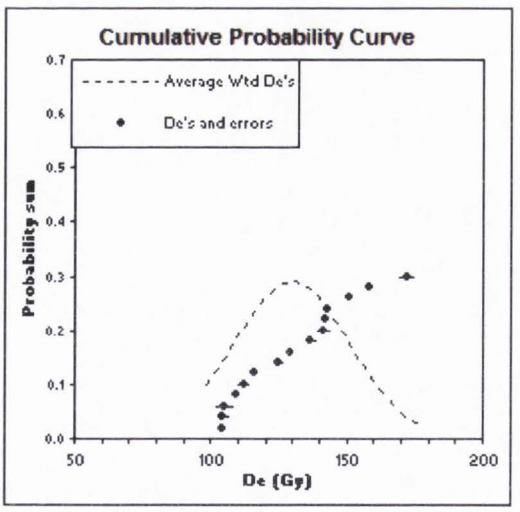

GC-05-65.5-17 **S3y, Lava Chuar**

UNL-1171

	De (Gy)	±	Age (ka)	±
wt Mean =	**129.80**	**21.39**	**46.1**	**8.0**
Min =	103.81		36.9	6.4
Max =	171.84		61.0	10.6
S.D. =	21.39	used here		
Standard error =	5.52			
Random Errors=	16.68	%		
Systematic Error=	4.65	%		
Total Error=	17.31	%		
Bin Width =	10	**Gy**		
n =	15	**Disks**		
		+/-		
dose rate=	2.82	0.13	**Gy/ka**	
U =	3.10	0.2	**ppm**	
Th =	5.80	0.5	**ppm**	
K2O =	1.79	0.04	**wt. %**	
Rb2O=	60.7	2.4	**ppm**	
H2O=	2.0	3.0	**wt. %**	
Cosmic=	0.23	**Gy/ka**		
depth =	0.3	**m**		
latitude=	36	**degrees (north positive)**		
longitude=	-112	**degrees (east positive)**		
elevation=	0.90	**km asl**		

De (Gy)	Error	Age (ka)	±
103.81	**0.37**	36.87	6.38
104.45	**2.62**	37.10	6.42
105.08	**3.60**	37.32	6.46
109.41	**0.52**	38.86	6.73
111.85	**2.31**	39.73	6.88
115.63	**1.59**	41.07	7.11
124.39	**2.26**	44.18	7.65
128.95	**1.09**	45.80	7.93
136.60	**2.34**	48.52	8.40
141.24	**2.81**	50.17	8.69
142.04	**1.48**	50.45	8.73
142.81	**0.10**	50.73	8.78
150.62	**1.75**	53.50	9.26
158.27	**1.29**	56.22	9.73
171.84	**3.45**	61.04	10.57

Sample descript: Collected from the base of a remnant of S3y materials near the mouth of Lava Chuar

UTM: Z 12, 426334E, 3999772N

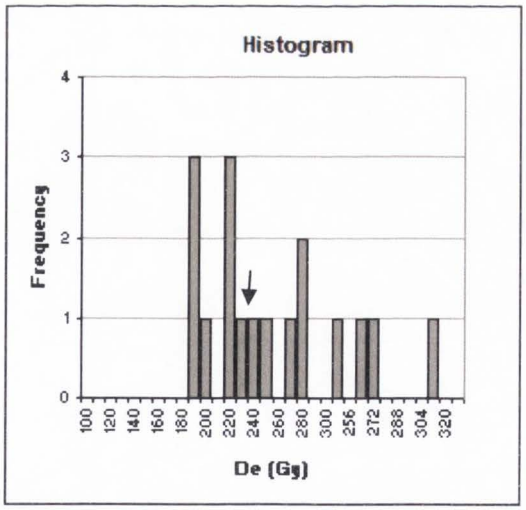

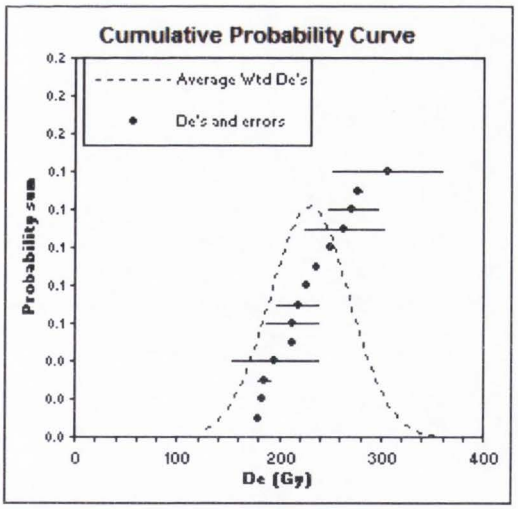

GC-05-65.5-18	S3, Lava Chuar			
UNL-1164				
	De (Gy)	±	Age (ka)	±
wt Mean =	229.81	39.12	61.3	11.0
Median =	222.39		59.3	10.6
Min =	180.06		48.0	8.6
Max =	305.43		81.4	14.6
S.D. =	39.12	used here		
Standard error =	10.46			
Random Errors=	17.24	%		
Systematic Error=	4.68	%		
Total Error=	17.87	%		

De (Gy)	Error	Age (ka)	±
180.06	1.32	48.02	8.58
183.42	1.35	48.91	8.74
184.49	7.82	49.20	8.79
195.89	44.49	52.24	9.33
212.25	0.13	56.60	10.11
212.80	26.92	56.75	10.14
217.92	23.01	58.12	10.38
226.85	1.72	60.50	10.81
236.01	0.39	62.94	11.25
249.38	5.02	66.51	11.88
263.43	40.88	70.25	12.55
271.84	25.73	72.49	12.95
277.56	5.80	74.02	13.23
305.43	55.60	81.45	14.55

Bin Width =	10	Gy	
n =	14	Disks	
		+/-	
dose rate=	3.75	0.17	Gy/ka
U =	3.40	0.2	ppm
Th =	11.80	1.1	ppm
K2O =	2.37	0.06	wt. %
Rb2O=	111.0	4.4	ppm
H2O=	0.6	3.0	wt. %

Cosmic=	0.15	Gy/ka
depth =	3.8	m
latitude=	36	degrees (north positive)
longitude=	-112	degrees (east positive)
elevation=	0.90	km asl

Sample descript: S3o from base of a pedestal near the Butte Fault

UTM: Z 12 425628E, 3999900N

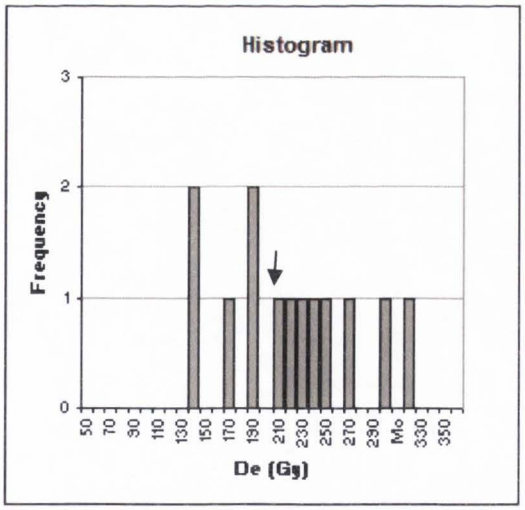

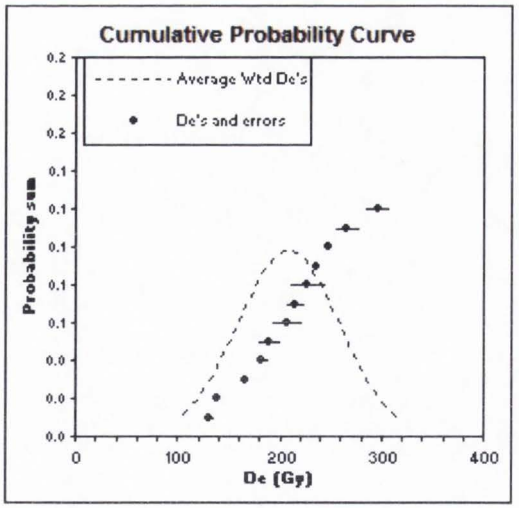

GC-05-65.5-15	S3, Lava Chuar			
UNL-1178				
	De (Gy)	±	Age (ka)	±
wt Mean =	208.50	50.01	57.5	14.1
Min =	131.30		36.2	8.9
Max =	296.34		81.7	20.1
S.D. =	50.01	used here		
Standard error =	14.44			
Random Errors=	24.11	%		
Systematic Error=	4.74	%		
Total Error=	24.57	%		

De (Gy)	Error	Age (ka)	±
131.30	4.32	36.19	8.89
138.21	4.77	38.10	9.36
165.92	0.81	45.74	11.24
181.78	6.63	50.11	12.31
189.85	11.59	52.34	12.86
206.72	15.60	56.99	14.00
214.94	9.13	59.25	14.56
226.92	18.00	62.56	15.37
235.58	5.19	64.94	15.95
248.52	3.51	68.51	16.83
265.97	12.08	73.32	18.01
296.34	12.71	81.69	20.07

Bin Width =	10	Gy	
n =	12	Disks	
		+/-	
dose rate=	3.63	0.16	Gy/ka
U =	2.40	0.2	ppm
Th =	10.20	0.9	ppm
K2O =	2.73	0.07	wt. %
Rb2O=	104.5	4.2	ppm
H2O=	2.4	3.0	wt. %
Cosmic=	0.16	Gy/ka	
depth =	3.0	m	
latitude=	36	degrees (north positive)	
longitude=	-112	degrees (east positive)	
elevation=	0.90	km asl	

Sample descript: Collected from an S3 exposure in a gully in the lower trunk of Lava Chuar

UTM Z12, 423845E,4000932N

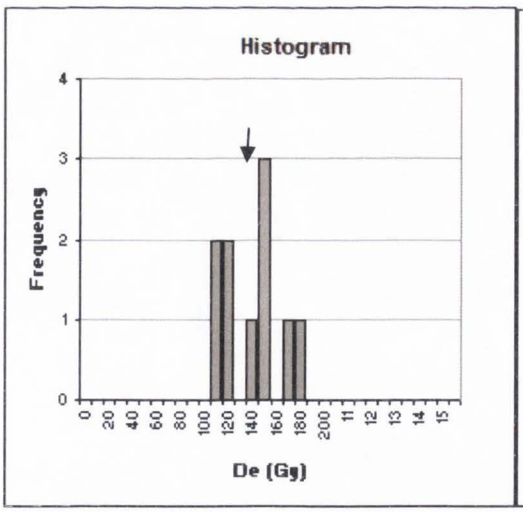

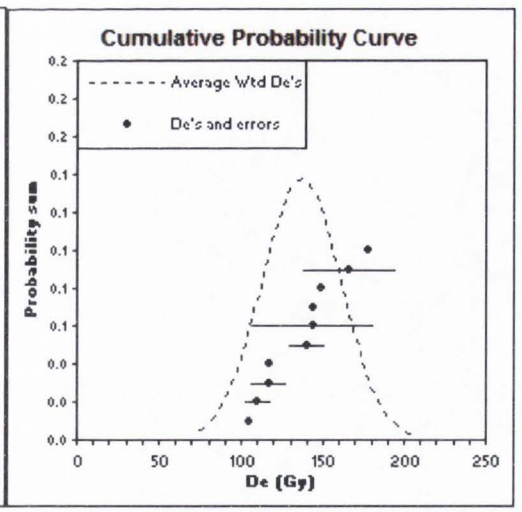

					De (Gy)	Error	Age (ka)	±
GC-06-65.5-01	S3, Lava Chuar				104.46	0.19	73.46	13.63
UNL-1442								
	De (Gy)	±	Age (ka)	±	109.89	8.15	77.28	14.34
wt Mean =	136.75	24.28	96.2	17.8	116.63	11.38	82.01	15.22
					117.46	0.65	82.60	15.33
Min =	104.46		73.5	13.6	139.65	11.68	98.20	18.22
Max =	177.74		125.0	23.2	143.48	38.80	100.89	18.73
					143.91	0.18	101.19	18.78
S.D. =	24.28	used here			148.51	0.38	104.43	19.38
Standard error =	7.68				165.74	28.81	116.55	21.63
					177.74	1.09	124.98	23.20
Random Errors=	17.94	%						
Systematic Error=	4.75	%						
Total Error=	18.56	%						
Bin Width =	10	Gy						
n =	10	Disks						
		+/-						
dose rate=	1.42	0.06	Gy/ka					
U =	1.00	0.1	ppm					
Th =	3.20	0.3	ppm					
K2O =	1.07	0.03	wt. %					
Rb2O=	34.7	1.4	ppm					
H2O=	0.5	3.0	wt. %					
Cosmic=	0.07	Gy/ka						
depth =	10.0	m						
latitude=	36	degrees (north positive)						
longitude=	-112	degrees (east positive)						
elevation=	0.90	km asl						

Sample descript: S3 surface, S4 sediments from the upper trunk of Lava Chuar

UTM: Z 12, 422070E,4002569N

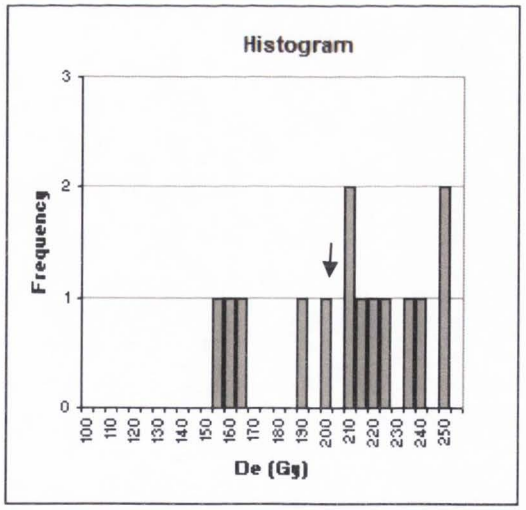

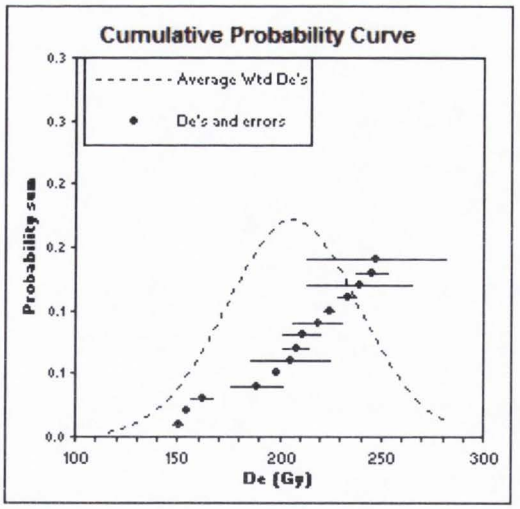

GC-05-67-14 **S3, Comanche**
UNL-1165

	De (Gy)	±	Age (ka)	±
wt Mean =	**206.26**	**32.44**	**62.4**	**10.4**
Min =	150.26		45.5	7.6
Max =	247.67		74.9	12.4
S.D. =	32.44	used here		
Standard error =	8.67			
Random Errors=	15.90	%		
Systematic Error=	4.80	%		
Total Error=	16.61	%		
Bin Width =	5	**Gy**		
n =	14	**Disks**		
		+/-		
dose rate=	3.30	0.15	**Gy/ka**	
U =	2.30	0.2	**ppm**	
Th =	8.00	0.7	**ppm**	
K2O =	2.57	0.06	**wt. %**	
Rb2O=	94.2	3.8	**ppm**	
H2O=	0.2	3.0	**wt. %**	
Cosmic=	0.07	**Gy/ka**		
depth =	11.5	**m**		
latitude=	36	**degrees (north positive)**		
longitude=	-112	**degrees (east positive)**		
elevation=	0.90	**km asl**		

De (Gy)	Error	Age (ka)	±
150.26	**3.88**	45.47	7.55
155.05	**1.20**	46.92	7.79
162.01	**6.15**	49.02	8.14
188.54	**13.75**	57.05	9.48
198.33	**0.75**	60.01	9.97
205.29	**20.27**	62.12	10.32
208.04	**7.54**	62.95	10.46
211.07	**10.14**	63.87	10.61
218.83	**13.11**	66.21	11.00
224.45	**3.61**	67.92	11.28
233.35	**5.14**	70.61	11.73
239.33	**26.93**	72.42	12.03
245.40	**8.54**	74.25	12.33
247.67	**35.20**	74.94	12.45

Sample descript: Collected from a small sand lense ~1m from the base of an S3 in the trunk of Comanche

UTM: Z 12, 426473E 3996301N

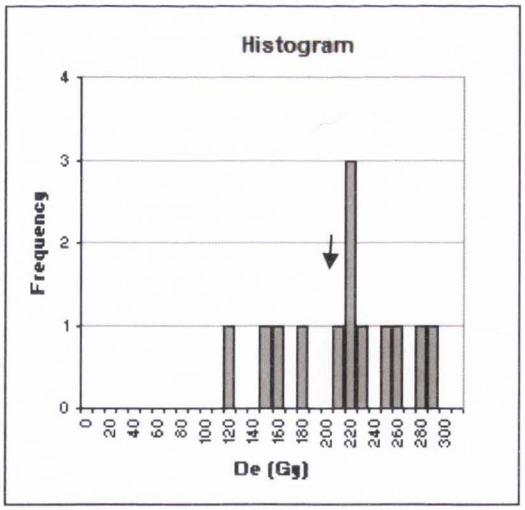

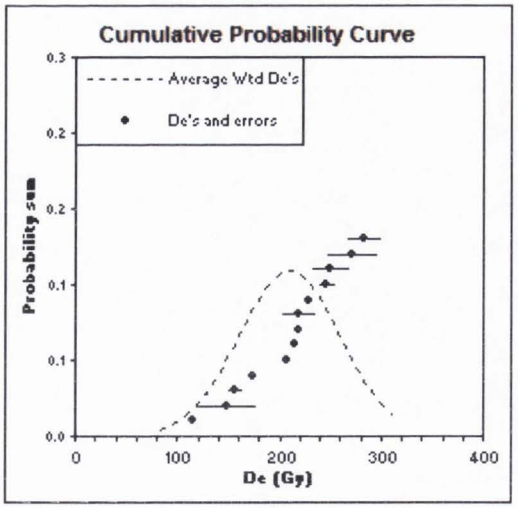

					De (Gy)	Error	Age (ka)	±
GC-04-67-01	S3, Comanche				114.36	0.28	31.44	2.66
UNL-1322					148.38	29.02	40.79	3.46
	De (Gy)	±	Age (ka)	±	155.93	7.43	42.87	3.63
wt Mean =	209.94	13.79	57.7	4.9	173.14	0.81	47.60	4.03
Min =	114.36		31.4	2.7	207.75	0.07	57.11	4.84
Max =	282.67		77.7	6.6	215.07	3.35	59.13	5.01
					218.27	0.44	60.01	5.08
S.D. =	49.72	used here			218.35	16.99	60.03	5.09
Standard error =	13.79				227.57	3.25	62.56	5.30
					246.53	8.70	67.78	5.74
Random Errors=	6.98	%			250.00	19.18	68.73	5.82
Systematic Error=	4.80	%			271.18	25.23	74.55	6.32
Total Error=	8.47	%			282.67	17.27	77.71	6.58

Bin Width =	10	Gy	
n =	13	Disks	
		+/-	
dose rate=	3.64	0.16	Gy/ka
U =	2.90	0.2	ppm
Th =	8.40	0.8	ppm
K2O =	2.73	0.07	wt. %
Rb2O=	99.8	4.0	ppm
H2O=	0.2	3.0	wt. %

Cosmic=	0.07	Gy/ka
depth =	10.7	m
latitude=	36	degrees (north positive)
longitude=	-112	degrees (east positive)
elevation=	0.90	km asl

Sample descript: Collected from a shaley lense ~1.5 meters from the base of an S3o exposure in the trunk Comanche

UTM: Z 12, 426473E 3996301N

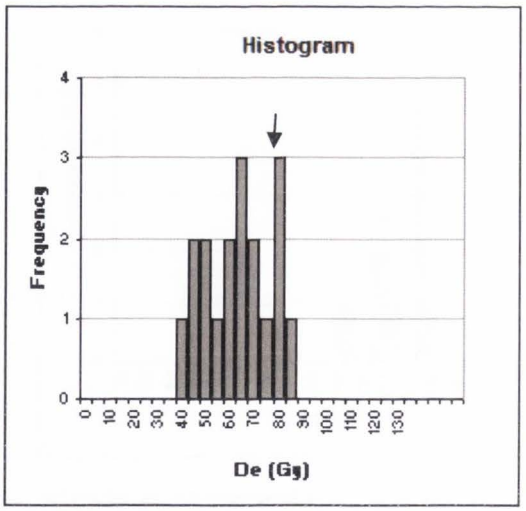

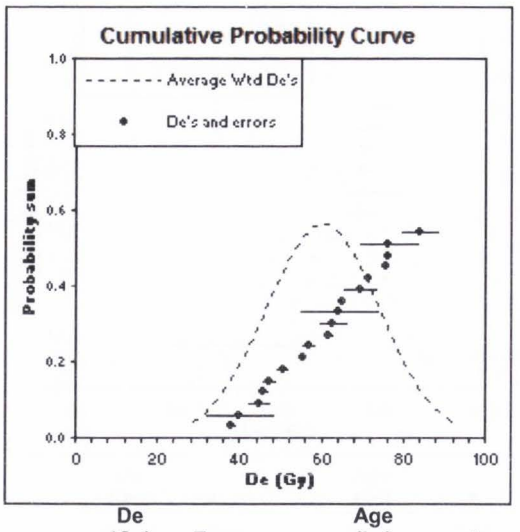

GC-05-67-09 C3, Comanche
UNL-1174

	De (Gy)	±	Age (ka)	±
wt Mean =	60.23	13.83	38.5	9.1
Min =	37.80		24.1	5.7
Max =	84.13		53.7	12.7
S.D. =	13.83	used here		
Standard error =	3.26			
Random Errors=	23.12	%		
Systematic Error=	4.77	%		
Total Error=	23.61	%		
Bin Width =	5	Gy		
n =	18	Disks		
		+/-		
dose rate=	1.57	0.07	Gy/ka	
U =	1.60	0.1	ppm	
Th =	4.10	0.4	ppm	
K2O =	1.07	0.03	wt. %	
Rb2O=	39.7	1.6	ppm	
H2O=	0.2	3.0	wt. %	
Cosmic=	0.00	Gy/ka		
depth =	65.0	m		
latitude=	36	degrees (north positive)		
longitude=	-114	degrees (east positive)		
elevation=	0.21	km asl		

De (Gy)	Error	Age (ka)	±
37.80	1.38	24.15	5.70
40.04	8.66	25.58	6.04
44.66	2.84	28.52	6.74
45.59	1.27	29.12	6.88
46.97	2.06	30.00	7.08
50.35	1.78	32.16	7.59
55.49	0.08	35.44	8.37
56.60	1.90	36.15	8.54
61.50	1.54	39.29	9.28
62.81	3.69	40.12	9.47
64.32	10.10	41.08	9.70
65.00	1.12	41.52	9.80
69.30	4.37	44.27	10.45
71.31	0.12	45.55	10.76
75.76	0.89	48.39	11.43
76.16	0.12	48.65	11.49
76.31	7.48	48.74	11.51
84.13	4.92	53.74	12.69

Sample descript: Reworked colluvium near the headwaters of Comanche Creek.

UTM: Z 12 428074E,
3995502N

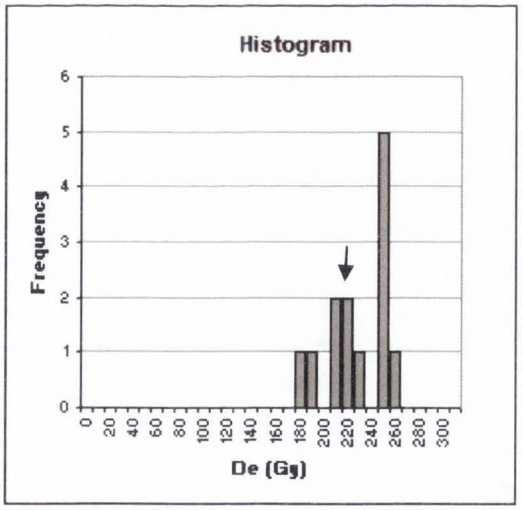

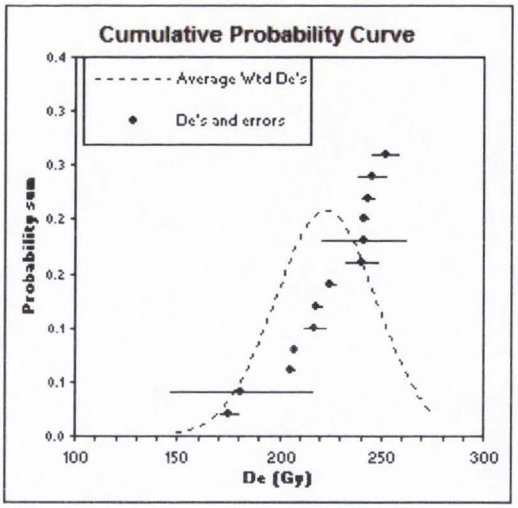

GC-04-67-03, S3 Comanche
UNL-1170

	De (Gy)	±	Age (ka)	±
wt Mean =	**222.62**	**24.72**	**77.3**	**9.5**
Min =	175.21		60.8	7.5
Max =	251.72		87.4	10.8
S.D. =	24.72	used here		
Standard error =	6.86			
Random Errors=	11.34	%		
Systematic Error=	4.79	%		
Total Error=	12.31	%		

	De (Gy)	Error	Age (ka)	±
	175.21	**5.32**	60.81	7.48
	181.31	**35.31**	62.93	7.75
	205.66	**3.04**	71.38	8.79
	207.31	**0.62**	71.95	8.86
	217.44	**6.05**	75.46	9.29
	218.52	**3.75**	75.84	9.33
	225.15	**3.33**	78.14	9.62
	240.77	**8.65**	83.56	10.29
	241.14	**21.35**	83.69	10.30
	241.35	**2.56**	83.76	10.31
	243.08	**3.75**	84.37	10.38
	245.43	**7.47**	85.18	10.48
	251.72	**7.04**	87.36	10.75

Bin Width =	10	**Gy**	
n =	13	**Disks**	
		+/-	
dose rate=	2.88	0.13	**Gy/ka**
U =	1.90	0.1	**ppm**
Th =	6.80	0.6	**ppm**
K2O =	2.24	0.06	**wt. %**
Rb2O=	82.0	3.3	**ppm**
H2O=	0.2	3.0	**wt. %**

Cosmic=	0.09	**Gy/ka**
depth =	8.0	**m**
latitude=	36	**degrees (north positive)**
longitude=	-112	**degrees (east positive)**
elevation=	0.90	**km asl**

Sample descript: Mainstem sands from the center of the complicated deposit at the mouth of Comanche

UTM: Z 12 425844E, 3997021N

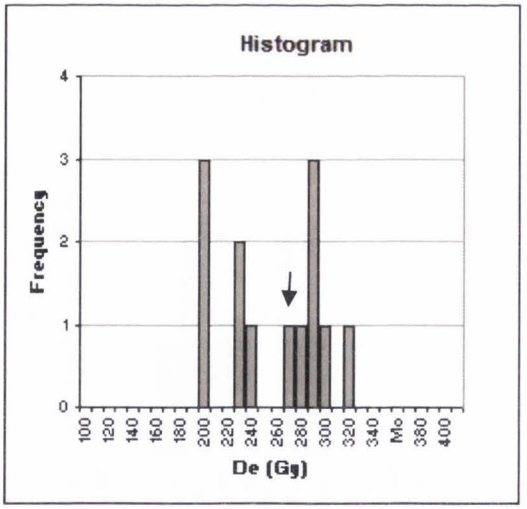

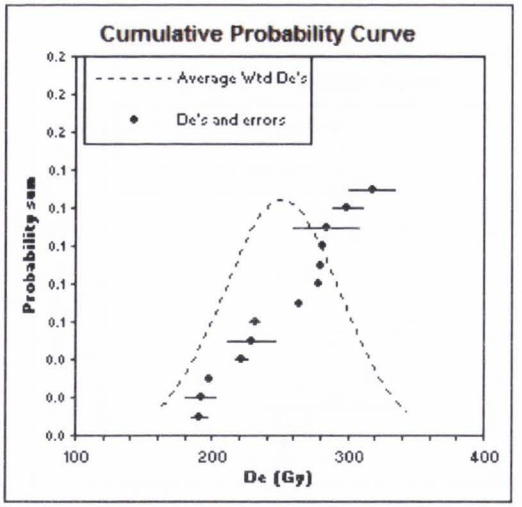

GC-05-65.5-06 **S4, Lava Chuar**

UNL-1130

	De (Gy)	±	Age (ka)	±
wt Mean =	**251.28**	**43.03**	**100.5**	**18.0**
Min =	190.77		76.3	13.7
Max =	317.32		126.9	22.8
S.D. =	43.03	used here		
Standard error =	11.94			
Random Errors=	17.30	%		
Systematic Error=	4.81	%		
Total Error=	17.95	%		
Bin Width =	10	**Gy**		
n =	13	**Disks**		
		+/-		
dose rate=	2.50	0.11	**Gy/ka**	
U =	1.90	0.1	**ppm**	
Th =	6.50	0.6	**ppm**	
K2O =	1.90	0.05	**wt. %**	
Rb2O=	71.6	2.9	**ppm**	
H2O=	0.4	3.0	**wt. %**	
Cosmic=	0.02	**Gy/ka**		
depth =	30.0	**m**		
latitude=	36	**degrees (north positive)**		
longitude=	-114	**degrees (east positive)**		
elevation=	0.21	**km asl**		

De (Gy)	Error	Age (ka)	±
190.77	**7.56**	76.30	13.70
191.72	**12.15**	76.68	13.77
198.26	**3.43**	79.30	14.24
221.24	**5.70**	88.49	15.89
228.86	**19.02**	91.53	16.43
231.07	**4.64**	92.42	16.59
264.28	**0.80**	105.70	18.98
278.01	**2.64**	111.19	19.96
280.44	**2.01**	112.16	20.14
281.08	**3.28**	112.42	20.18
283.92	**26.08**	113.55	20.39
299.66	**12.81**	119.85	21.52
317.32	**17.57**	126.91	22.79
336.81	**44.31**	134.71	24.19

Sample descript: Taken from within 1m of a local strath of the S4 in the upper trunk of Lava Chuar

UTM: Z 12, 421891E,4002799N

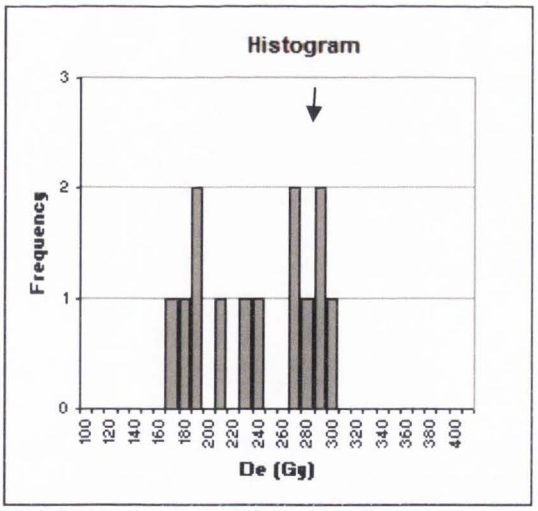

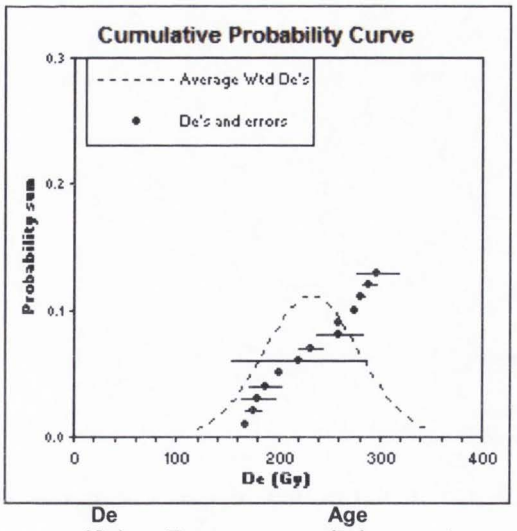

GC-04-67-04 31, Comanche
UNL-1167

	De (Gy)	±	Age (ka)	±
wt Mean =	232.95	46.94	89.2	18.5
Min =	168.66		64.6	13.4
Max =	297.54		113.9	23.6
S.D. =	46.94	used here		
Standard error =	13.02			
Random Errors=	20.29	%		
Systematic Error=	4.15	%		
Total Error=	20.71	%		

De (Gy)	Error	Age (ka)	±
168.66	3.42	64.55	13.37
175.26	9.58	67.08	13.89
180.37	18.71	69.04	14.30
188.11	17.55	72.00	14.91
200.13	5.00	76.60	15.87
220.38	67.89	84.35	17.47
231.91	13.43	88.77	18.38
260.03	24.27	99.53	20.61
260.21	3.59	99.60	20.63
274.49	3.35	105.06	21.76
281.62	5.99	107.79	22.32
289.69	8.67	110.88	22.96
297.54	22.53	113.88	23.59

Bin Width =	10	Gy	
n =	13	Disks	
		+/-	
dose rate=	2.61	0.10	Gy/ka
U =	2.60	0.2	ppm
Th =	4.90	0.4	ppm
K2O =	1.81	0.05	wt. %
Rb2O=	58.5	2.3	ppm
H2O=	0.1	0.1	wt. %
Cosmic=	0.14	Gy/ka	
depth =	4.0	m	
latitude=	36	degrees (north positive)	
longitude=	-114	degrees (east positive)	
elevation=	0.90	km asl	

Sample descript: M4 sands collected near the top of the complicated outcrop at the mouth of Comanche

UTM: Z 12 425843 E, 3997022N

APPENDIX D: PLATES

Plates 1 and 2 show the locations where age samples and total station transects were taken. Unit descriptions can be found in Anders (2003).

Plate 1: Surficial Geologic Map of Lava Chuar with OSL Sample and Cross Section Locations

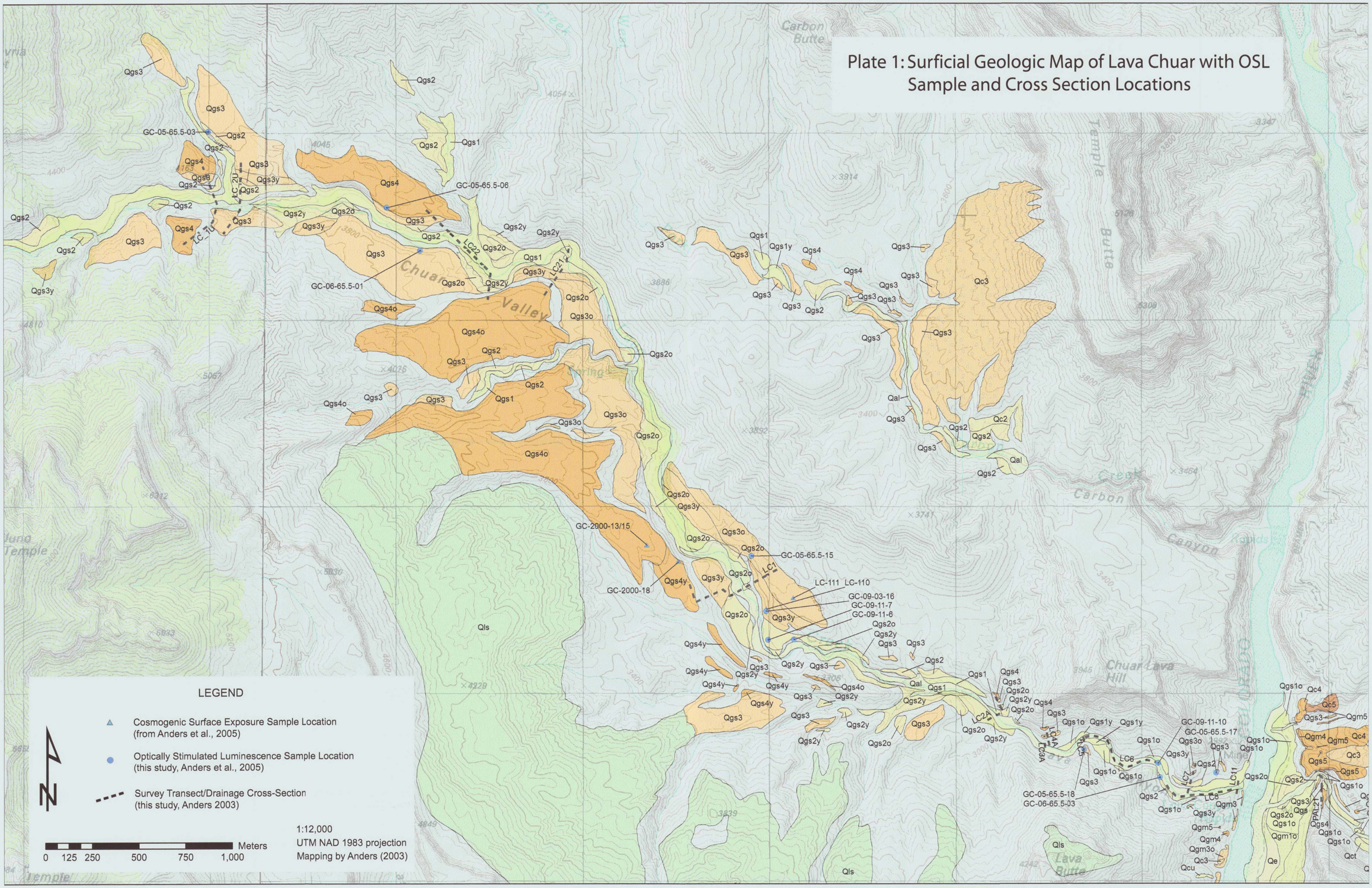

LEGEND

- Cosmogenic Surface Exposure Sample Location (from Anders et al., 2005)
- Optically Stimulated Luminescence Sample Location (this study, Anders et al., 2005)
- Survey Transect/Drainage Cross-Section (this study, Anders 2003)

N

0 125 250 500 750 1,000 Meters

1:12,000
UTM NAD 1983 projection
Mapping by Anders (2003)

Plate 2: Surficial Geologic Map of Comanche with OSL Sample and Cross Section Locations